G-quadruplex formation in mouse macrophages changes the immune response to bacterial infection

Doctoral thesis

to obtain a doctorate (PhD)

from the Faculty of Medicine

of the University of Bonn

Melanie Kastl

from Cologne, Germany

2024

Written with authorization of
the Faculty of Medicine of the University of Bonn

First reviewer: Prof. Dr. Katrin Paeschke

Second reviewer: Prof. Dr. Eva Kiermaier

Day of oral examination: 24.11.2023

For the clinic and policlinic for translational oncology
Director: Prof. Dr. Peter Brossart
and
For the institute for clinical chemistry and clinical pharmacology
Director: Prof. Dr. Gunther Hartmann

Table of Contents

List of abbreviations

ASC	Apoptosis-associated speck-like protein containing a CARD
AIM2	absent in melanoma 2
ALRs	Absent in melanoma-2-like receptors
ATAC Seq	Assay for Transposase-Accessible Chromatin using sequencing
BRAC1	Breast cancer 1
CARD	Caspase activation and recruitment domain
CCL3	CC-chemokine ligand 3
CD40	Cluster of differentiation 40
CD80	Cluster of differentiation 80
cGAS	Cyclic GMP-AMP synthase
ChIP	Chromatin immunoprecipitation
CLR	C-type lectin receptors
CTD	C-terminal domain
CTLD	C-type lectin-like domains
CUT&Tag	Cleavage under targets and tagmentation
DEGs	Differentially expressed genes
DHX36	DEAH-box helicase 36
DNA	Desoxyribonucleic acid
E. coli	*Escherichia coli*
EGR1	Early growth response protein 1
FACS	Fluorescence activated cell sorting
FANCJ	Fanconi anemia complementation group J helicase
G4	G-quadruplex
iBMDMs	immortalized bone-marrow-derived macrophages
IFI16	Interferon gamma inducible protein 16
IFN	Interferon
IKK	IκB kinase
IL	Interleukin
IP10	Interferon gamma-induced protein 10
IRF3	Interferon regulatory factor 3
IRF3	Interferon regulatory factor 3
ITAM	Immunoreceptor tyrosine-based activation motif
IκB	Inhibitor of κB
LBP	LPS-binding protein
LGP2	Laboratory of genetics and physiology 2
LPS	Lipopolysaccharide
LRR	Leucine-rich repeat
MAPK	Mitogen-activated protein kinase

MAZ	Myc-associated zinc-finger protein
MD-2	Myeloid Differentiation factor 2
MDA5	Melanoma differentiation-associated protein 5
MHC	Major histocompatibility complex
MyD88	Myeloid differentiation factor
NACHT	Domain present in NAIP, CIITA, HET-E and TP1
NAIP	NLR family, apoptosis inhibitory protein
NBD	Nucleotide-binding domain
NEMO	NF-κB essential modulator
NFKBIZ	NF-κB inhibitor zeta
NF-κB	Nuclear factor 'kappa-light-chain-enhancer' of activated B-cells
NHEJ	Non-homologous end joining
NIK	NF-κB inducing kinase
NLR	Nucleotide-binding oligomerization domain-like receptors
NLRC	NLR family CARD domain containing
NLRP	NOD-, LRR- and pyrin domain-containing protein
NOD	Nucleotide-binding and oligomerization domain
PAMP	Pathogen-associated molecular pattern
PD-L1	Programmed death ligand 1
PDS	Pyridostatin
PQS	Potential quadruplex-forming sequences
PRRs	Pattern recognition receptors
PYD	Pyrin domain
RD	Repressor domain
RIG-I	Retinoic acid inducible gene I
RLRs	RIG-I-like receptors (RLRs)
RNA	Ribonucleic acid
ROS	Reactive oxygen species
RQC	RecQ C-terminal domain
RTEL1	Regulator of telomere elongation helicase 1
STAT	Signal transducer and activator of transcription
STING	Stimulator of interferon genes
TAMs	Tumor associated macrophages
TBK1	TANK-binding kinase 1
TIR	Toll-interleukin-1R domain
TIRAP	TIR domain containing adaptor protein
TLR	Toll like receptor
Tn5	Transposase 5 (hyperactive form for tagmentation)
TNF	Tumor necrosis factor
TRAM	TRIF-related adaptor molecule
TRIF	Toll-interleukin-1 receptor domain-containing adaptor inducing IFN beta

1 Introduction

1.1 Importance of the immune response

The goal of organisms is to preserve cellular and genome stability and stay healthy [1,2]. Several aspects contribute to human health, such as the immune system and cellular functions that maintain genome stability [1,3]. Most eukaryotes, including humans, live in a symbiosis with bacteria that support cellular function and contribute to the overall health of the organism [4]. For example, 10^{14} is an estimate of the number of microorganisms present in the human gastrointestinal tract [5]. However, specific exogenous factors such as invading pathogenic microorganisms challenge our health [2]. Higher eukaryotes, including humans, have a complex immune system that detects and eliminates invading pathogens such as bacteria, viruses, and fungi [2]. In addition to pathogens, the immune system can also detect and eliminate also intrinsic factors that challenge the organism, for example, diseased, damaged, or apoptotic cells [6].

A complex network of cooperating cells, tissues, and organs is the basis of the immune system [2]. The immune system can be divided into two branches: the innate and the adaptive immune response [7]. In the first instance the innate immune cells sense the toxic challenge, secrete destructive substances such as hydrolases and finally eliminates them [2,8]. If the infection is not destroyed by this process, additional adaptive immune cells with specialized, systemic, and memory functions are recruited [2]. This process involves multiple immune cells cooperating in an orchestrated manner [9]. Disruptions in the immune response or changes in the specificity of the immune cells have pathophysiological consequences: underactivity can lead to infections and tumors of immunodeficiency, whereas overactivity can lead to allergic and autoimmune diseases [3]. An example of the disruption of the host immune response is provided by pathogenic bacteria such as *Yersinia* species [10]. These pathogens use their type three secretion system to inject six effectors that, for example neutralize the host phagocytic activity [10,11]. Most notably, the spread of the Gram-negative bacterium *Yersinia pestis* in 1347 caused an estimated two hundred million deaths (“Black Death”) [12]. The discovery of antibiotics drastically limited the spread of pathogenic bacterial infections [13]. However, the emergence of multi-resistant bacterial pathogens poses a threat to human health [14].

1.1.1 Innate immune system response

As stated above the immune system in vertebrates has two branches: the innate immune system and the adaptive immune system (Figure 1) [15]. The innate immune system, also called general, is a broad and rapid response to foreign microorganisms within hours [2]. It is a non-specific response that is present from birth and provides immediate protection against a broad range of conserved pathogenic patterns [2]. The first line of defense consists of mechanical and chemical barriers such as skin, saliva, and mucus [16]. If pathogenic microorganisms pass through this first barrier, they can be recognized by cells of the innate immune system that aim to eliminate the pathogen [2]. Innate immune cells recognize common pathogen surface molecules, called pathogen-associated molecular patterns (PAMPs) [17]. PAMPs are conserved within a microorganism type, are essential for its survival, and their molecular characteristics are not present in the host and can therefore be classified as “non-self” [17]. Examples include lipopolysaccharide (LPS), which is part of the outer membrane of Gram-negative bacteria, or chitin, which is part of the fungal cell wall [18,19]. Immune cells can also recognize apoptotic or damaged host cells, by specific released damage-associated molecular patterns (DAMPs) [17]. Recognition of PAMPs and DAMPs is mediated by extracellular or intracellular pattern recognition receptors (PRRs) [17,18]. Extracellular PRRs are localized at the cell membrane and recognize for example LPS [17]. Whereas intracellular PRRs are in the cytoplasm of the cell or in distinct vesicles like endosomes and recognize for example viral nucleic acids [20]; see Chapter 1.1.3 on PRRs.

The seven major cell types of the innate immune system and their function are briefly summarized below (Figure 1):

(1) Macrophages: Early in the immune response, macrophages are one of the first cells at the infection site [2]. Macrophages recognize and phagocytose (engulf and digest) microorganisms [2]. They present the lysed pathogenic proteins, as an antigen to migrating T cells [21,22]. Macrophages secrete cytokines to recruit other immune cells to the infection site [2]. Furthermore, macrophages contribute to tissue homeostasis by clearance of apoptotic cells [23]. For more details on macrophages, see Chapter 1.1.6.

(2) Dendritic cells: Similar to macrophages, they are derived from monocytes [23]. Dendritic cells express a wide range of PRRs to detect changes in the environment, such as the presence of PAMPs and DAMPs [24]. Dendritic cells are also phagocytic cells [21]. In contrast to tissue-resident macrophages they are highly migratory cells and move from tissues to B cell and T cell zones in lymphoid organs and activate T cells (B cells and T cells see below) [23]. They present antigens on their surface to T cells in local lymphoid tissues and thus are the main antigen-presenting cells [21,24].

(3) Neutrophils: Among the white blood cells, neutrophils are the most abundant [21]. Upon cytokine activation they emigrate from the bone marrow to the blood and to the tissues [25]. Similar to macrophages, neutrophils also phagocytose pathogenic microorganisms [21]. In addition, they release granules containing antimicrobial compounds such as cathepsins by degranulation [25]. Neutrophils release reactive oxygen species to eliminate extracellular microorganisms and secrete cytokines to further recruit immune cells [25].

(4) Natural killer cells: Natural killer cells play a role in eliminating virus-infected cells [21]. Natural killer cells recognize the presence of “alert” signals on the host surface [26]. Host cell apoptosis is achieved through release of perforin and granzymes [21]. By secreting interferon-gamma, natural killer cells mobilize antigen-presenting cells to the site of infection [21].

(5) Basophils: Basophils are the least abundant granulocytes in the human blood and play a role in the defense against parasites [27]. Through degranulation, they release histamine to improve the blood flow [28]. Their secretion of interleukin-4 stimulates other immune cells, for example the activation of B-cells [28].

(6) Eosinophils: Eosinophils play a role against parasites [21]. They have phagocytic properties and are essential for clearance of parasites that are too large for phagocytosis [21]. Through degranulation, they release mediators stored in their granules such as eosinophil peroxidase to eliminate invaders [29]. They are also involved in lymphocyte recruitment through the secretion of a variety of cytokines [30].

(7) Mast cells: Upon the coordinated effects of integrins, cytokines, and adhesion molecules, mast cells migrate to the infection site [31]. Mast cell granules contain proteases such as tryptase, and histamine and heparin to regulate the blood flow [31].

The innate and adaptive immune system are supported by the complement system [32]. The complement system, or complement cascade, is a network of tightly regulated proteins with essential functions in host defense [33]. More than 30 proteins, either blood-soluble or membrane-bound, are part of the complement cascade and are activated in a sequential enzymatic cascade [33]. For example, the membrane attack complex is made of the complement proteins: C5b-9, C6, C7 and C8 (and C9) [33]. The complement system leads to the opsonization of pathogenic microorganisms, thereby facilitating or enabling the elimination by phagocytotic cells [33]. It also enhances the clearance of apoptotic cells [33].

1.1.2 The adaptive immune system

The adaptive immune response, also called specialized, is not present at birth and develops over time [15]. It has a slower response than the innate immune system, usually within days [15]. The cells of the adaptive immune system specifically and effectively identify and target the pathogen and “remember” it, providing long-term protection against specific pathogens (called immunological memory) [34]. Antigen-presenting cells, such as dendritic cells and macrophages, are an important link between the innate and adaptive immune system [2]. The main effector cells of the adaptive immune cells are T cells and B cells (Figure 1) [15].

(1) T cells: The primary site of T cell development is the thymus [35]. T cells are present at low frequencies and undergo clonal expansion after activation [35]. Antigen presentation is required for proliferation and differentiation [36]. The strength and duration of exposure to the antigen and co-stimulatory stimulation affects the differentiation process of T memory cells and effector cells (can be divided into CD4+ and CD8+) [36]. Antigen-presenting cells such as phagocytes present via major histocompatibility complex II antigens to CD4+ T cells [37]. CD4+ T cells can differentiate into T helper cells [37]. T helper cells maximize the bactericidal activity of phagocytes, activate CD8+ T cells and determine B cell antibody

class switching [37]. CD8+ T cells recognize via MHC I antigens and can directly kill infected cells, and thus also known as killer T cells [38].
(Note: MHC I are present on almost all cells and result from proteasomal degradation in the cell and are transported via the ER to the cell surface. CD8+ T-cells can thus identify for example virus-infected cells by the presence of viral antigens [39]. MHC II is only present on antigen-presenting cells such as macrophages and dendritic cells and B cells and is recognized by CD4+ T cells [39]. The antigens presented on MHC II result from lysosomal degradation after phagocytosis [39].)

(2) B cells: B cells are characterized by their successive rearrangement by expression of the surface markers immunoglobulin (Ig) heavy (H) and light (L) gene segments [40]. B cells undergo a process of maturation and selection to exclude self-antigen binding [40]. After antigen recognition, B cells present “their” antigen to CD4+ T cells via MHC II and receive activation signals [40]. The predominant role of B cells is the production of antibodies (humoral immunity) [40]. Binding of the antibody to the antigen neutralizes the pathogen or marks it for elimination [41].

During antigen-dependent activation B cells and T cells, B cells and T cells can develop to memory cells [42]. Memory B cells are persistent antigen-specific B cells generated during infection, and B cell and T cell memory is the basis for immunological memory of lasting antibody titers [43]. These memory cells are essential for the second and faster response when encountering the pathogen again [44]. The generation and maintenance of memory cells is also the basis for the success of vaccination [44].

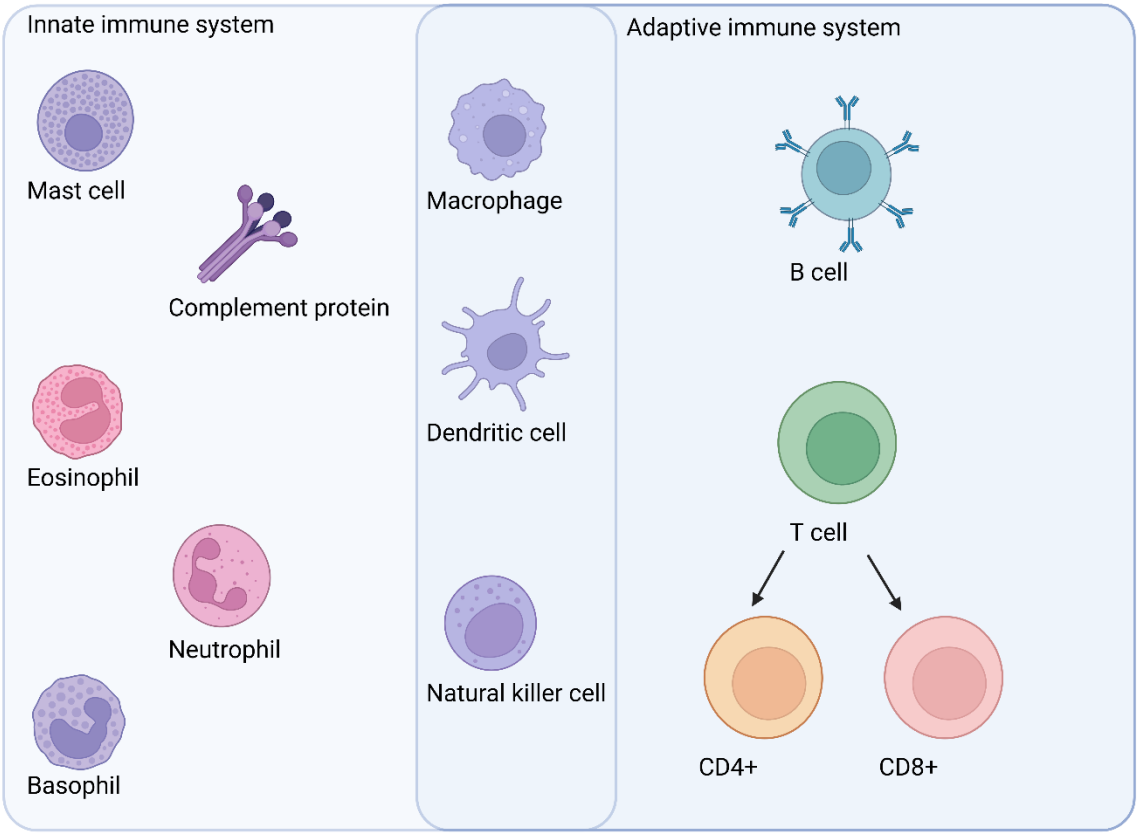

Figure 1: Simplified overview of the cells of the innate and adaptive immune system. The innate immune system provides the first and rapid response to pathogenic microorganisms. Part of the innate immune response are soluble factors such as the complement system and several cellular components such as granulocytes (basophil, neutrophil and eosinophil), mast cells, macrophages, dendritic cells and natural killer cells. The adaptive immune response is slower than the innate immune response but provides antigenic specificity and memory. Part of the adaptive immune response are antibody producing B cells and T cells. T cells can be further classified into CD4+ and CD8+ T lymphocytes. Macrophages and dendritic cells present antigens to B cells and T cells and thus provide a link between the innate and adaptive immune system. Natural killer cells belong to the innate immune system, however, based on their morphologic similarity and expression they are more similar to lymphocytes. Figure created with Biorender.com based on [45,46].

1.1.3 Pattern recognition receptors (PRRs)

PRRs can specifically recognize and bind a wide range of molecular features present on pathogens, called PAMPs, and those on damaged/ apoptotic host cells, called DAMPs (Table 1) [17]. Most pathogens contain a variety of PAMPs and are therefore recognized by a combination of PRRs that activate specific signaling pathways [47]. Different pathogenic microbes require a dynamic and versatile orchestration of PRR signaling to specifically inhibit pathogenic spread with limited damage to host cells [47]. PRRs have a ligand recognition domain, an intermediate domain, and an effector domain [17]. Most PRRs can be classified into five families based on protein domain, structural homology and specific target (Table 1) [17].PRRs at the cell membrane (extracellular) recognize for example fungal cell wall components such as chitin [18,19]. Intracellular PRRs can recognize for example viral nucleic acids inside the cell [20].

Upon ligand binding, PRRs recruit adaptor molecules through the effector domain to initiate downstream signaling pathways leading to specific gene expression changes such as inflammatory mediators [17,48]. The hallmark of PRR activation is the secretion of pro-inflammatory cytokines that either directly neutralize the pathogen or attract other immune cells such as phagocytes in a paracrine manner [17,49]. PRR recognition and signaling will be discussed in more detail in the next section 1.1.4 using TLR4 recognition of LPS as an example.

Table 1: Overview of pattern recognition receptors (PRRs) in the innate immune response [17,50]

Item	PRR	Domain	Site(s) of action
Toll-like receptors (TLRs)	TLR1-9 TLR10 (human) TLR11-13 (mouse)	LRR, TIR	Cell surface, endosomes
Nucleotide-binding oligomerization domain-like receptors (NLRs)	NOD1-2 (/NLRC1-2) NLRC3-5 NLRP1-9 and 11-14 NAIP1, 2, 5, 6	LRR, NBD	Cytoplasm, endosomal membrane
RIG-I-like receptors (RLRs)	RIG-I MDA5 LGP2	(RD)-CTD-DexD/H helicase domain–CARD	Cytoplasm
C-type lectin receptors (CLRs)	Dectin-1-2	CTLD–ITAM	Cell surface
Absent in melanoma-2-like receptors (ALRs)	AIM2 IFI16	HIN-200-PYD	Cytoplasm

Nucleotide-binding and oligomerization domain (NOD), NLR family CARD domain containing (NLRC), NOD-, LRR- and pyrin domain-containing protein (NLRP), NLR family, apoptosis inhibitory protein (NAIP), Retinoic acid inducible gene I (RIG-I), Melanoma differentiation-associated protein 5 (MDA5), Laboratory of genetics and physiology 2 (LGP2), Absent in melanoma 2 (AIM2), Interferon gamma inducible protein 16 (IFI16), Leucine-rich repeat (LRR), Toll/IL-1R domain (TIR), Nucleotide-binding domain (NBD), Repressor domain (RD), C-terminal domain (CTD), Caspase activation and recruitment domain (CARD), C-type lectin-like domains (CTLD), Immunoreceptor tyrosine-based activation motif (ITAM), Pyrin domain (PYD).

1.1.4 LPS recognition by TLR4

Among the PRRs is the toll like receptor (TLR) family (Table 1) [50]. The family members differ in their location and are functionally subdivided into cell membrane TLRs (TLR1,2,4,5,6,10) and intracellular TLRs or nucleic acid sensors (TLR3,7,8,9) [48]. TLR4 is a member in the TLR family (see Table 1) and induces a pro-inflammatory response upon pathogen recognition [51]. TLR4 is mainly expressed on myeloid immune cells such as monocytes, macrophages and dendritic cells [52]. TLR4 specifically recognizes LPS, which is part of the outer membrane of Gram-negative bacteria (Figure 2A-B) [48]. TLR4 can also recognize other PAMPs such as fungal-derived mannans [48]. However, data indicate that TLR4 can also be activated by DAMPs such as high mobility group box protein 1 and hyaluronic acid, which are released during tissue injury [53,54]. TLR4 has an extracellular LRR domain, a hypervariable domain, a transmembrane domain, and a conserved cytoplasmic Toll/IL-1R domain (TIR) domain [52].

LPS in the serum is transported by LPS-binding protein (LBP) to the LRR structural protein CD14 on the surface of e.g. macrophages (Figure 2B) [17,52,55]. CD14 lacks an intracellular domain for signal transduction [52]. CD14 transfers the bound LPS molecule to the complex of TLR4 together with myeloid differentiation factor 2 (MD2), which is stably associated with the extracellular part of the receptor (Figure 2B) [51,53,54]. LBP and CD14 only seem to enhance the TLR4 signaling and are not necessarily required for TLR4 recognition [52,56]. The conserved part of LPS, the acyl chains and phosphate groups of lipid A, are essential for the TLR4/MD-2 binding (Figure 2B) [51]. After ligand binding, TLR4 receptors homodimerize through the TIR domains, leading to conformational changes [52]. This recruits the cytoplasmic TIR domain containing adapter molecules to initiate intracellular signaling [52].

TLR4 can trigger two pathways named after the adaptor proteins (Figure 2B):

1) Myeloid differentiation factor (MyD)-dependent pathway, with TIR domain containing adaptor protein (TIRAP) and MyD88 adaptor proteins in the plasma membrane [52]. This pathway regulates early NF-κB activation leading to cytokine production such as IL-12 [52].

2) Toll-interleukin-1 receptor domain-containing adaptor inducing IFN beta (TRIF)-dependent pathway, where TRIF-related adaptor molecule (TRAM) and TRIF adaptor proteins start in early endosomes after receptor endocytosis [51]. This pathway also regulates the interferon regulatory factor 3 (IRF3) transcription factor, leading to type I interferon secretion [52]. It also leads to TNF-alpha secretion and TNF-alpha binding to its receptor upregulates NF-κB [52]. In addition, it induces the expression of co-stimulatory molecules such as cluster of differentiation 40 (CD40) and CD80 [52]. Macrophages constitutively express the cell surface tumor necrosis factor receptor superfamily member CD40 [57]. CD40 activation induces cytokine synthesis and the upregulation of MHC-II and co-stimulatory molecules such as CD80 [57]. CD40 stimulation is mediated by CD4+ T cells via CD40 ligand (CD154) [58].

Endocytosis of the TLR4 receptor terminates the MyD-dependent pathway and activates the TRIF-dependent pathway [51]. The termination of the TRIF-dependent pathway depends on its following endosome maturation and lysosomal degradation of TLR4 [51]. The lysosomal degradation contributes to the termination of the inflammatory immune response [51].
Thus, the two adaptor protein pathways are activated consecutively and depend on the redistribution of activated TLR4 from the plasma membrane to endosomes [51]. Both pathways activate two different sets of cytokines with partial redundancy [51]. Both pathways activate the NF-κB pathway leading to expression of pro-inflammatory cytokines [51,52]. The TRIF-dependent pathway can also activate the IRF3 transcription factor leading to expression of type I interferons [51,52].

The cellular level of TLR4 and its signaling must be tightly regulated [51]. If the TLR4 inflammatory signaling is exaggerated or uncontrolled during an infection, it can lead to sepsis, septic shock and even death [51].

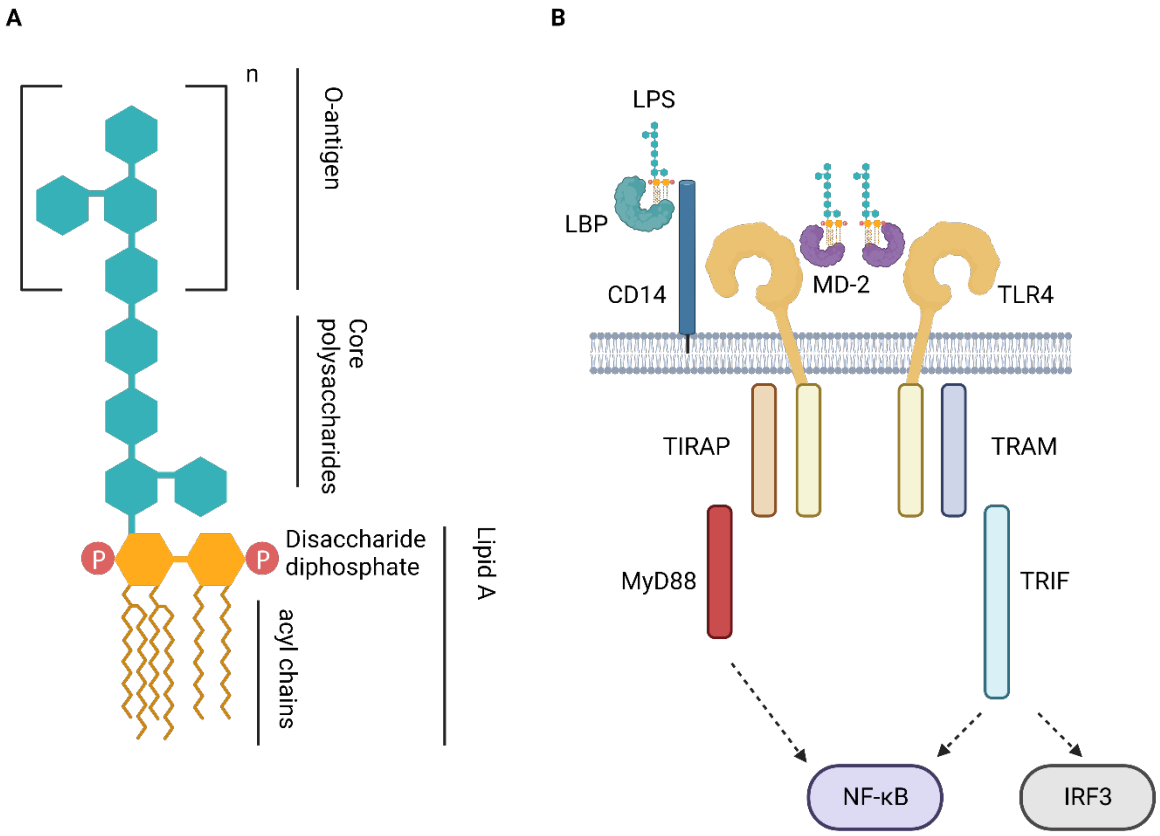

Figure 2: Overview of the lipopolysaccharide (LPS) structure and its recognition by Toll like receptor 4 (TLR4).
A) Structural details of LPS from Gram-negative bacteria. LPS is amphipathic and consists of three different regions: lipid A (hydrophobic), core polysaccharides and O-antigen (n can be up to 40 repeats of polysaccharide chains). B) LPS is transported by LBP to CD14 and recognized by the TLR4/MD-2 receptor complex. The signaling can be divided in MyD88-depent and independent pathway. Both pathways lead to proinflammatory cytokine transcription via NF-κB. The MyD-independent pathway via TRIF also leads to activation of IRF3. Cluster of differentiation (CD14); lipopolysaccharide-binding protein (LBP); TIR domain containing adaptor protein (TIRAP); TRIF-related adaptor molecule (TRAM); Myeloid differentiation factor 88 (MyD88); toll-interleukin-1 receptor domain-containing adaptor inducing IFN beta (TRIF); Myeloid Differentiation factor 2 (MD-2); Nuclear factor 'kappa-light-chain-enhancer' of activated B-cells (NF-κB); interferon regulatory factor 3 (IRF3). Figure created with Biorender.com and adapted from [52,59,60].

1.1.5 NLRP3 inflammasome assembly

Among the PRRs is also the NLR family (Table 1) [50]. The NLR family differs in their type of the N-terminal domain and can be divided into four groups (acidic transactivation, pyrin, caspase recruitment domain (CARD), and baculoviral inhibitory repeat (BIR)-like domains) [61]. The NOD-, LRR-, and pyrin domain-containing protein 3 (NLRP3) is a member in the NLR family and acts as an intracellular sensor that detects various PAMPs and DAMPs that lead to inflammasome assembly (Figure 3) [50,62]. Inflammasome assembly occurs in a two-step process: first, the priming signal and in the second step, the activation signal [63]. The priming signal from PAMPS, DAMPs or cytokines, such as TLR ligands (see Chapter 1.1.1), leads to the upregulation of NF-κB, pro-IL-1 beta, and NLRP3 [63]. The activation signal can be extracellular ATP, viral RNA or potassium ionophores [63,64]. The inflammasome includes the sensor NLRP3, the adaptor apoptosis-associated speck-like protein containing a CARD (ASC), and the effector caspase 1 (Figure 3) [62]. NLRP3 harbors a pyrin domain, a domain present in NAIP, CIITA, HET-E and TP1 (NACHT domain) that has ATPase activity and is thus essential for NLRP3 self-assembly and function, and a leucine-rich repeat (LRR) domain that is crucial for autoinhibition by backfolding onto the NACHT domain [62]. ASC has a pyrin domain and a caspase recruitment domain [62]. Caspase 1 also has a caspase recruitment domain and two catalytic subunits (p20 and p10) [62]. To activate NLRP3, ion fluxes are required as a stimulus [62]. For example ATP leads to calcium influx via its trimeric ion channel (P2X purinoceptor 7) and potassium efflux [62]. The potassium efflux leads to endoplasmatic reticulum linked calcium store release [62]. Another example is nigericin, a microbial toxin from *Streptomyces hygroscopicus* [62]. Nigericin is a potassium hydrogen ionophore that promotes potassium efflux leading to IL-1 beta maturation [62,65–67]. NLRP3 activation further promotes ionic flux events such as potassium and chloride efflux, calcium mobilization, and sodium influx [63]. It is supposed that potassium efflux leads to NLRP3 conformational changes [63].

When the NLRP3 inflammasome is activated, NLRP3 oligomerizes via the NACHT domains (Figure 3), interacts with ASC via the pyrin-pyrin interaction, and ASC filament formation is initiated; large aggregates are formed, called “ASC specks” [62]. Via CARD-CARD interaction ASC recruits caspase 1, initiating its self-cleavage and activation [62].

Activated caspase 1 then cleaves pro-IL-1 beta (Figure 3) and pro-IL-18, as well as gasdermin D, which gets incorporated into the membrane and leading to pores that cause pyroptosis [62].

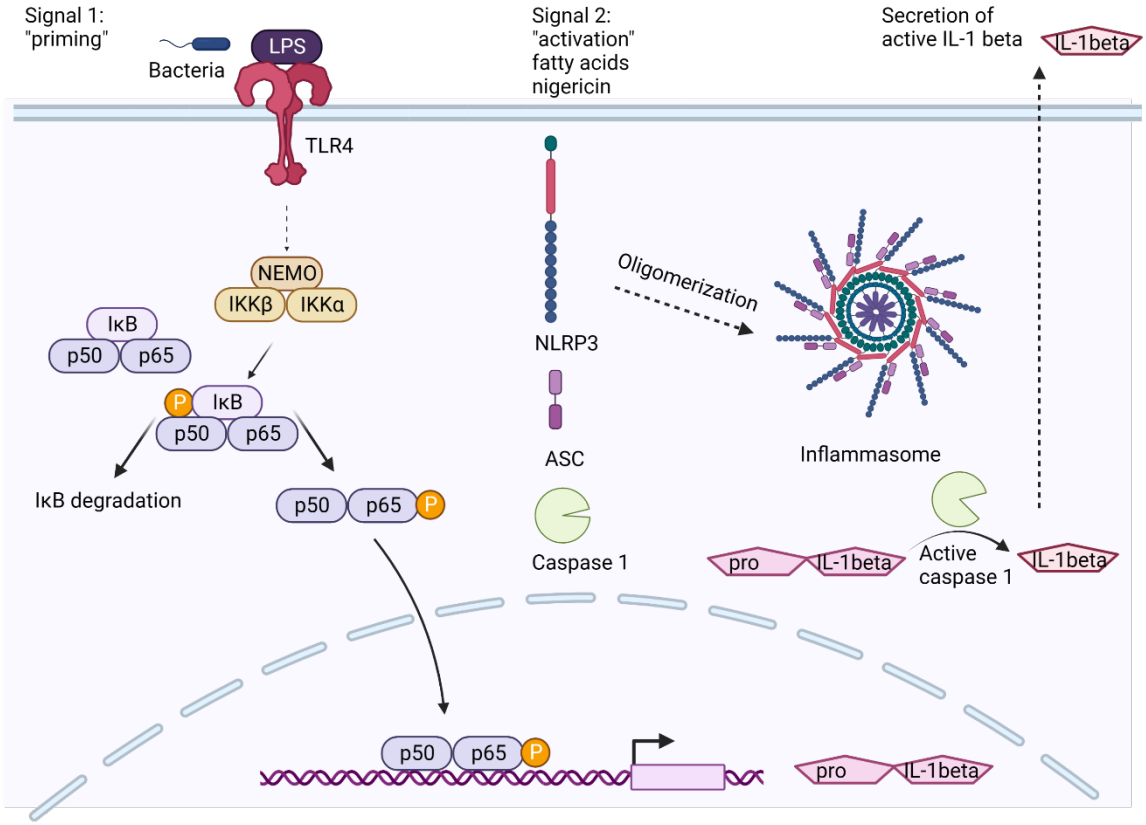

Figure 3: Host response to bacterial infection.
Stimulation by lipopolysaccharide, which is part of the outer membrane of Gram-negative bacteria, is recognized by TLR4. This leads to the degradation of IκB and translocation of p50 and p65 (subunits of the transcription factor NF-κB) to the nucleus after phosphorylation of p65. NF-κB binding leads to the expression of inflammatory cytokines such as IL-1 beta. IL-1 beta is expressed as an inactive precursor and is cleaved by activated caspase 1. Caspase 1 is activated after stimulation with a second stimulus such as nigericin, which causes oligomerization of the inflammasome. Created with Biorender.com based on [68–71]. Lipopolysaccharide (LPS); Nuclear factor 'kappa-light-chain-enhancer' of activated B-cells (NF-κB); Inhibitor of kB kinase-related kinase (IKK), Toll like receptor (TLR), NF-κB essential modulator (NEMO), NOD-, LRR- and pyrin domain-containing protein 3 (NLRP3), Apoptosis-associated speck-like protein containing a CARD (ASC).

1.1.6 Role of macrophages

1.1.6.1 Macrophages origin

Macrophages were first described by Metchnikoff in 1894 while studying immune mechanisms in primitive animals [72]. Macrophages in adult tissues are either derived from circulating monocytes or are established before birth and are resident (Figure 4) [73]. These resident macrophages are derived from primitive yolk sac macrophages (primitive hematopoiesis) or embryonic fetal liver monocytes [73–75]. They are partially maintained by local proliferation [73]. During embryogenesis, they colonize organs in each tissue and contribute to tissue development (Figure 4) [76]. Depending on its location every macrophage type has a name, such as microglia in the brain and Kupffer cells in the liver [73]. Each tissue-resident macrophage population has a distinct phenotype [77]. They exhibit different expression profiles that are tissue-specific and serve the developmental and homeostatic needs of the tissue [77]. During adulthood, pluripotent hematopoietic stem cells in the bone marrow give rise to monocytes (Figure 4) [78]. Circulating monocytes in the blood enter into damaged tissue following chemokine gradients from macrophages at the site of infection [78]. These circulating monocytes mature into macrophages and outnumber the tissue-resident macrophages [78].

Growth factors and cytokines released by the local tissue lead to phenotypic and functional characteristics of the of recruited and resident macrophages [78]. The environmental signals regulate the expression of specific transcription factors that shape the role and phenotype of the macrophages [77]. However, these hematopoietic stem cell-derived macrophages also replenish to the macrophage population in many tissues, and together with yolk sac-derived monocytes contribute to tissue function and homeostasis (Figure 4) [76].

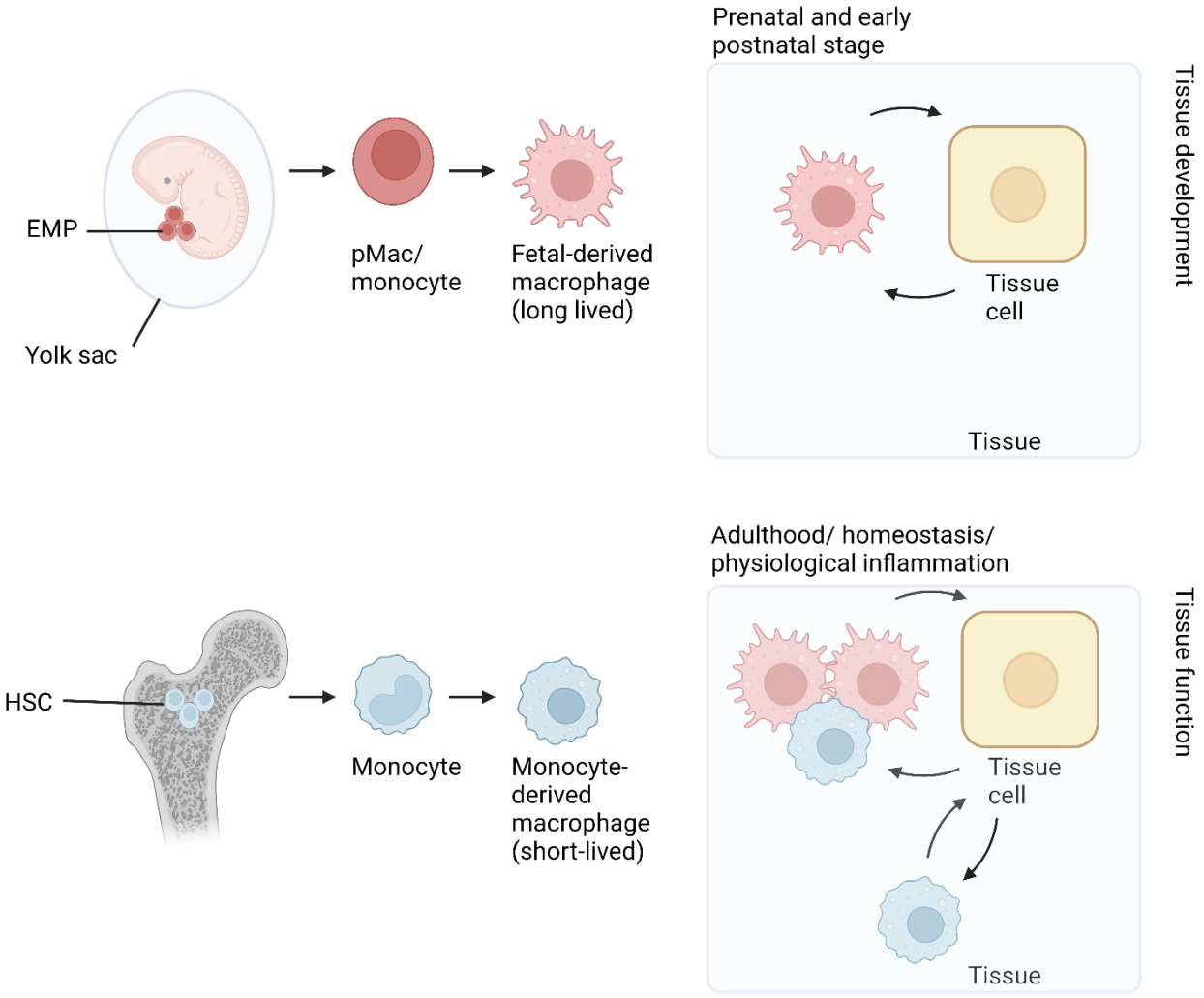

Figure 4: Origin and contribution of macrophages to tissue development and function.
Yolk sac erythro-myeloid progenitors (EMPs) are the source of pre-macrophages (pMac) and monocytes. They differentiate into tissue-resident macrophages that are long-lived with high self-renewal capacity. EMP-derived macrophages are responsible for the tissue development. Hematopoietic stem cells (HSCs) are the source of monocyte-derived macrophages during early postnatal stage and adulthood. They are short-lived and require replenishment from monocytes. During homeostasis or inflammation, they support and contribute to tissue function. Figure created with Biorender.com based on [76].

1.1.6.2 Macrophages function

Based on function and activation, macrophages can be classified as classically activated (M1) macrophages and alternatively-activated (M2) macrophages [79]. The microbial component LPS can polarize macrophages to the M1 state [79]. The M1 state is characterized by an inflammatory response and the production of inflammatory cytokines such as IL-6 and the overexpression of cell surface markers such as CD80 [79]. M1 macrophages are involved in phagocytosis and lysis of pathogens as well as antigen presentation [80]. M2 macrophages are characterized by an anti-inflammatory response, polarized by IL-4 [80]. M2 macrophages contribute to tissue repair [79]. However, this M1/M2 classification is obsolete as further complexity is discovered [81].

The main characteristic task of macrophages is phagocytosis [78]. Macrophages express a wide range of TLRs to recognize PAMPs and DAMPs [82]. This is important for (1) tissue homeostasis and (2) pathogen clearance for the innate immune response and subsequent antigen presentation to the adaptive immune system [76,78].

(1) Macrophages are present in all organs and maintain tissue homeostasis by recycling dead cells or debris via engulfment of particles (phagocytosis) [78,83]. They perform organ-specific functions, for example, Kupffer cells clear senescent red blood cells and thus maintain iron homeostasis [77]. Neurons and astrocytes, for example, release colony-stimulating factor 1 and IL-34 to maintain microglia in the central nervous system niche and function [76]. Microglia clear for example dead neurons and therefore ensure neural network maintenance [76,84].

(2) During infection, monocyte-derived macrophages follow chemotactic signals and recognize pathogens at the site of infection via PRRs (see also Chapter 1.1.1) [78,85]. Macrophages also express complement receptors (CR1 and CR3) to bind opsonized targets [86]. Macrophages digest phagocytosed pathogens in phagolysosomes containing several hydrolases [78,87]. The phagolysosome with the resulting pathogen peptides (12-25 amino acids) fuses with endoplasmatic reticulum-derived vesicles containing MHC II molecules [78]. They are transported to the cell surface and presented to B or T lymphocytes, particularly T helper cells [78,88]. Three signals are required for T cell

activation and its clonal expansion [89]. First, the T cell receptor interacts with the MHC-peptide complex [89]. Second, a complex costimulatory molecule between T cell (CD28) and macrophage (expression of maturation markers such as CD80) are required [89]. Third, cytokine secretion from in local environment by macrophages and other immune cells [89]. Phagolysosome-associated enzymes promote the production of reactive oxygen species (ROS) to eliminate the pathogenic microorganisms [78,90].

In addition, macrophages recruit and activate other immune cells such as dendritic cells, T cells, eosinophils and basophils by secreting proinflammatory cytokines [91,92]. Binding of PAMPs by TLRs leads to activation of the NF-κB signal pathway, which orchestrates the cytokine expression [78,93]. For example, interleukin-1 beta (IL-1 beta) and tumor necrosis factor alpha (TNF alpha) lead to increased vascular permeability and lymphocyte activation, whereas interleukin-12 (IL-12) activates natural killer cells [78,94,95]. Because of its central role, the NF-κB signal pathway will be discussed in Chapter 1.1.7.

1.1.7 NF-κB signaling pathway

The NF-κB transcription factor family is essential for the inflammatory and apoptotic responses [78]. It consists of five subunits: NF-κB1/ p50, NF-κB2/ p52, p65/ RELA, RELB, and c-REL1, which can homo- or heterodimerize [78,96–99]. They all have an N-terminal Rel-homology domain (named after their homology to the retroviral oncoprotein v-Rel), a conserved DNA binding and dimerization domain [100]. The Rel-homology domain has two beta barrel domains that can bind DNA in the major groove [101]. p65, RELB and c-REL have C-terminal transcriptional activation domain and thus p50 and p52 require them in the dimer for transcription activation [102]. Three dimensional structure of the transactivation domain is missing, putatively it leads to recruitment of co-activators [103]. NF-κB1 and NF-κB2 are expressed as inactive precursors, p105 and p100, respectively [100]. They have C-terminal ankyrin repeats that inhibit the protein activity and require proteolysis prior to activation [100].

NF-κB proteins are inactive in the cytoplasm and bound by the inhibitor IκB (IκB) complex [78,104]. The activation of NF-κB proteins involves the canonical and the noncanonical pathway [105]. The canonical pathway is activated for example by several

ligands of cytokine receptors, PRRs, TNF receptor family members, T cell receptor, and B cell receptor (Figure 3) [105]. The activation leads to degradation of IκBα through site-specific phosphorylation of the IκB kinase (IKK) complex [105].The IKK complex includes the catalytic serine protein kinases IKKα and IKKβ and the scaffold, sensing NF-κB essential modulator (NEMO also called IKKγ) (Figure 3) [105]. Phosphorylation of IκB leads to its proteasomal degradation [100,106]. This leads to nuclear translocation of NF-κB dimers such as p50/p65 or p50/c-REL1 (Figure 3) [105]. The dimers bind to 10 bp, called κB sites (consensus motif is 5´-GGGRNYYYCC-3´; R= purine, N= any nucleotide, Y= pyrimidine) [107].

Alternatively, the noncanonical pathway is activated by certain receptor binding, such as B-cell activating factor [100]. This activates NF-κB inducing kinase (NIK), leading to activation and phosphorylation of IKKα [100]. IKKα facilitates the processing of p100 to p52, which dimerizes with RELB [78,100]. In addition, a variety of post-translational modifications of the proteins involved further orchestrate the regulation and function of the NF-κB pathway, such as p65 phosphorylation sites that modulate the activity and promote transactivation [108,109]. Since NF-κB is a master regulator of most cytokines [110], those relevant for this PhD study are listed below focusing on the major and early cytokines according to the literature in the innate immune response [111–113]. Additionally, IL-10 was chosen based on its anti-inflammatory effect in contrast to the inflammatory cytokines [114]. The cytokines were also selected based on their potential to fold G4s, exemplary the IL-1 beta and TNF alpha promoters are shown (Supplementary figure 1).

IL-1 beta is a proinflammatory cytokine produced by monocytic lineage cells and stimulated by PAMPs or DAMPs [115,116]. It is synthesized as an inactive precursor, is cleaved into mature IL-1 beta by caspase 1 upon a second PAMP or DAMP stimulus, and finally secreted [116,117]. IL-1 beta circulates even to the brain and can induce fever [118,119].

IFN beta is produced by almost all cell types in response to DNA and RNA and has antiviral and antiproliferative effects [120,121]. It reduces antigen presentation and changes the cytokine expression, but it was also shown to resolve bacterial inflammation [121,122].

IL-6 is a proinflammatory cytokine playing a role in cell differentiation and proliferation and contributes to the expression of acute inflammation genes [123]. IL-6 is mainly produced by macrophages and monocytes and promotes B cell differentiation [123,124].

IL-10 has an anti-inflammatory effect by inhibiting the activity of macrophages, T helper cells, and natural killer cells and is produced by macrophages, dendritic cells, B cells, and T cells [114]. IL-10 limits the expression of proinflammatory cytokines [114]. Although these cells are necessary for pathogen clearance, they can damage the tissue if not tightly regulated [114].

TNF alpha is an inflammatory cytokine produced by macrophages and monocytes and contributes to necrosis or apoptosis [125]. It is produced by macrophages and natural killer cells and raised research interest to its ability to induce necrosis of tumors [126].

IL-18 is expressed by macrophages and dendritic cells and pro IL-18 is constitutively expressed but requires processing by caspase 1 [118]. It contributes with IL-12 to the T cell population activation and differentiation by inducing interferon γ [127].

IP-10 triggers an inflammatory response and serves a chemoattractant mainly for lymphocytes [128]. It is interferon γ induced [129] and plays a role in chemotaxis, apoptosis via activation of caspase 3, and cell growth [130,131].

IL-12 is a proinflammatory cytokine produced by phagocytic cells leading to interferon γ production and promotes T helper cell activation [132].

1.2 Structural aspects of DNA and RNA

Both DNA and RNA can adopt multiple secondary structures. Apart from the canonical B-DNA (right-handed helix), DNA can have alternative conformations such as cruciform and triplexes [133], and RNA can fold into loops, bulges, hairpins, and helices [134]. Not only are these structures predicted from sequence motifs, but they have been shown to form and play functional roles *in vivo* [133]. Among the stable secondary structures are G-quadruplexes (G4s).

1.2.1 G-quadruplex structures

It has been known since 1910 that guanylic acid can form a gel and suggested that guanine-rich regions could self-assemble [135]. Later, X-ray diffraction proved that guanylic acids form tetrameric structures in which four guanines form a square planar arrangement and stacking of these G-quartets forms a G-quadruplex (G4) structure [133,136]. G4s form in guanine-rich regions of DNA and RNA [137]. Guanines bind via Hoogsten hydrogen bonds to form a planar array stabilized by a monovalent cation in the center (mostly K^+ and Na^+) [138]. The consensus G4 motif is G_{3+}-N_{1-7}-G_{3+}-N_{1-7}-G_{3+}-N_{1-7}-G_{3+}-N_{1-7} [137]. Non-consensus quadruplex-structures with longer loops have been shown to impact biological processes *in vivo* [139], and G-columns with only two guanines have also been shown to fold *in vitro* [140–142]. G4s are highly thermodynamically stable structures with melting temperatures up to 72°C [143]. The properties of the stabilizing cation influence the stability of the G4 (K^+>Na_+>NH_4^+>Li^+) [140,144]. In addition, the G4 stability depends on the loop length [133]. Long loops lead to less stable G4s because they are counteracted by the effects of entropy [140,145].

The topology formation can vary from intermolecular to intramolecular folded (Figure 5) [146,147]. Based on the strand orientation they can vary from parallel to hybrid to antiparallel (Figure 5) [146,148]. A parallel G4 has parallel G-tracts, whereas an antiparallel G4 has two parallel and two antiparallel G runs (Figure 5) [140]. A mixture of one parallel and three antiparallel G-tracts, called hybrid, is also possible [146].

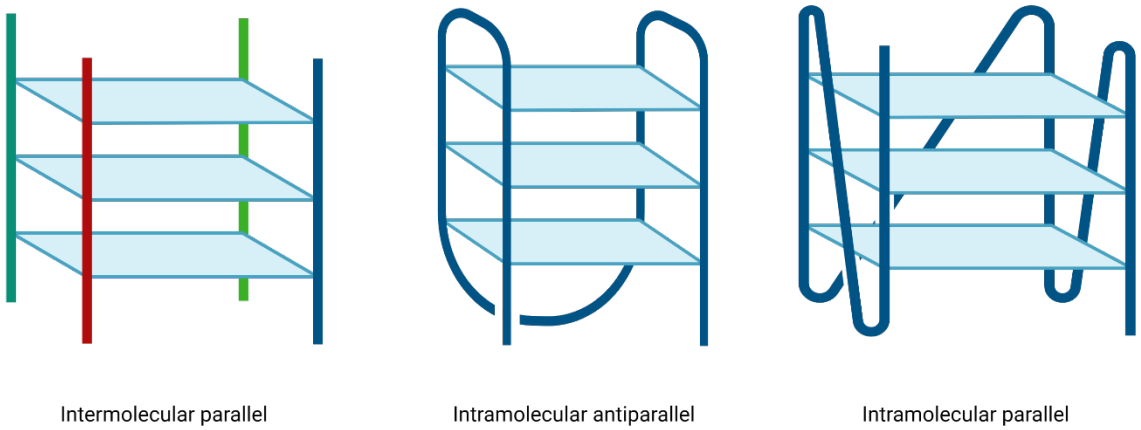

Figure 5: G-quadruplex (G4) topologies.
G4s can fold in guanine-rich regions and can vary based on the strand orientation from parallel to antiparallel and can vary with the number of participating molecules from inter- to intramolecular. Figure created with Biorender.com.

1.2.2 General characteristics of G-quadruplex

The folding potential and location of G4s are conserved in most species and their number has increased during evolution from lower to higher organisms [149–151]. G4s are not randomly distributed across the genome, highlighting their potential as functional elements [152]. G4s are enriched at telomeres, promoters, and splicing sites [152–154].
Putative G-quadruplex sequences (PQS) are based on computational prediction using a consensus motif [155]. However, they neglect non-conical long loop structures and lack information on whether they fold under physiological conditions [155,156]. High-throughput sequencing has identified experimentally observed G4s in all organisms sequenced to date, e.g. 434,272 G4s in humans and 797,789 G4s in mice [155]. The abundance of G4s varies dynamically depending on the cell cycle or cell type, making it pivotal to regulate the folding and unfolding of G4s [157–159].

The dynamic folding and unfolding of G4s is tightly regulated by G4 binding proteins, stabilizing proteins, and unwinding proteins/ helicases [160]. Human nucleolin is an example of an RNA G4 stabilizing protein involved in chromatin decondensation, transcription, translation and cell proliferation [157,161]. An example of a DNA G4 binding protein is the human Myc-associated zinc-finger protein (MAZ), which functions as a transcriptional

regulator [157,162]. Fanconi anemia complementation group J helicase (FANCJ) resolves G4s during DNA replication with the assistance of DEAH-box helicase 36 (DHX36), which promotes the bypass of the replication factors [163]. The two helicases have partially redundant functions to ensure the robustness of the unwinding process [163]. Misregulation of G4 folding and unwinding has severe consequences, for example defects in the G4 unwinding helicases are associated with diseases such as Werner and Bloom syndromes [164]. Werner´s syndrome leads to premature aging and a high risk of cancer, and Bloom´s syndrome to dwarfism, immunodeficiency and several types of cancer [165-167]. Both helicases can unwind DNA G4s *in vitro* [168,169]. The diseases share mutations in the RQC (RecQ C-terminal domain), the G4 DNA binding domain [168]. The genomic instability in the absence of the helicases leads to the early cancer development [168].

Thus misregulation in the un/-folding and localization of G4s promotes their biologically significant role in the disease development [170]. This led to the research interest in synthetic compounds that interact with G4s and serve as a tool to regulate G4s and study their function in detail [171]. Much attention has been focused on the characterization and synthesis of G4 ligands, and more than 2000 G4 stabilizing ligands have been described [172,173]. These small chemical compounds often share common features such as an aromatic core [171]. The aromatic core allows for π-π stacking with the G-tetrads [171]. The binding affinity of the G4/ligand complex, measured by the dissociation constant K_D, is a pivotal parameter in the ligand synthesis [171]. The K_D is in the µM range for most of the ligands [171].

G4 ligands have become an interesting target in cancer therapy, because several oncogene promoters are G4-rich, such as KRAS, one of the most mutated oncogenes, and the c-Myc oncogene [174–177]. C-Myc overexpression has a poor prognosis in cancer therapy and G4 stabilization has been shown to repress the transcription [178–181]. CX-5461 is a G4 ligand tested in clinical trials with breast cancer 1/2 (*BRAC1/2*)-deficient tumors [182]. CX-5461 was shown to block replication forks and cause DNA damage [182]. Failure of the BRCA and non-homologous end joining (NHEJ) pathways to repair the DNA damage led to the selective lethality in the *BRAC1/2*-deficient tumors [182].

One of the well-known and established ligands is pyridostatin (PDS). PDS is widely used due to its high specificity and affinity for G4s (K_D 490 nm) and thermal stability [183–185]. The aromatic ring of PDS matches with the G-tetrad planes and enhances the π-π stacking, and thus achieving the specificity for G4s [183]. PDS has been used in combination with other methods and technologies, for example to visualize G4 formation in human cells and in next-generation experiments to map G4s in the human genome [155,156,158,183]. PDS induced polymerase stalling and decreased the proliferation of several cancer cell lines through DNA damage-induced cell cycle arrest [186]. Due to its outstanding molecular characteristics and broad application in the G4 field, PDS was also used in this study.

1.2.3 Existence of G-quadruplexes *in vivo*

In silico predictions using the G4 consensus motif revealed PQS in functional elements in the genome, and G4s have been shown to fold *in vitro* [136,187,188]. Whether they fold *in vivo* has been actively debated in the past, but experimental evidence has established their existence *in vivo* and revealed their functional roles [133,189–191].

First, the presence of helicases indirectly demonstrates the need for of the cell to regulate and resolve G4 formation (see Chapter 1.2.2). Second, the aforementioned conservation of G4s between organisms and their enrichment at functional sites in the genome demonstrates their favorable biological role in evolution [133,149]. The first experimental evidence for G4s was the visualization by immunofluorescence with the telomeric G4-specific single-chain antibody fragments Sty3 and Sty49 in the ciliate *Stylonychia lemnae* [192]. Later, G4s could also be visualized in fixed human cells with the development of the single-chain structure-specific antibody BG4 [158]. Treatment with PDS increased the BG4 signal, whereas treatment with DNase 1 abolished the signal, and thus clearly demonstrating G4 formation *in vivo* [158]. The development of a fluorescent G4-specific probe (SiR-PyPDS) allowed the real-time detection of G4s in living cells [193]. This technique revealed the fluctuation of folding and unfolding as well as cell cycle dependent G4 formation [193]. Thus previous hypotheses of this dynamic process were experimentally confirmed in living cells [193].

BG4 was used to develop a G4 genome-wide chromatin immunoprecipitation-DNA sequencing (ChIP-Seq) method [189]. This was the first approach to map G4s genome-wide in human cells [189]. Thus, *in silico* predictions of the G4 locations were confirmed and G4 landscapes of twelve different species were generated by G4-seq (a polymerase stop assay) [155]. These data showed that experimentally observed G4s were enriched, for example, in promoters, suggesting their role as functional elements [155]. The G4 landscape of different breast tumors revealed differentially enriched G4s regions [194]. These regions were associated with the promoters of highly transcribed genes [194]. Differences in the differentially enriched G4s correlated with distinct transcription factor programs [194]. These data clearly demonstrated the functional role of G4s as hubs for transcription factors and their role as biomarkers and drug targets in cancer therapy [194].

1.2.4 Biological functions of G-quadruplexes

Several experiments have shown that folded G4 structures have both positive and negative effects on various cellular functions [152,191,195,196]. In the following, I will briefly describe the current knowledge on the biological relevance of DNA G4s for (1) telomeres, (2) replication, (3) transcription, and (4) genome stability.

(1) The highest number of predicted G4s is found at telomeres (TTAGGG repeats) [197,198]. At telomeres, G4s are thought to act as a capping structure to protect against degradation by nucleases, thus contributing to telomere maintenance (Figure 6) [152,199,200]. G4s at telomeres affect the telomerase binding and activity and putatively act as a negative regulator of telomerase elongation [201]. G4 formation at telomeres has been shown to contribute to the organization of telomeres to the nuclear scaffold, called tethering, in ciliates [202,203].

(2) Approximately 90% of human replication origins contain PQS [204–206]. During replication, the DNA double helix is transiently single-stranded, allowing G4s to fold [207]. G4 formation during replication causes stalling of the DNA polymerase and thus the replication fork to stall (Figure 6) [207,208]. Helicases such as FANCJ resolve G4s during replication or single-strand DNA binding proteins such as replication protein A coat the lagging strand and unfold G4s [209,210]. *In vivo* evidence is lacking whether the impact of the

G4 formation on the leading or lagging strand is greater [207]. Due to the discontinuous nature of the lagging strand, it is hypothesized to be more accessible for G4 formation [211].

(3) *In silico* analysis revealed that G4 motifs are enriched in promoters of oncogenes and regulatory genes, whereas they are underrepresented in housekeeping genes and tumor suppressor genes [133,212,213]. G4s have been implicated as transcriptional repressors by inhibiting the polymerase progression and leading to transcription termination (Figure 6) [152,214,215]. This `roadblock´ model was supported by the finding that G4 stabilization of the predicted G4 in the c-Myc oncogene led to its downregulation [179,216]. The model was further supported by follow-up experiments on other G4 formations in oncogenes such as c-KIT [217]. These studies relied mainly on ligands and *in vitro* data, neglecting endogenous gene expression [216]. Genome-wide experiments such as BG4 ChIP-Seq have shown that G4s are enriched at promoters of highly transcribed genes and thus may function as transcriptional enhancers rather than repressors (Figure 6) [194,216,218,219]. How G4 formation might affect transcription initiation could be by facilitating transcription factor binding and thus serving as a `hub´ for several transcription factors such as the transcription factor E2F4 [196]. Alternatively, G4 formation could also contribute to activate gene expression via guanine oxidation [216]. G4s in promoters are highly susceptible to guanine oxidation by reactive oxygen species, which can lead to direct gene activation [220,221]. In summary, G4s at promoters are a key regulatory element for transcription [216].

(4) Uncontrolled G4 folding and stabilization poses a risk of genome instability, and G4 motifs overlap with DNA double-strand break sites [133,222]. G4s challenge genome stability by stalling the replication fork, altering transcription, and inducing mutations [209,222–226]. The correct unfolding is regulated by helicases, thus maintaining genome stability [227]. However, in the absence of helicases G4 formation challenges genome stability [191,228]. At telomeres, for example, mutation of the G4-resolving helicase regulator of telomere elongation helicase 1 (RTEL1) leads to a “fragile telomere” phenotype, a replication stress-induced break formation [203,229–231]. The G4s sites are hotspots for DNA breakage, leading to deletions and other chromosome rearrangements [232–234]. Despite of the role of G4s in contributing to DNA damage, they can also stimulate DNA repair pathways [228,235].

It is hypothesized that G4 formation caused by replication fork stalling are processed by homologous recombination to restart replication [228,236,237]. This is supported by the finding that homologous recombination factors such as exonuclease 1 are involved in the binding and unwinding of G4s [228,238].

In summary, G4s play a role in diverse biological processes and whether their effect is positive or negative depends largely on the control of their folding and unwinding.

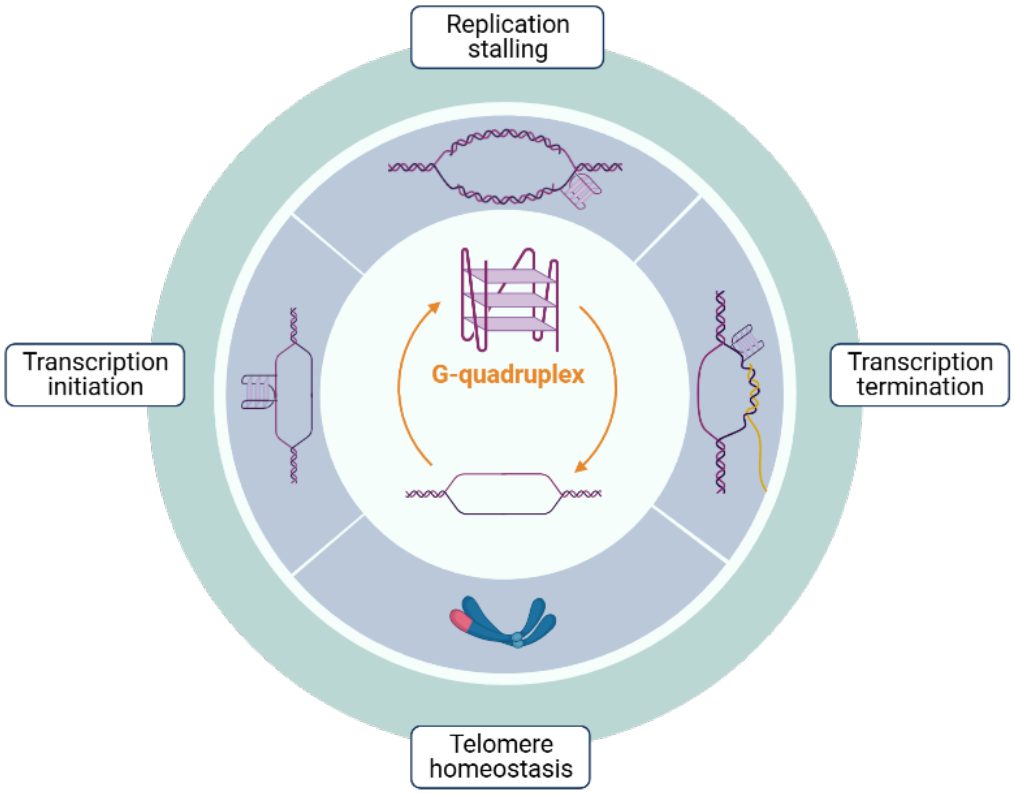

Figure 6: Biological relevance of G-quadruplexes (G4s).
G4s can influence a variety of biological processes: G4s can cause the stalling of the replication fork, maintain telomere homeostasis, and can cause the initiation and termination of the transcription. The figure was created with Biorender.com.

1.2.5 Immune system and G-quadruplexes and consequences of G4 stabilization

G4 stabilization is used as a target in cancer therapy [182,239]. First of all, it reduces the accessibility to telomerase [239,240]. Upregulated telomerase activity, which allows replication without telomere shortening, is a problem in the majority of cancer cells [241]. Second, G4 stabilization challenges the genome stability (see also Chapter 1.2.4) and could thus contribute to increased apoptosis rates and autophagy in cancer cells [239,242,243]. Finally, G4s targeted in the promoter of oncogenes such as c-Myc reduce the expression of oncogenes (see also Chapter 1.2.4) [179]. Consistent with this, G4 ligand treatment was shown to reduce the pancreatic tumor cell growth in xenografts [244].

A hallmark of cancer is prolonged inflammation [245]. Whether it contributes to tumor initiation or to its growth is largely context dependent [246]. Nevertheless, as tumors proliferate, the immune landscape in the tumor microenvironment changes [246]. The tumor microenvironment alters the myeloid cells into an immunosuppressive state, e.g. by secreting immunosuppressive mediators such as IL-10 [246,247]. In this context, tumor-associated macrophages (TAMs) are discussed as a link between cancer and inflammation [248]. TAMs express high levels of IL-10 and low levels of IL-12 [249–252]. The missing IL-12 production results in a lack of NK cell activation and thus facilitates tumor progression [251,252]. TAMs produce programmed death ligand-1 (PD-L1), and binding to its receptor PD-1 can cause T cell apoptosis, further contributing to immune suppression [252,253]. It is therefore not surprising that the presence of TAMs indicates poor clinical outcome in cancer treatment [252,254].

However, experimental evidence is lacking on how the immune system is affected by the G4 ligand treatment. It has been shown that prolonged chemical G4 stabilization induced micronuclei formation in cancer cells and that this DNA damage activated the cytoplasmic STING (stimulator of interferon response cGAMP interactor 1) [255]. This led to an interferon β response in the cells, thus triggering an innate immune response [255]. Therefore, the data highly suggest a link between G4 ligand treatment in cancer cells and an immune system response [255].

1.3 Aim of this thesis

Diseases caused by bacteria and the limit for therapeutical approaches, such as antibiotic resistance, can be life-threatening. Targeting G4s is a promising novel therapeutic strategy against cancer such as breast cancer, but apart from the above-mentioned biological functions of G4s, little is known about their relevance and role in immune cells. In addition, TAMs play an important role in cancer proliferation, but experimental evidence on how and when G4s are formed in macrophages is lacking. As G4s are known to positively and negatively impact cellular functions, I predict that it may modulate the host defense against bacteria in macrophages.

The primary aim of this thesis is to shed light on the function of G4 formation in mouse macrophages and how it impacts the immune response to bacterial infection. It is important to understand the molecular mechanisms by which G4s affect the immune response in order to target and modify it in the future in therapeutical approaches such as cancer treatment. As part of this thesis, I investigated how G4s influence the immune response to bacterial infection in macrophages.

2 Material and Methods

2.1 Methodology

2.1.1 Bacteria cell culture

All *E. coli* strains were grown on LB agar plates at 37°C. Single colonies were transferred to LB liquid growth medium and grown overnight at 37°C and 200 rpm agitation. All plates and media contained the appropriate antibiotic concentration (100 µg ml^{-1} ampicillin, 50 µg ml^{-1} kanamycin). OD600 was checked by a spectrophotometer. For cryo-conservation 600 µl bacterial overnight culture were mixed with 50% glycerol and stored at -80°C. For transformation 50 µl chemical-competent DH5α *E. coli* cells were thawed and 10 ng plasmid DNA were added and incubated for 30 min on ice. The heat shock was carried out at 42°C for 30 sec and the suspension was placed back on ice for 5 min. 450 µl SOC medium were added followed by incubation for 30 min at 37°C at 500 rpm agitation. The bacteria were collected by centrifugation (1 min 8000 *xg*), resuspended in 100 µl SOC medium and spread on appropriate LB agar plates. The plates were incubated overnight at 37°C.

2.1.2 Eukaryotic cell culture

iBMDMs (immortalized bone marrow-derived macrophages) were received from the Abdullah laboratory and originally isolated from femur and tibiae and immortalized by SV40 virus transformation [256]. The iBMDMs were cultivated in Dulbecco´s modified Eagle´s medium (DMEM) supplemented with 10% (v/v) fetal bovine serum (FBS) and 100 U ml^{-1} Penicillin-Streptomycin (PenStrep) and for the RAW-Blue™ NF-kB SEAP reporter cells the medium was supplemented in addition with 100 µg ml^{-1} zeocin and 100 µg ml^{-1} normocin and all cells were grown at 37°C and 5% CO_2. Confluent cells (iBMDMs) were passaged by washing with PBS and dethatched by addition of Trypsin-EDTA. The reaction was stopped by the addition of new media and cells were seeded in new dishes and if required counted by using a hemocytometer. For cryo-conservation a cell suspension was centrifuged (200 *xg*, 5 min) and resuspended in freezing medium (DMEM plus 10% FBS plus 10% DMSO) to a final concentration of $3 \cdot 10^6$ cells/ml and every aliquot contained 1 ml cell suspension. The stocks were frozen in the Mr. Frosty ™ freezing container at -80°C for one week and long-term stored at -150°C. The cells were

kept for a maximum of 20 passages before a new vial was thawed. The stocks were thawed at 37°C and added to a 15 ml reaction tube containing DMEM. The cells were centrifuged for 5 min at 200 *xg* and the pellet was resuspended in 10 ml DMEM, transferred to a 10 cm cell culture petri dish and incubated at 37°C and 5% CO_2. For the RAW-Blue™ NF-kB SEAP reporter cells the first passage after thawing was performed without selective antibiotics (zeocin and normocin) and cells were passaged at 80% confluency using a cell scraper (not trypsin).

2.1.3 Treatment of macrophages

If not indicated otherwise the cells were seeded the day before and treated the next morning with 25 µM PDS and/ or 200 ng/ml LPS or H_2O_2 for 4 h or with nigericin for 1 h at 37°C with 5% CO_2.

2.1.4 AlamarBlue™ assay

The metabolic activity after PDS and LPS was performed by using the AlamarBlue™ assay. The iBMDMs were seeded ($6 \cdot 10^4$ cells per well) in triplicate in a black bottom clear 96 well plate and treated the next morning. Afterwards 10 µl of 10% AlamarBlue™ solution was added to a final volume of 100 µl and incubated at 37°C for 3 h. The Thermo Scientif™ Fluorskan™ FL plate reader was used to measure the emission at 590 nm.

2.1.5 Protein biochemistry

2.1.5.1 Protein isolation from eukaryotic cells

The cells were seeded in a six well plate ($3 \cdot 10^5$ cells per well) the evening prior to the treatment and collected using a cell scraper. The cells were collected by resuspension in 50 µl 1:6 diluted SDS loading dye supplemented with 1:1000 diluted benzonase. The samples were incubated for 5 min at RT and either processed for western blot analysis or stored at -20°C.

2.1.5.2 SDS-polyacrylamide gel electrophoresis (SDS-PAGE)

The proteins were separated according to their molecular weight by denaturing discontinuous sodium dodecyl sulphate polyacrylamide gel electrophoresis (SDS-PAGE). The 12% separating and 4% stacking gel contained 0.1% SDS and the polymerization was achieved by ammonium persulfate (1:100) and tetramethylethylendiamin (1:1000). 6x SDS loading dye was added to the samples to a final concentration of 1x, denatured for 5 min at 95°C and 20 µl protein sample were loaded per well. The run was performed at 100 V for ca. 2 h using 1x SDS running buffer.

2.1.5.3 Coomassie staining

The SDS-PAGE gel was covered with Coomassie staining solution and incubated for 1 h at RT under agitation. Afterwards destaining solution was added for 30 min under agitation and the gel was kept in distilled water.

2.1.5.4 Western blot

The SDS-PAGE gel was used for subsequent analysis by western blot. The blotting sandwich was assembled (whatman paper, nitrocellulose membrane, SDS gel and whatman paper) after all components were soaked with blotting buffer. The semi-dry blotting was adjusted to 1 h with 2 mA per cm^2 gel size. For blocking the membrane incubated for 1 h with TBS-T +5% BSA. The membrane was incubated overnight at 4°C under rotation with the according primary antibody in TBS-T +5% BSA. Three washes for 10 min with TBS-T were performed prior to incubation with the corresponding fluorescent secondary antibody (1 h at RT under rotation). Again three washes for 10 min with TBS-T were performed and subsequent detection with the BioRad Molecular Imager ChemiDOC XRS Imaging System with automatically calculated detection times was performed. In order to quantify the protein intensities ImageJ (Fiji) was used [257].

2.1.5.5 BG4 purification

The BG4 purification protocol was established in the Balasubramanian laboratory [158] and modified in the Marco Di Antonio laboratory. In short, BL21 cells containing the pSANG10-3F-BG4 plasmid were expanded overnight in 50 ml 2x TY medium supplemented with

50 mg/ml kanamycin and 1% glucose at 30°C with 200 rpm agitation. The next morning 10 ml overnight culture were used to inoculate one liter 2x TY medium and cells were grown for 24 h at 18°C with 200 rpm agitation. The culture was centrifuged (4000 *xg*, 30 min, 4°C). The pellet was resuspended in 100 ml TES buffer supplemented with protease inhibitor. Afterwards 1:5 diluted TES buffer supplemented with 20 µl benzonase and 5 mM $MgCl_2$ were added and the lysate was centrifuged (8000 *xg*, 20 min, 4°C). The supernatant was filtered (0.45 µm). For the column 3 ml cobalt resin were washed with 10 CV PBS and the cell lysate was pipetted on the column and the bead-cell lysate mixture was incubated for 30 min at 4°C in rotation. The column was washed with 3 CV wash buffer and the protein was eluted with three times 5 ml elution buffer. The elution buffer was exchanged with intracellular salt buffer and concentrated by using Amicon® Ultra-15 centrifugal filters with 10 kDa cutoff (MERCK). The purity of BG4 was checked by SDS-PAGE and Coomassie staining. The concentration was quantified by using Qubit fluorometer (ThermoFisher).

2.1.6 RNA biochemistry

2.1.6.1 RNA purification from cells and 3´RNA-Seq

The cells were seeded in a six well plate ($3 \cdot 10^5$ cells per well) the evening prior to the treatment and collected by addition of 500 µl TRIzol (Thermo Fisher Scientific) per well and followed by incubation for 5 min. 100 µl chloroform were added, vortexed and incubated for 3 min. Centrifugation (12,000 *xg*, 15 min, 4°C) was used for phase separation and the upper phase was transferred to a new tube containing one volume of isopropanol. The samples were mixed and incubated on ice for 20 min. The RNA was pelleted by centrifugation (20,000 *xg*, 10 min, 4°C), washed with 75% ethanol and dried for 5 min. The pellet was resolved in appropriate amount of ddH_2O and a Nanodrop device was used for determining the concentration. For 3´RNA-Seq the samples were processed by the Next Generation Sequencing Core Facility from the Medical Faculty in Bonn (HiSeq 2500 V4, 10 M raw reads, 1x150 bp). The Partek® Flow® Software was used for data analysis. The sequencing reads were aligned to the mm10 genome using the STAR method [258]. To check the representation of G4s in the PDS treated samples, the DNA G4

map from mouse [155] was correlated with the 3´RNA-Seq using http://yeast.genomes.nl/mouse.html (by Victor Guryev).

2.1.6.2 Reverse transcription

In order to perform reverse transcription the Quantitect RT Kit (Qiagen) was used according to the manufacturer's instructions. In brief, 500 ng RNA were mixed with 1 µl 7x gDNA wipe-out-buffer and incubated for 2 min at 42°C. Afterwards 0.5 µl reverse transcriptase, 0.5 µl primer mix and 2 µl 5x buffer were added per sample and incubated for 15 min at 42°C followed by 3 min at 95°C.

2.1.6.3 Quantitative Polymerase Chain Reaction (qPCR)

The obtained cDNA was diluted 1:20. 3 µl cDNA were mixed with 6 µl SYBR Green mastermix and 3 µl primer mix (1 µM forward and reverse primer). The qPCR was performed in technical replicates in a 96-well plate using the BioRad CFX96 RealTime System.

Step	Time	Temperature	Cycle
Initial denaturation	3 min	95°C	1x
Denaturation	15 s	95°C	
Annealing	20 s	60°C	40x
Elongation	30 s	72°C	

2.1.7 Molecular biological experiments

2.1.7.1 Fluorescent microscopy to detect G4 structures (BG4 staining)

Macrophages ($8 \cdot 10^4$) were seeded on sterile coverslips (14 mm diameter) in 24 well-plates. For fixation the cells were incubated for 5 min at RT with pre-fix solution. After two brief washes with the fix solution, the cells were fixed with fix solution for 10 min at RT. The cells were washed once with PBS and permeabilized by addition of the permeabilization solution for 3 min at RT. Next the cells were washed three times in agitation for 5 min at RT. The cells were blocked in blocking solution in agitation for 1 h at RT and afterwards incubated with 2 µg BG4 per slide in blocking buffer in agitation for 2 h at RT. Next, the cells were washed three times with wash solution in agitation each for

10 min, followed by incubation with a rabbit antibody against the FLAG epitope in blocking buffer for 1 h in agitation at RT. The cells were washed three times as described above and the cells were incubated with anti-rabbit Alexa Flour® 488 diluted in blocking buffer for 1 h at RT in agitation. The cells were washed again and the cover slips were mounted with Fluoroshield with DAPI (Sigma-Aldrich). The slides were imaged (DAPI and Alexa Fluor 488) using a Zeiss Axio observer five and at least 100 nuclei per slide/ condition were captured. For quantification of the nuclear G4 levels ImageJ (Fiji) was used [257]. The BG4 stained picture was redirected to the DAPI picture and the particles were analyzed and the integrated density divided by the area was chosen to be displayed as fold change compared to the untreated samples.

2.1.7.2 BG-flow (BG4 staining using FACS)

Instead of analyzing the G4 levels by BG4 IF, we developed in our laboratory a method to use FACS analysis to perform the BG4 staining, called BG-flow [259]. In brief, the samples are trypsinized for collection and all steps are performed in tubes. The steps are identical to BG4 IF (see 2.1.7.1) except that the cells were centrifuged (1,500 rpm, 5 min) after every step. At the end the cells were resuspended with 3 ml PBS and transferred to FACS tubes.

2.1.8 System-wide experiments

2.1.8.1 CUT&Tag

The cells were trypsinized and adjusted to $2 \cdot 10^5$ cells per condition with wash buffer. The samples were centrifuged (600 *xg*, 4 min, 4°C) and the pellet was resuspended with antibody binding buffer and centrifuged again. The pellet was resuspended in antibody binding buffer supplemented with BG4 (0.01 mg/ml) and incubated under rotation at 4°C overnight. The samples were centrifuged (600 *xg*, 4 min), washed 3x with 200 µl Dig-Wash-BSA buffer and resuspended in DIG-Wash-BSA buffer supplemented with anti-FLAG antibody and incubated for 1 h at RT under rotation. Afterwards the samples were centrifuged and washed again and the pellet was resuspended with anti-mouse antibody in Dig-Wash-BSA buffer and incubated for 1 h at RT under rotation. The samples were centrifuged and washed and the tagmentation was started by addition of the Tn5 assembly

mix (15 µl Tn5, 3.2 µl mosaic adapter A&B) diluted in DIG-Wash-BSA buffer and incubated for 1 h under rotation at RT. The samples were centrifuged, washed with Dig-Wash-BSA buffer and resuspended in 200 µl tagmentation buffer, followed by incubation at 37°C for 1 h. The tagmentation was stopped by the addition of EDTA (0.5 M), SDS (10%) and proteinase K (10 µl of 10 mg/ml). The gDNA was extracted with phenol/chloroform and quantified with Qubit. The protocol and reagents including the Tn5 were kindly provided by the Simon Elsässer laboratory [260].

2.1.8.2 ATAC-Seq

The cells ($5 \cdot 10^4$) were washed with PBS and the pellet after centrifugation (200 *xg*, 5 min) was resuspended with 50 µl ATAC lysis buffer and centrifuged (500 *xg*, 10 min, 4°C). The pellet was resuspended with 50 µl transposition reaction mix and incubated at 37°C for 30 min. The DNA was isolated using the Qiagen MinElute cleanup kit according to the manufacturer's instructions and eluted in 10 µl elution buffer. The samples were sequenced at the Cologne Center for Genomics (50 M reads, paired end 2x150 bp). Partek Flow® was used for the analysis and the reads were aligned to the mm10 genome using Bowtie2 [261].

In cooperation with Jasper Spitzer the further ATAC-Seq analysis was done. The ATAC reads were trimmed using cutadapt (V1.18) [262] and aligned to the mm10 reference genome using bowtie2 (V2.4.5) [261]. Reads were deduplicated using Picard (V2.26.10) (https://github.com/broadinstitute/picard) and sorted using samtools (V1.14) [263]. Sorted and filtered reads were used for peak calling with macs2 (V2.2.7.1) [264]. Consensus peaks per condition were created using IDR (v2.0.4.2) [265]. Motif enrichment for TF binding was performed using HOMER (V4.11) [266]. Differentially accessible regions were called using diffbind (V3.10) [267] and correlated to 3´RNA-Seq data using Pearson correlation. G4 motif discovery followed the published consensus motif [137], using the Biostrings R package (V2.68.1) [268] to identify peaks with motifs based on the consensus peaks. For peak motif distribution, only the 1000 most common motifs per condition were considered. Read distribution around peaks was visualized using deeptools (V3.5.2) [269], computeMatrix and, plotHeatmap. Visualizations were created using R [270] and the tidyverse packages [271].

2.1.8.3 NF-kB ChIP Seq

The cells ($1 \cdot 10^7$) were seeded in a 15 cm petri dish. Cross-linking was performed by adding 0.5 ml 30% formaldehyde (vol/vol) to 15.5 ml growth medium and the cells incubated for 10 min at RT with 30 rpm shaking. Addition of 0.12 M glycine and incubation for 10 min was used to stop the cross-linking reaction. The cells were washed twice with 10 ml cold PBS and scraped for collection. The cells were pelleted (300 *xg*, 5 min, 4°C), washed with PBS and centrifuged again. The cell pellet was resuspended in 0.8 ml hypotonic buffer (Chromatrap) and incubated on ice for 10 min. The mixture was centrifuged (5,000 *xg*, 5 min, 4°C) and resuspended in 1 ml lysis buffer (Chromatrap) and incubated for 10 min. The sonication was performed using a Covaris connected to a cooling system. The sonication mode was 20 cycles (30 sec on/ 30 sec off). The DNA was isolated using the MinElute kit (Qiagen) according to the manufacturer´s instructions and the sample was eluted with 20 µl and the fragment size distribution was checked on a 2% (wt/vol) agarose gel.

2 µg antibody were added per sample containing 5 µg chromatin (except for the input) and incubated at 4°C overnight under rotation. The next morning, 80 µl Dynabeads-Protein G washed with washing buffer were added per sample and incubated at 4°C for 2 h under rotation. The beads were washed three times with washing buffer using a metal stand on a magnet. The DNA was eluted by the addition of 75 µl TE buffer supplemented with 2 µl proteinase K and incubated at 65°C for 3 h and 16 h at 4°C. The DNA was isolated using the MinElute kit and the final elution volume was 25 µl. The sequencing was performed at the Cologne center for genomics (paired end, 2x 150 bp, 50 M reads).

2.1.9 Macrophage specific experiments

2.1.9.1 Maturation marker (CD40 and CD80) staining

The cells were trypsinized and adjusted to $1 \cdot 10^6$ cells/ml and collected by centrifugation. The cells were washed once with PBS, centrifuged and resuspended in FACS buffer containing the appropriate antibodies (MTG+MTDR, MTG+MitoSox, CD40, CD80) and incubated for 30 min on ice or for 30 min at 37°C for the mitochondrial marker (MTG, MTDR, MitoSox). The cells were centrifuged and washed again with FACS buffer and

proceeded for Flow cytometry analysis (Canto I) and appropriate single stains and FMOs were included. The FlowJo (FlowJo LLC) software was used for the analysis.

2.1.9.2 Phagocytosis uptake assay

The cells were trypsinized and adjusted to $2 \cdot 10^6$ cells/ml. The heat-inactivated *Salmonella* mCherry strain (provided by the Abdullah laboratory) was adjusted to $4 \cdot 10^7$ CFU/ml. The medium containing the bacteria was supplemented with 50 µl/ml normal mouse serum (NMS) (provided by the Abdullah laboratory) or as control only medium and incubated for 15 min at 37°C. Afterwards 0.5 ml cells were mixed with 0.5 ml bacteria or medium and incubated for 1 h in a tube rotator at 37°C. The cells were collected by centrifugation (1,500 rpm, 5 min), washed once with FACS buffer and resuspended in FACS buffer containing the appropriate antibodies (L/D, CD11b, F4/80) and incubated for 30 min on ice. The cells were centrifuged and washed again with FACS buffer and proceeded for Flow cytometry analysis (Fortessa II). The FlowJo (FlowJo LLC) software was used for analysis.

2.1.9.3 Phagocytosis killing assay

The cells ($5 \cdot 10^5$) were seeded in medium without antibiotics and infected with 50 µl *Listeria* (MOI 5). The medium was replaced with DMEM supplemented with gentamycin (100 µg/ml) after 30 min. After 1 h and after 4 h the cells were washed twice with PBS and incubated with 500 µl lysis buffer for 5 min. Afterwards the lysate was diluted (1:10 dilution for 5 times) with distilled water and 20 µl dilution was plated on BHI plates. The plates incubated overnight at 37°C and the colonies were counted the next morning and the CFU/ml was calculated.

2.1.9.4 Procartaplex assay

The supernatants of treated iBMDMs were collected in triplicates. The Procartaplex 9 Plex assay (Thermo Fisher Scientific) was performed according the manufacturer´s instructions, the MFI was measured and the concentrations were calculated by the Thermo Fisher Scientific software based on the standard curves.

2.1.9.5 RAW-Blue cell QUANTI-Blue assay (Invivogen)

The RAW-Blue NF-kB SEAP reporter cell line is commercially available. They are derived from RAW 264.7 cells and express a secreted embryonic alkaline phosphatase (SEAP) upon NF-kB activation. The SEAP secretion was detected by using the QUANTI-Blue assay according to the manufacturer's instructions. In brief, $1 \cdot 10^5$ cells were per well seeded in 96-well plate using DMEM without selective antibiotics. 10 µl of RAW-Blue cell supernatant was mixed with 190 µl QUANTI-Blue solution and incubated for 6 h at 37°C. The solution was mixed and SEAP levels were measured with a SpectraMax M5e spectrophotometer at 630 nm.

2.1.9.6 HTRF IL-1beta

The supernatants of treated iBMDMs were collected in triplicates and the kit was used according to the manufacturer's instructions. In brief, 8 µl sample, 8 µl medium, 4 µl antibody mix and 16 µl standard were mixed and incubated overnight at RT in the dark. A SpectraMax M5e plate reader was used (665 and 620 nm).

3 Results

3.1 G4 formation in mouse macrophages can be stabilized by PDS

G4s play a role in variety of biological processes such as transcription [272–274] and replication [275] and have recently been discussed as a target in cancer therapy [239]. Since tumor development can be influenced by immune cells [276], there is an urgent need to analyze G4 folding and their role in immune cells. Among the immune cells, macrophages are widely used model systems for phagocytosis or oxidative burst, for example [277].

The first research question was to address whether G4s can form in mouse macrophages. In order to monitor G4 levels via immunofluorescence, the structure-specific single chain antibody BG4 was used [158]. As indicated by a low but specific punctate nuclear signal, G4s were detected in the nucleus of untreated iBMDMs (Figure 7A). Although G4s can fold in the cytoplasm, the cytoplasmic signal was not detectable and thus neglected for this study.

As a tool to study G4-mediated mechanisms, G4s can be stabilized by G4 specific ligands [183]. Due to its high specificity among the G4 ligands, the small molecule PDS was chosen [183]. Since G4 stabilization poses a challenge for genome stability that can cause DNA damage [133,186,222], western blot was performed after PDS treatment to analyze the γH2AX levels, a DNA double strand marker. It was shown that four hours incubation with 25 µM PDS did not lead to DNA double-strand breaks (Figure 7D). Unlike the positive control H_2O_2, which lead to γH2AX foci after four hours incubation with 6 mM H_2O_2 (Figure 7D). Macrophages supply a lot of energy for phagocytosis and production of antimicrobial compounds such as ROS [278,279], thus the mitochondrial fitness and cellular metabolism of macrophages is sensitive and could be compromised by ligand treatment. An Alamarblue assay was performed to monitor the metabolic activity of iBMDMs treated with PDS. The assay confirmed that iBMDMs were metabolically active after four hours treatment with 25 µM PDS (Supplementary figure 2). Using FACS analysis with the specific mitochondrial tracker (MitoTracker™ Green, MitoTracker™ Deep Red, MitoSOX™), it was demonstrated that four hours ligand treatment did not compromise the mitochondrial fitness of iBMDMs (Supplementary figure 2).

Four hours treatment with 25 µM PDS significantly increased the number of BG4 foci by 1.5 fold compared to untreated (Figure 7A-B). Thus the iBMDMs are sensitive for PDS treatment. Since four hours treatment with 25 µM PDS increased the nuclear BG4 level without impacting the mitochondrial and metabolic activity, this concentration and treatment time was used for all subsequent studies. G4s can impact cellular functions positively and negatively and thus it was investigated next how it affects macrophages function during fighting bacterial infections. Lipopolysaccharide (LPS) treatment (200 ng/ml) for four hours was used to mimic a bacterial infection by inducing a TLR4 response [280]. Nuclear BG4 levels did not change after LPS treatment compared to untreated (Figure 7B). Interestingly, the four hours co-treatment with PDS and LPS did not reveal any significant differences in the nuclear BG4 foci level compared to the untreated cells (Figure 7B). To validate the G4 levels with a different technique, we established a new method using flow cytometry, called BG-flow [259]. The BG-flow experiments showed as well a significant 1.5 fold nuclear and cytoplasmic BG4 level increase for the PDS treated cells and similar BG4 levels in the PDS and LPS co-treated cells like the untreated cells (Figure 7C). Thus the results obtained by immunofluorescence for the nuclear BG4 levels were confirmed (Figure 7C).

Next, it was investigated whether G4s can impact macrophage function when they are stabilized prior to the LPS treatment. In this time course experiment pre-treatment of macrophages with 25 µM PDS for four hours followed by the addition of LPS for four hours was applied (total treatment time for eight hours). The hypothesis was that PDS pre-treatment would increase the nuclear BG4 level again, unlike simultaneous treatment of PDS and LPS. Indeed, pre-treatment of PDS followed by LPS treatment significantly increased the nuclear BG4 level by 1.5 fold (Figure 7B). Vice versa, pre-treatment of LPS for four hours followed by the addition of PDS for 4 hours, was hypothesized to unvarying G4 levels. It was confirmed that LPS pre-treatment did not increase the nuclear BG4 level compared to untreated (Figure 7B). In the following the PDS and LPS co-treatment (for four hours) was used for further experiments. Overall, LPS treatment did not alter the nuclear BG4 level, but it demolished the G4 level increase by PDS in the double treatment without decreasing the total BG4 level.

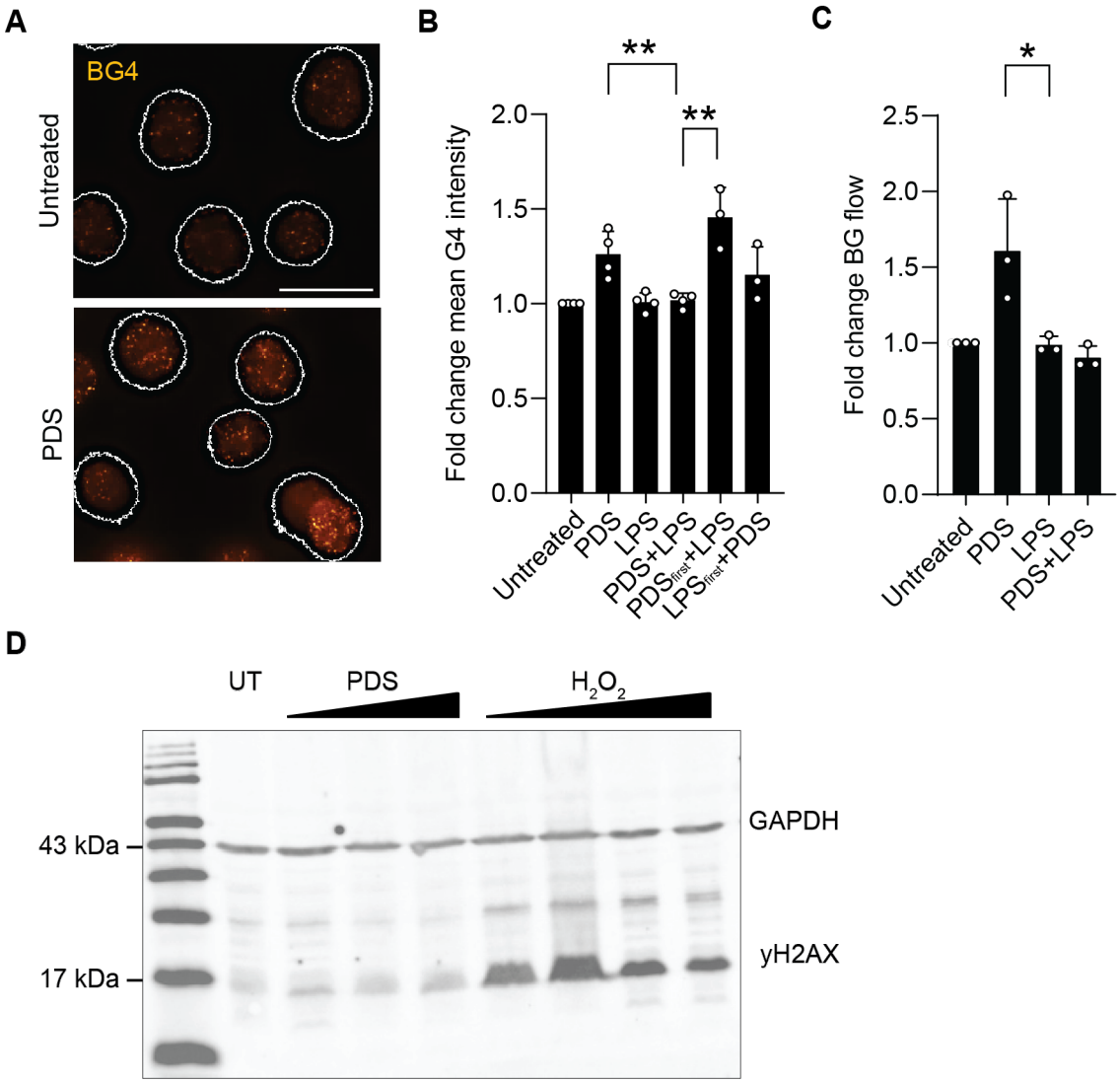

Figure 7: G-quadruplex (G4) quantification in mouse macrophages.
A) iBMDMs (immortalized bone marrow derived macrophages) were treated with PDS (25 µM) and/or LPS (200 ng/ml) for four hours or with PDS first and then with LPS (total eight hours when indicated with "first") and vice versa. Immunofluorescence showing orange BG4 foci in the nucleus (white line are the boundary of the DAPI signal). The scale bar represents 10 µm. B) The graph displays the nuclear BG4 quantification. At least 100 nuclei were counted per condition and four biological replicates are shown. C) The immunofluorescence data were validated by BG4 flow cytometry (BG-flow) and normalized over the untreated sample. The mean fluorescence intensity was analyzed of the BG4 signal (FL1 channel). Three biological replicates are shown. D) Western blot analysis of γH2AX after PDS (25, 50 and 100 µM) and H_2O_2 treatment (1, 3, 6 and 12 mM) for four hours and GAPDH as loading control. Example of one western blot out three replicates is shown. UT=Untreated; p-value≤0.05=*; p-value≤0.01=** (unpaired t-test); scatter plot mean with SD.

3.2 G4 stabilization by PDS does not alter the phagocytosis behavior but slightly decreases the expression of maturation markers

Since the total G4 level was not affected when macrophages are activated by LPS, the next step was to investigate the role of G4s in phagocytosis. Macrophages engulf microorganisms such as pathogenic bacteria and can trigger an adaptive immune response by presenting antigens [281]. Therefore, it was evaluated whether G4 stabilization by PDS can influence the phagocytic uptake and lysis/ killing of bacteria. To analyze the phagocytic uptake rate, pre-treated iBMDMs with PDS and/ or LPS were incubated with a *Salmonella* strain labelled with the mCherry reporter gene. The mCherry signal was detected by flow cytometry and reflected the engulfed bacterial rate. The geometric mean of the mean fluorescence intensity was around 3,000 for all conditions (Figure 8A). Thus pre-treatment with PDS and/ or LPS did not alter significantly the phagocytic uptake rate of mCherry labelled *Salmonella* (Figure 8A). Next, the phagocytotic killing of PDS pre-treated iBMDMs was investigated using *Listeria* infection. As a positive control, iBMDMs were pre-treated with IFNγ (100 ng/ml for 20 hours). The infection was followed by macrophages lysis and plating of the lysate to count the remaining *Listeria* colonies. The *Listeria* colony formation reflected the iBMDMs phagocytotic lysis/ killing behavior. PDS pre-treatment did not change the *Listeria* colony formation compared to untreated, for untreated and PDS the colony formation is around ten (Figure 8B). IFNγ and PDS plus IFNγ pre-treatment slightly decreased (not significant) the *Listeria* colony formation to lower than five, indicating increased phagocytotic killing behavior of the iBMDMs (Figure 8B). Conclusively, G4 stabilization does not affect the phagocytic behavior of macrophages.

The macrophages response to pathogenic microorganisms includes the overexpression of maturation markers such as CD40 and CD80 to orchestrate the inflammatory process such as T cell activation [89]. Thus, the next step was to investigate if G4 stabilization can impact the maturation marker expression. The expression of CD40 and CD80 was analyzed by flow cytometry analysis. The iBMDMs were pre-treated with PDS and/ or LPS for four hours. Pre-treatment with LPS increased (not significantly) the maturation marker expression of CD40 and CD80 1.5 fold (Figure 8C-D). Pre-treatment with PDS had no effect on the maturation marker expression compared to untreated (Figure 8C-D).

Whereas G4 stabilization decreased the expression in the co-treatment with LPS and PDS compared to LPS treatment alone (Figure 8C-D). To conclude, G4 stabilization by PDS does not affect the maturation marker expression of CD40 and CD80, but it inhibits the overexpression of CD40 and CD80 in the co-treatment with LPS.

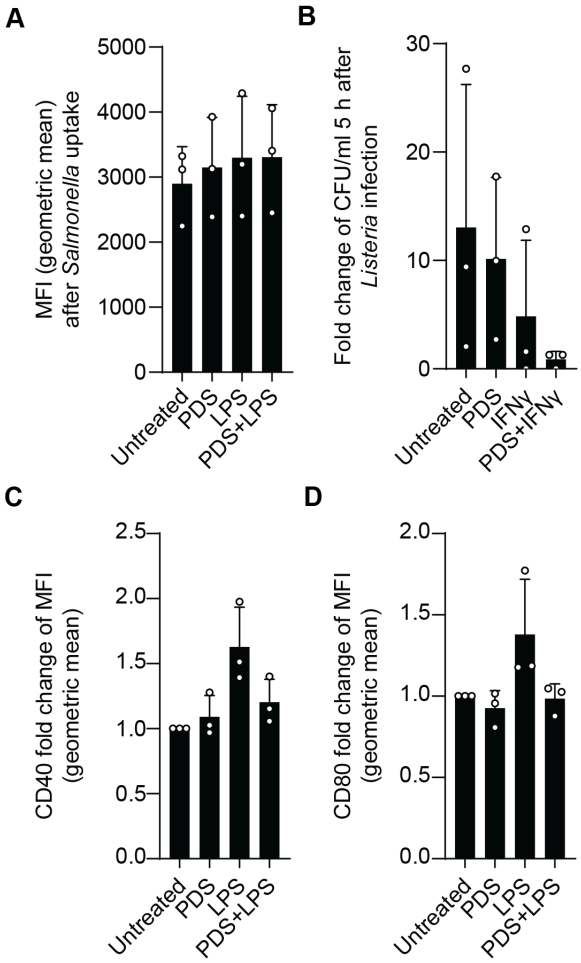

Figure 8: Phagocytosis behavior and maturation marker expression after G-quadruplex stabilization.
G4 formation does not impair phagocytosis and slightly decreases the maturation marker expression. iBMDMs (immortalized bone marrow derived macrophages) were treated with PDS (25 µM) and LPS (200 ng/ml) for four hours. A) mCherry labelled heat-inactivated Salmonella ($2 \cdot 10^8$ CFU/ml) were incubated for two hours with iBMDMs and FACS analysis was performed considering Cd11b+ and alive cells. B) iBMDMs were treated with 100 ng/ml IFNγ for 20 hours and infected for 5 h with Listeria (MOI 5). The cells were lysed and bacterial colonies were counted the next day. C-D) FACS-analysis of the activation marker CD40 and CD80 on alive cells. Three biological replicates are shown and data points are not significant (unpaired t-test); scatter plot mean with SD; MFI=mean fluorescence intensity. The experiments were performed in cooperation with Jennifer Szlapa and Konstantinos Symeonidis (Abdullah laboratory).

3.3 G4 formation reduces the cytokine-mediated immune response to bacteria

The observation that G4 stabilization inhibits the LPS-mediated overexpression of maturation markers, arose the question whether G4 stabilization leads to transcriptome-wide changes after co-treatment with LPS in macrophages. In order to analyze transcriptomic changes, iBMDMs were treated with PDS and/ or LPS, RNA was isolated and followed by 3´RNA-Seq. First of all, the 3´RNA-Seq analysis focused on overall changes (Figure 9), and later specifically analyzed the LPS-mediated cytokine immune response (Figure 10).

The highest proportion of down-regulated genes (2662 genes, 63.5%) was observed in the co-treatment of PDS and LPS, only 764 genes (49.5%) were significantly up-regulated (Figure 9A-B). Treatment with LPS resulted in up-regulation of 491 genes (31.8%) and downregulation of 968 genes (23.1%). The least transcriptomic changes were caused by PDS treatment: 149 genes (9.7%) were up-regulated and 35 genes (0.8%) were down-regulated (Figure 9A-B). The GO annotation overview shows that the PDS and LPS co-treatment led to the up-regulation of genes with kinase activity, whereas genes of the type I interferon-mediated signaling pathway were down-regulated (Figure 9C). The strong down-regulation in the PDS and LPS co-treatment is further illustrated by the volcano plots (Figure 9D-F). To exemplify the regulation of the cytokines, interleukin-1 beta (IL-1 beta) is highlighted: it is one of the highly up-regulated genes after LPS stimulation and is down-regulated in the PDS and LPS co-treatment (Figure 9E-F). Early growth response protein 1 (Egr1) is up-regulated in the PDS treatment (Figure 9D) and is known to have putative quadruplex sequences [282]. The up-regulated and down-regulated genes in the PDS treatment correlated significantly ($p<0.001$) with experimental mapped DNA G4s [155]. CC-chemokine ligand 3 (Ccl3), interferon gamma-induced protein 10 (IP10) and NF-κB1 and 2 are involved in the immune response [283–285] and up-regulated in the LPS treated samples (Figure 9E). Ccl3 and NF-κB inhibitor zeta (NF-κBIZ) are down-regulated in the PDS and LPS co-treatment (Figure 9F). Thus, the PDS and LPS treatments showed distinct patterns of the differentially expressed genes (DEGs).

A

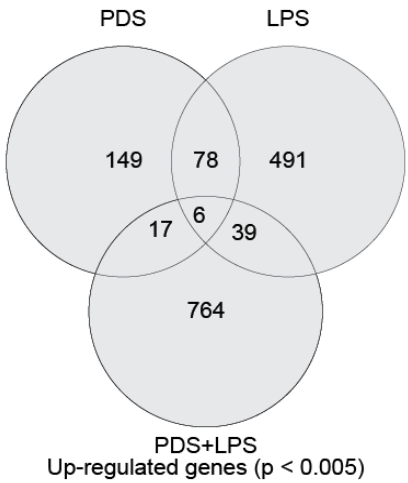

B

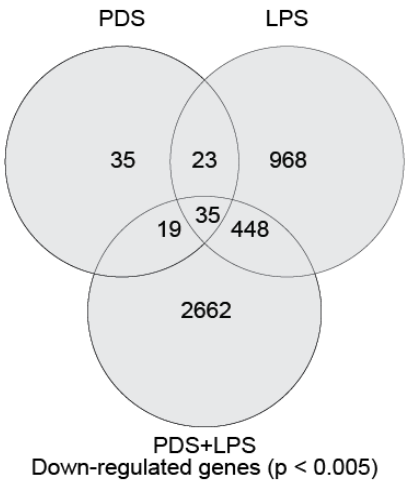

C

Condition	GO annotation
PDS up	Inflammatory response
	Defense response
	Signal transduction
LPS up	Regulation of response to stimulus
	Response to stress
	Immune system process
PDS+LPS up	Positive regulation of transferase activity
	Positive regulation of kinase activity
	Regulation of leukocyte chemotaxis
PDS down	Regulation of cytokine production
LPS down	Organic substance metabolic process
	Cellular metabolic process
	Histone H3-K4 methylation
PDS+LPS down	Regulation of intracellular estrogen receptor signaling pathway
	Positive regulation of lysosomal membrane permeability
	Regulation of lysosomal membrane permeability
	Positive regulation of protein complex assembly
	Negative regulation of type I interferon-mediated signaling pathway

D E F

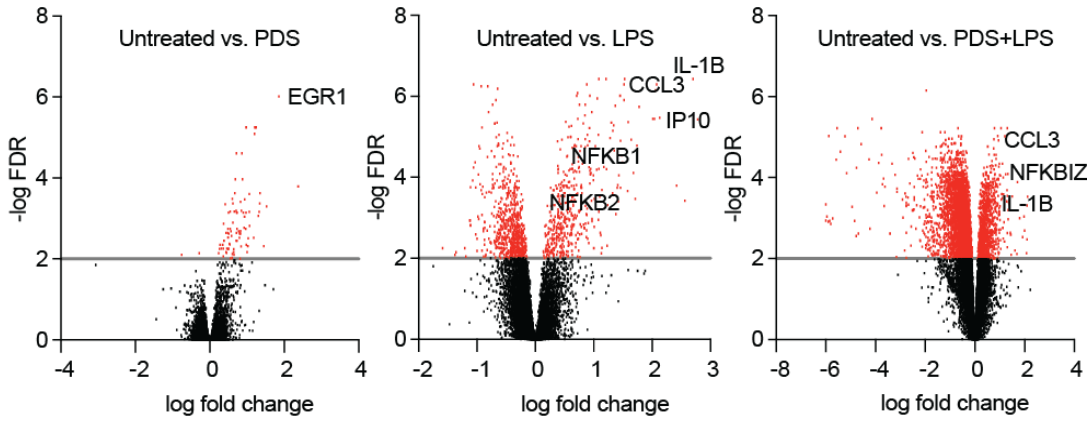

Figure 9: Transcriptome changes after 3´ RNA-Seq.
A-B) Venn diagrams of the significantly (p<0.005) regulated genes C) and their top three hit GO annotations. D-F) Volcano plots represent the negative logarithmic false discovery rate (FDR) on the y-axis and the logarithmic fold change on the x-axis. The transcripts identified as significantly differentially expressed (FDR<0.05) are colored in red. The 3´RNA-Seq was performed in three biological replicates.

Since cytokines were among the DEGs in LPS and in the PDS and LPS co-treatment, the analysis was further focused on cytokines. IL-1 beta is a pro-inflammatory cytokine involved in the host defense and signaling [117]. After macrophages are primed by exposure to pathogen-associated molecular patterns (PAMPs), IL-1 beta is expressed as an inactive precursor and is processed and secreted upon triggering by a second stimulus [117]. To validate the 3´ RNA-Seq results of IL-1 beta expression levels, RT-qPCR was performed (Figure 10A). Stimulation with LPS resulted in an upregulation (more than 10,000 fold) of IL-1 beta compared to untreated, whereas co-treatment with PDS and LPS significantly downregulated the expression (Figure 10A). The endotoxin nigericin was used as a second stimulus for the inflammasome to induce IL-1 beta processing and secretion [117]. IL-1 beta secretion levels were significantly upregulated to 12,000 pg/ml when primed with LPS and nigericin for eight hours (Figure 10B). In contrast to that, the IL-1 beta expression levels were significantly downregulated by triple treatment with PDS, LPS and nigericin (circa 1,000 pg/ml). The same trends were observed after four hours, although the total secretion levels were lower (and not significant) (Figure 10B).

The 3´ RNA-Seq heatmap of interleukins illustrates that the down-regulation (negative Z-score) after co-treatment with PDS and LPS was not only observed for IL-1 beta, but also for the interleukins in general (Figure 10C). The genes of the LPS-mediated immune response are highly up-regulated after LPS treatment (positive Z-score) and down-regulated after G4 stabilization and LPS treatment (Figure 10C).

In conclusion, IL-1 beta expression and secretion are decreased in the PDS and LPS treatment compared to LPS (Figure 10A-B). The expression of other cytokines, apart from IL-1 beta, showed the same expression profile and were also down-regulated after G4 stabilization by PDS (Figure 10C).

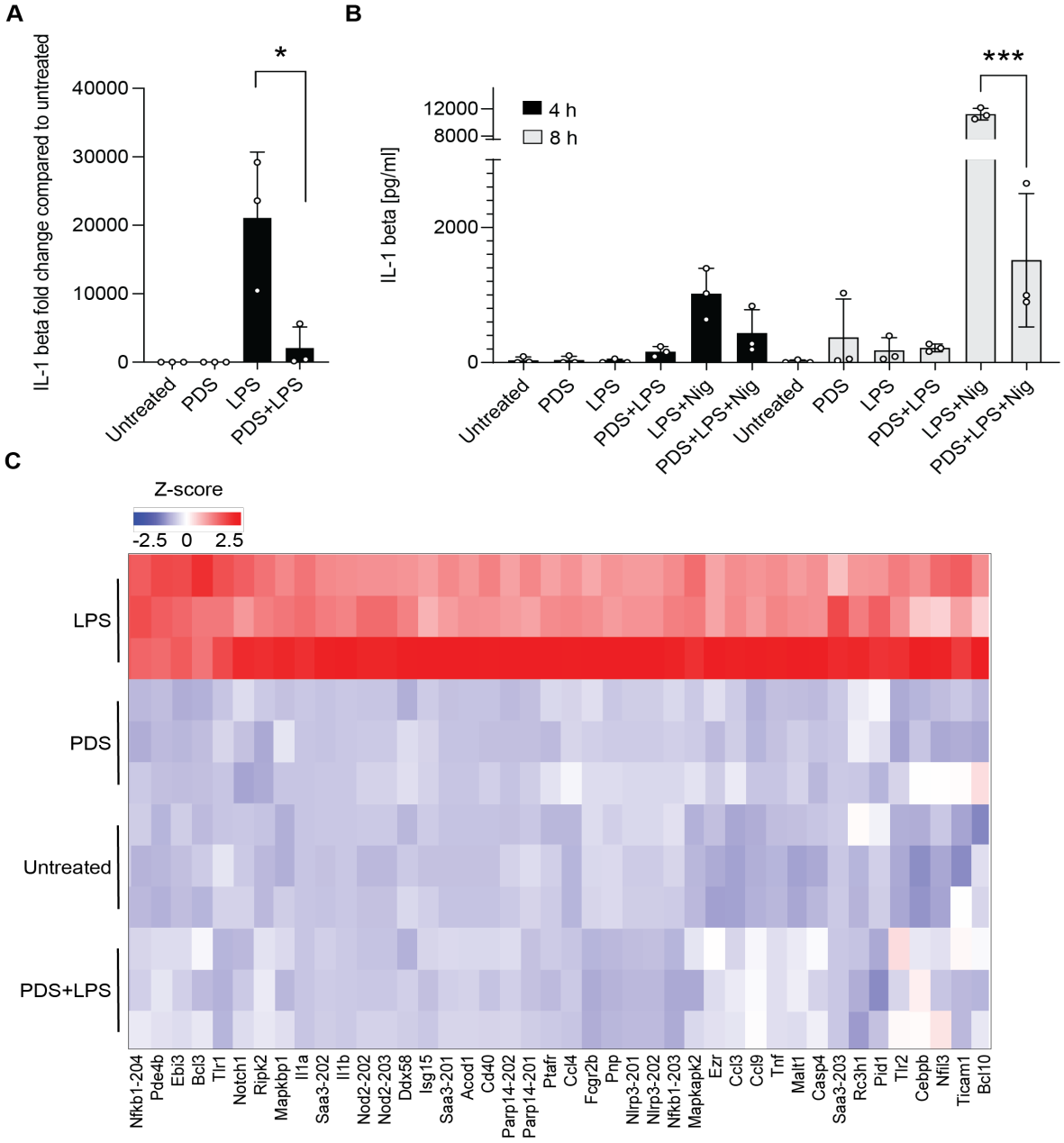

Figure 10: Figure 10: Cytokine expression after G4 stabilization.
A) IL-1 beta transcript level was measured by RT-qPCR four hours after treatment, normalized by GAPDH and the fold change is calculated compared to untreated. B) Additionally, IL-1 beta secretion was analyzed by HTRF using the supernatant after four and eight hours (10 µg/ml nigericin for one hour). C) Heat map of 3´RNA-Seq for subgroup of interleukins that are differentially expressed. The x-axis shows the gene names and for gene names that are listed more than once the transcript-ID is indicated. On the y-axis are three biological replicates displayed for every treatment. Z-score hierarchical clustering based on Euclidean distance measure and average linkage for the linkage analysis was used. Experiments were performed in three biological replicates; p-value≤0.05=*; p-value≤0.01=**; p-value≤0.0001=*** (unpaired t-test); scatter plot mean with SD. Figure panel B was performed in cooperation with Nathalia Rosero (Franklin laboratory).

Since exposure to the potent immune-activating stimulus LPS results in the secretion of a variety of other cytokines in addition to IL-1 beta to orchestrate and extend the inflammatory response [286,287], the ProcartaPlex™ assay was performed (Figure 11). This assay allows for the detection of multiple proteins in a single sample and was designed to quantify the cytokine secretion levels of interferon beta (IFN beta), interferon alpha (IFN alpha), interleukin-6 (IL-6), interleukin-10 (IL-10), tumor necrosis factor alpha (TNF alpha), interleukin-18 (IL-18), interferon gamma-induced protein 10 (IP-10 also known as C-X-C motif chemokine ligand 10 (CXL10)) and interleukin-12 (IL-12) (Figure 11A-H).

IFN beta secretion increased 300 pg/ml after LPS treatment and decreased significantly to 50 pg/ml after PDS and LPS co-treatment (Figure 11A). IFN alpha decreased significantly 10 pg/ml after G4 stabilization and LPS treatment (Figure 11B), whereas IL-6 decreased even 6,000 pg/ml in the LPS and PDS co-treatment compared to LPS treatment (Figure 11C). The secretion of the anti-inflammatory cytokine IL-10 decreased 10 pg/ml after PDS and LPS treatment (Figure 11D). TNF alpha secretion increased 5,000 pg/ml after LPS stimulation, whereas it decreased to 2,000 pg/ml after PDS and LPS co-treatment (Figure 11E). IL-18 only decreased slightly around 30 pg/ml (Figure 11F). IP-10 secretion increased to 2,000 pg/ml after LPS stimulation (Figure 11G) and IL-12 to 50 pg/ml (Figure 11H), for IP-10 and IL-12 the secretion levels after PDS and LPS treatment were too low to be detected. The secretion level of the untreated cells was always included as control and was always close to zero except for IL-18. To sum up, stimulation by LPS resulted in the secretion of the above mentioned cytokines (e.g. IFN beta and IL-6), whereas they were down-regulated by co-treatment with PDS and LPS (Figure 11A-H).

In conclusion, G4 stabilization affects the expression and secretion of important cytokines involved in mediating the immune response to bacteria (Figure 9 - Figure 11).

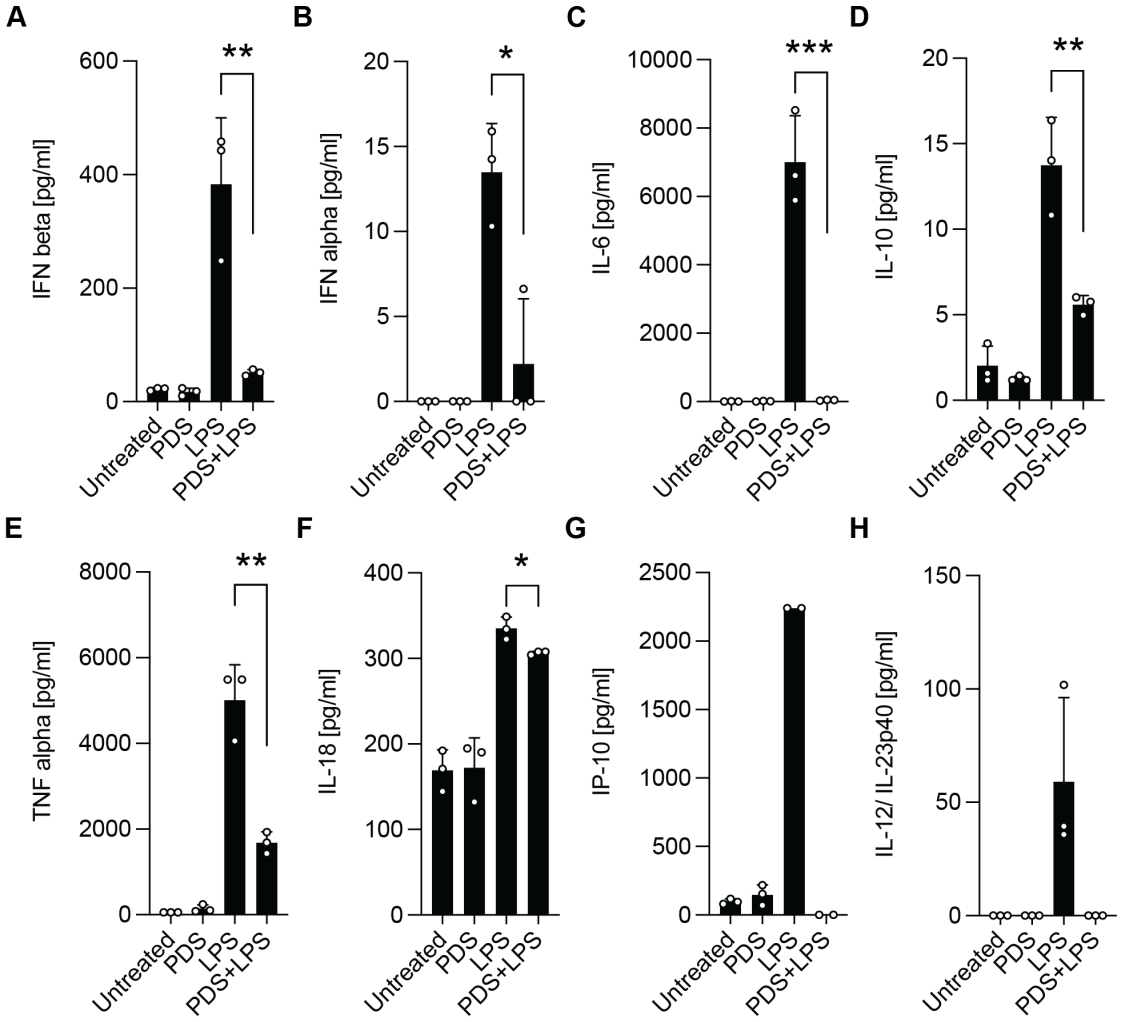

Figure 11: Cytokine secretion levels after G4 stabilization.
Cytokine secretion levels of iBMDMs four hours post treatment measured with ProcartaPlex™ Multiplex Immunoassay. For IP-10 and TNF alpha two values for LPS were higher than the standard and are displayed as the maximum of the highest standard. Three biological replicates are shown, p-value≤0.05=*; p-value≤0.01=**; p value≤0.0001=*** (unpaired t-test); scatter plot mean with SD. The experiment was performed in cooperation with Jennifer Szlapa (Abdullah laboratory).

3.4 G4 formation reduces the NF-κB activity

The collected data strongly suggested that G4 stabilization negatively affects the LPS-mediated immune response via cytokine expression and secretion. To further test this hypothesis, the signaling pathway of the involved and above tested cytokines was further investigated. IL-1 beta [288], IFN beta [289], IL-6 [290], IL-10 [291], TNF alpha [292], IP-10 [293] and IL-12 [294] are target genes of the transcription factor NF-κB. NF-κB is a master regulator of pro-inflammatory cytokine expression [105]. Thus, the role of G4 stabilization for the

transcription factor NF-κB was investigated. To quantify the NF-κB response to stimulation by LPS, the RAW-Blue™ NF-κB SEAP reporter cells (Invivogen) were used. Upon NF-κB activation, this cell line secretes an alkaline phosphatase that can be used for monitoring the activity level. Priming with LPS activated the transcription factor NF-κB by 3 fold, whereas co-treatment with PDS and LPS significantly reduced its activity by almost 2 fold (Figure 12A). The NF-κB subunit p65 is phosphorylated and translocated to the nucleus after LPS stimulation [295]. Western blot analysis showed that the total p65 protein levels did not change between PDS and/ or LPS treatments (Figure 12C). However, p65 was significantly less phosphorylated in the co-treatment of PDS and LPS compared to LPS (Figure 12B). G4 stabilization does not affect the p65 protein levels, but it alters the phosphorylation and reduces the NF-κB activity.

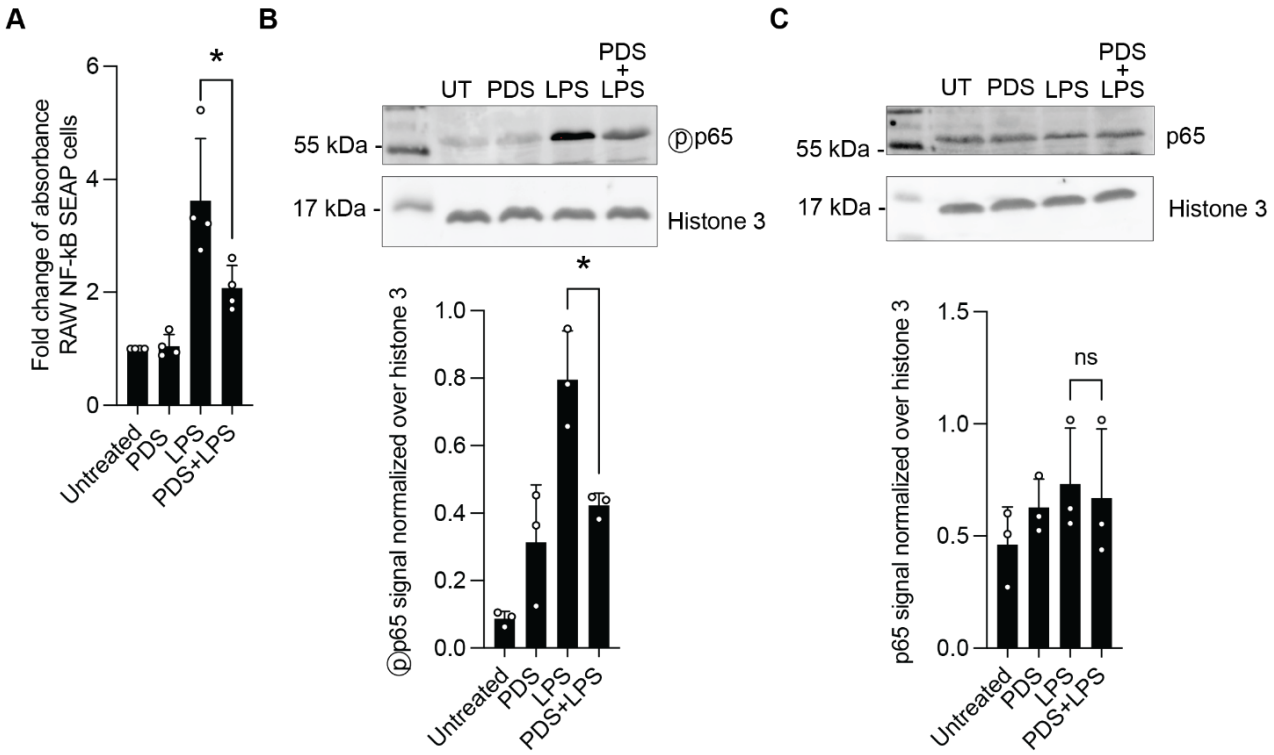

Figure 12: NF-κB activity after G4 stabilization.
NF-κB activity is negatively influenced by G4 stabilization via PDS. A) The RAW-Blue™ cells contain a secreted embryonic alkaline phosphatase inducible by NF-κB. SEAP secretion levels were monitored by measuring the absorbance at 630 nm after addition of QUANTI-Blue™ detection medium. B-C) NF-κB p65 protein levels were measured by western blot for iBMDMs four hours after treatment and quantified. UT=Untreated; Ⓟ=phosphorylated; At least three biological replicates are shown, p-value≤0.05=* (unpaired t-test); scatter plot mean with SD.

3.5 G4 stabilization alters the chromatin accessibility

To rule out if the observed expression changes in the LPS-mediated immune response after G4 stabilization correlate with G4 locations, a genome-wide G4 mapping was done. BG4 cleavage under targets and tagmentation (CUT&Tag) was performed in LPS and/ or PDS treated samples. BG4 CUT&Tag is an enzyme-tethering method used to map native G4s [260]. For the LPS-treated samples, 479 unique peaks were detected compared to the untreated samples and the peaks were enriched for experimental mapped DNA G4s ($p=0.052$) [155]. No unique peaks were observed for PDS and PDS+LPS treated samples compared to the untreated sample. The LPS peak regions were mapped to the corresponding genes (coding region of the genes) and Table 2 shows the first Amigo GO annotation hits for these genes. The proteins encoded by these 146 genes were analyzed in an interaction network (Supplementary figure 3) and several kinases were found [296]. Among the kinases were cyclin-dependent kinase 6 (Cdk 6) which regulates the G1/ S transition in the cell cycle, hematopoietic cell kinase (Hck) which is important for signaling transmission in the innate immune response, protein kinase C epsilon type (Prkce) which is associated with cytoskeletal proteins, and abelson murine leukemia viral oncogene homolog 1 (Abl1), a tyrosine-protein kinase involved in cytoskeleton remodeling following extracellular stimuli [296]. In addition, regulatory associated protein of mtor (Rptor), which is involved in cell growth, survival and autophagy was detected in the protein interaction network (Supplementary figure 3) [296].

Table 2: First hits of GO annotation for genes from called peaks by CUT&Tag for the LPS treatment

Condition	GO annotation
LPS	cell surface toll-like receptor signaling pathway innate immune response activating cell surface receptor signaling pathway cellular response to stimulus

To further investigate how G4 stabilization has genome-wide effects, the chromatin landscape became the focus of research. Changes in the chromatin landscape have been reported to be associated with LPS stimulation [297–300]. G4s fold predominantly in open chromatin regions [196]. Therefore, I asked whether G4 stabilization affects the chromatin remodeling induced by LPS stimulation. To investigate the chromatin landscape, an assay for transposase-accessible chromatin using sequencing (ATAC-Seq) was performed in LPS and/ or PDS treated iBMDMs. This assay takes advantage of the hyperactive Tn5 that cuts open chromatin regions.

The analysis first focused on general alterations observed in the ATAC-Seq and in the second part focused on the correlation with G4s. The samples clustered into two categories: in untreated or LPS treated samples and in PDS or PDS plus LPS treated samples. In the first category 26,931 and 32,386 peaks were detected, whereas in the second category 10,438 and 18,544 peaks were detected (Figure 13A). The majority of the peaks were detected at the transcription start site (TSS) (Figure 13B).The transcription start site plots show that the transposase accessible regions were highly accessible in the untreated and LPS treated samples, whereas the TSS sites were barely accessible in the PDS and PDS plus LPS treated samples (Figure 13C-F).
The ATAC-Seq reads from LPS correlated significantly with differentially expressed genes in the 3´RNA-Seq (correlation of linear regression 0.4) (Supplementary figure 4). The PDS and PDS plus LPS readouts did not correlate with the differentially expressed genes in the 3´RNA-Seq (data not shown).

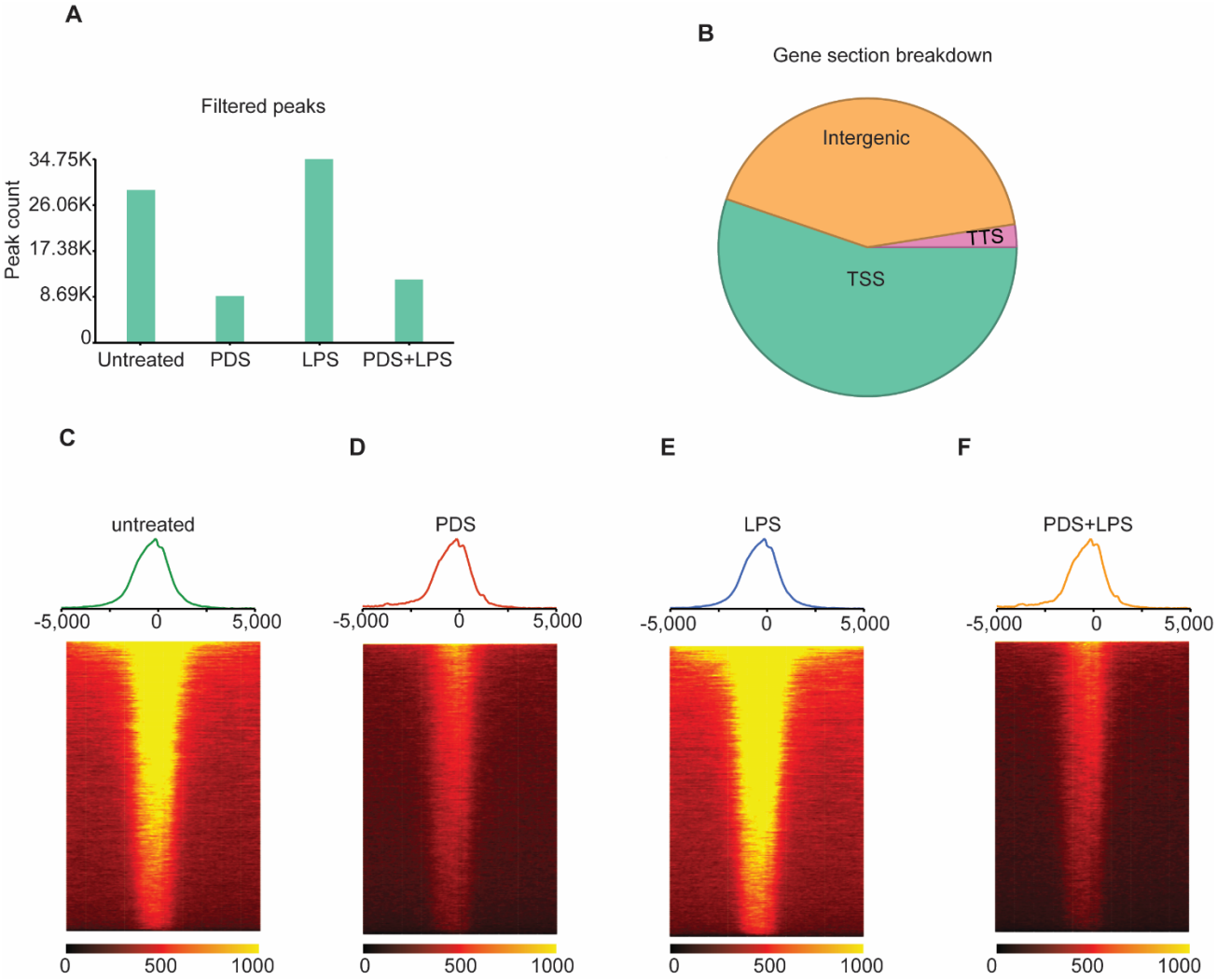

Figure 13: Chromatin landscape after G4 stabilization (ATAC-Seq).
A) Peak calling (using MACS2) results from ATAC (Assay for Transposase-Accessible Chromatin) Sequencing for iBMDMs treated for four hours. B) The cake chart displays the category of the previous called peaks. C-F) Coverage heat maps showing the density of mapped reads 5000 bp upstream and downstream of the Ensembl annotated TSS labelled as 0. Each peak represents a horizontal line and the heatmap shows the accessibility around the peaks. TSS=Transcription start site; TTS= Transcription termination site. ATAC-Seq was performed for n = 3 and the results for n = 1 are displayed in this figure, however n = 2 und n = 3 showed similar results.

These differences in the accessibility were also reflected in the transcription factor motif enrichment. Untreated and LPS treatment showed similar motifs among the ATAC-Seq peaks (Supplementary figure 5). The p65 subunit of the NF-κB motif was highly enriched in LPS compared to untreated samples (Figure 14A). The NF-κB motifs (p50, p52, p65) were significantly enriched in LPS compared to PDS plus LPS (Figure 14B). This role and involvement of NF-κB is consistent with previous data presented in this study (Figure 12).

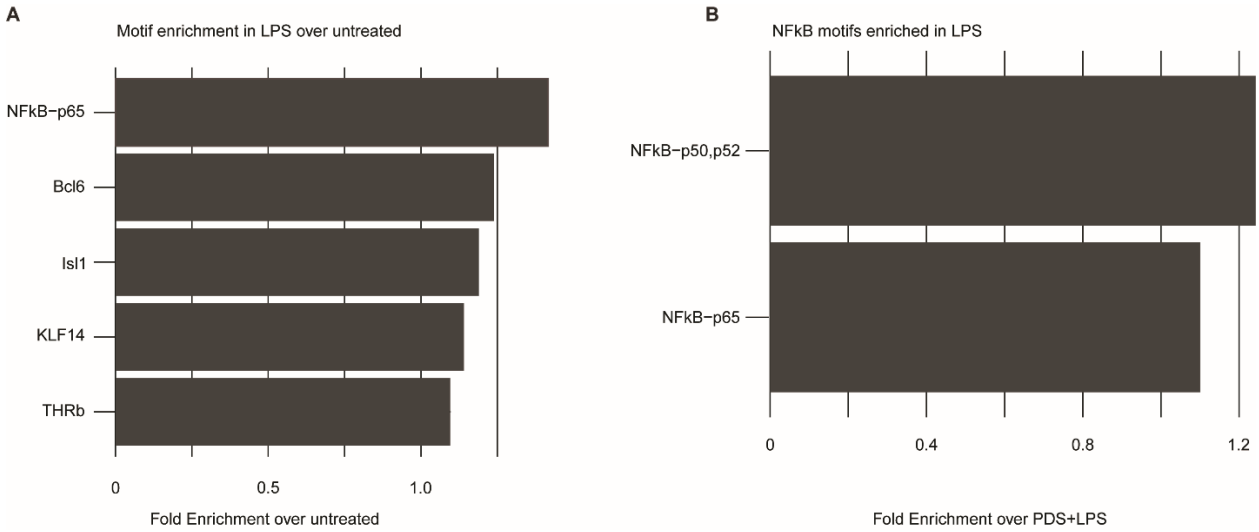

Figure 14: Motif enrichment for ATAC-Seq peaks.
(A) The motif enrichment shows the enriched motifs in the LPS treated sampled over the untreated samples. (B) The NF-κB motifs are enriched significantly ($p<0.005$) in LPS treated samples over PDS plus LPS treated samples. Nuclear factor 'kappa-light-chain-enhancer' of activated B-cells (NF-κB); B-cell lymphoma 6 (Bcl6); Insulin gene enhancer protein (Isl1); Krueppel-like factor 14 (KLF14); thyroid hormone receptor beta (THRb). All three biological replicates of the ATAC-Seq were considered. In cooperation with Jasper Spitzer (Schmidt laboratory).

The next step was to correlate the ATAC-Seq peaks with the G4 consensus motif [137]. As expected, the PDS treated samples had more G4 motifs enriched in their peaks compared to untreated and LPS treated samples (Supplementary figure 6). The G4-containing peaks were broader than the baseline (/no G4-containing) peaks (Figure 15A). In addition, the G4 motif composition varied between the treatments. In the untreated and LPS treated samples, the G-tracts had more Gs (magenta fraction) and in the PDS and PDS plus LPS treated samples the loop length was longer (yellow fraction) (Figure 15B).

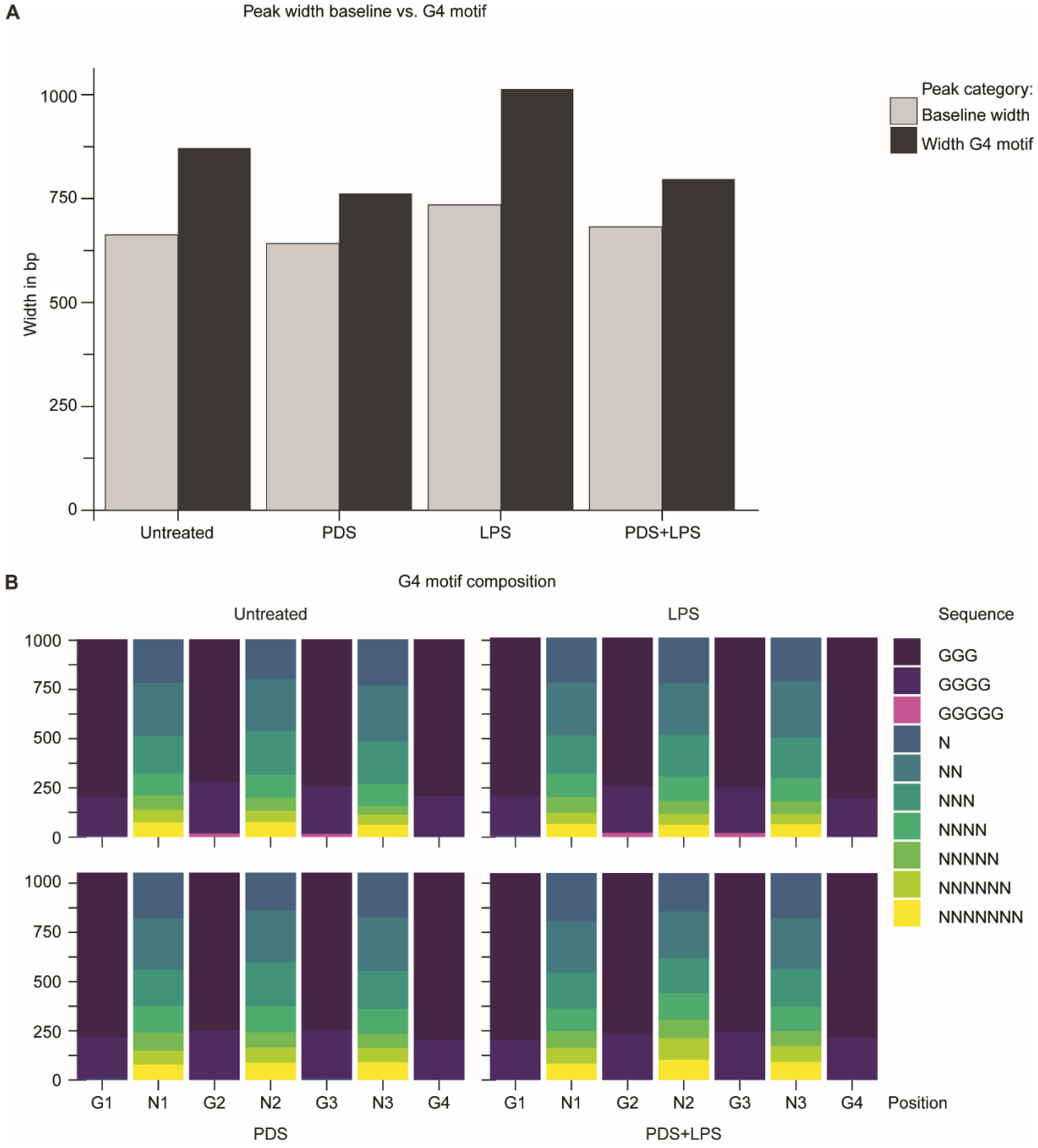

Figure 15: The ATAC-Seq peak correlation to G4 motifs.
(A) The ATAC-Seq peak width analyzed based on the presence of a G4 motif or not (=baseline). (B) The ATAC-Seq peaks were analyzed based on the motif composition (G= G-tetrad; N= loop). The y-axis shows the peak count. All three biological replicates of the ATAC-Seq were considered. In cooperation with Jasper Spitzer (Schmidt laboratory).

Next, it was addressed whether G4s have an impact on the surrounding chromatin accessibility. The untreated peaks from peak start to end plus 1 kb upstream and downstream were plotted in a heat map and divided into non-G4 and G4 motif containing peaks. Based on this division from the untreated samples, these loci were also plotted in the other treatments. In untreated and LPS treated samples the G4-containing peaks are more accessible, broader and more diffuse compared to PDS treated samples (Figure 16A). G4 motif sites are more accessible compared to non-G4 motif sites, even in the PDS and PDS plus LPS treated samples. The non-G4 motif sites are less accessible than the G4 sites (Figure 16A).

To investigate whether G4 formation has a broader influence on the chromatin landscape, a 5 kb window was analyzed in the next step. The G4 motif containing peaks resulted in more accessible chromatin in the 5 kb window (Figure 16B). The G4-containing peaks are even in the 5 kb window more diffused compared to the non-G4-containing peaks (Figure 16B).

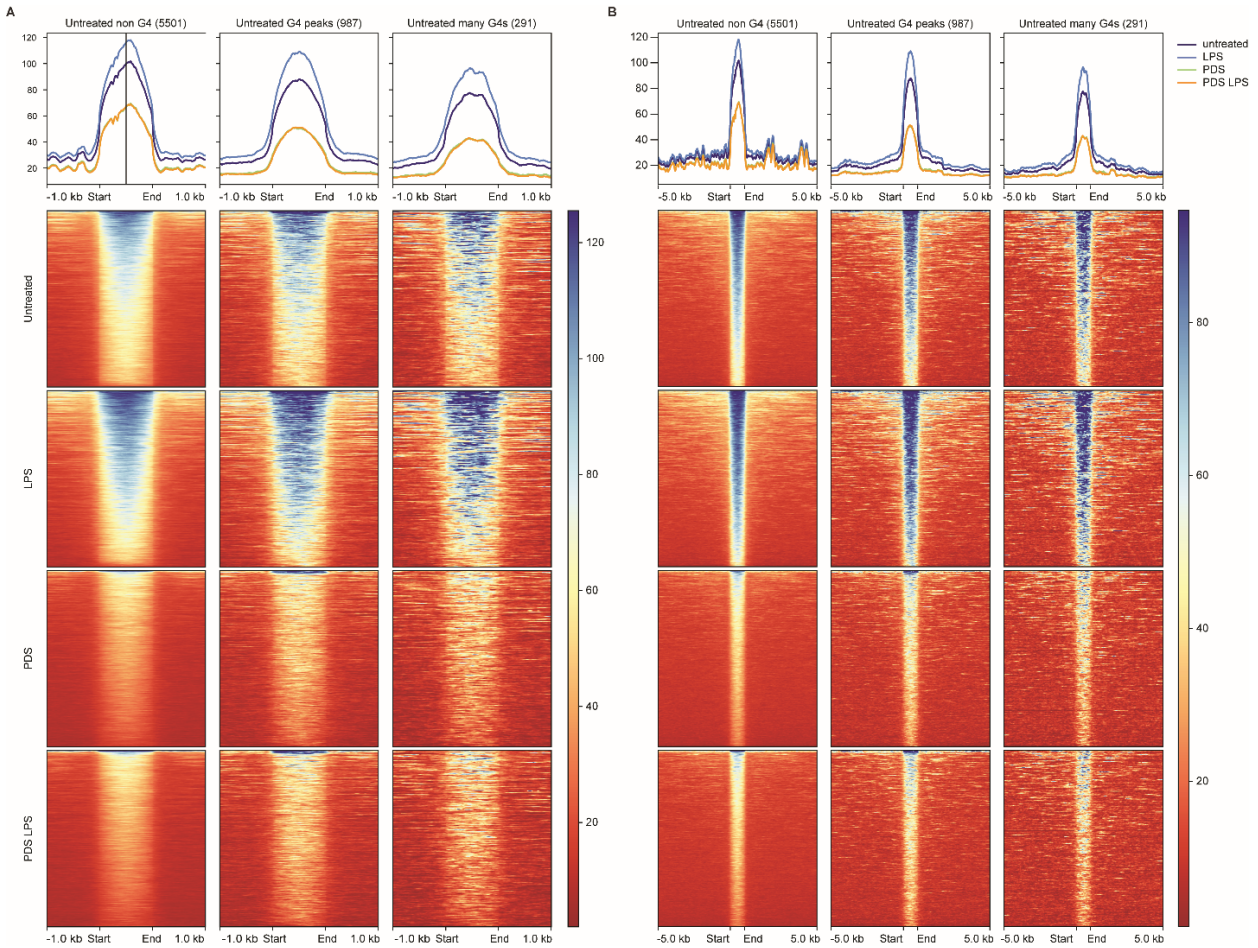

Figure 16: ATAC-Seq peak window in correlation to G4 motifs.
The ATAC-Seq peaks from the untreated samples were visualized in a color-coded heatmap based on their accessibility in a 1 kb window (A) and a 5 kb window (B) up- and downstream of the peak start (=start) and peak end (=end). The same loci were visualized for the other treatments as well. The peaks were categorized based on the presence of no G4 motif, one G4 motif or more than one G4 motif. The orange (PDS+LPS) and green (PDS) line are almost overlapping and thus only partially visible. All three biological replicates of the ATAC-Seq were considered. In cooperation with Jasper Spitzer (Schmidt laboratory).

4 Discussion

The aim of this thesis was to understand the contribution of secondary nucleic acid structures, in particular G4s, to macrophage function. Since G4 structures are known to impact gene expression and other cellular pathways [152], I predicted that they would also influence essential pathways within macrophages. G4 structures change dynamically during the cell cycle and also change in response to endogenous stimuli [133,193]. Thus, I predicted that G4 formation would change in response to macrophage activation, where it contributes to macrophage function. The cells of the innate immune system, such as macrophages, effectively clear bacterial infections by recognizing conserved PAMPs through PRRs [17]. However, in certain disease settings the immune system can be compromised [3]. Whereas underactivity can lead to infections and tumors of immunodeficiency, overactivity can lead to allergic and autoimmune diseases [3]. Immunodeficiency can have several causes: Primary immunodeficiencies are caused by congenital changes in the specificity of the immune cells and are classified according to the cell type that causes the disease [301]. Secondary immunodeficiencies can be caused by exogenous factors such as viral infections [301]. An example of a primary immunodeficiency of phagocytes is the chronic granulomatous disease [301]. Patients are extremely susceptible to certain bacteria and fungi, such as *Staphylococcus aureus* or *Aspergillus* species [302], and the intracellular survival of pathogens causes the granuloma formation [301]. It is a mostly X-chromosomal linked disorder [301]. Patients have mutations in the NADPH oxidase, which is required by phagocytic cells like macrophages to form reactive oxygen species to clear the pathogens [302].

Furthermore, changes in immune activation are also discussed to impact treatment and disease outcome. For example, bacterial infections during cancer therapy are a high risk and the most common complication during treatment due to drug-induced immunosuppression, leading to infection-related death [303–305]. Here, chemotherapy and radiation therapy change the leucocyte number (neutropenia) and can disrupt anatomical barriers, which are the main contributors to immune defects [304].

Different cellular processes contribute to the immune cell activation and are affected in disease settings [301,306]. How macrophages contribute to disease outcomes is under investigation, for example macrophages clear toxic proteins in neurodegenerative diseases such as Alzheimer's disease or Parkinson's disease [307]. G4s have been implicated as transcriptional, translational, and epigenetic regulatory elements of disease factors [170]. For example, defects in the RecQ C-terminal domain of the DNA G4 unwinding helicases Werner and Bloom cause severe syndromes, the Werner and Bloom syndromes, respectively [168]. To date, a clear picture of how cellular alterations and G4 levels contribute to immune cell functions is lacking.

In addition to infections, cells of the immune system influence the tumor progression [308]. For example, in early tumor stages, natural killer cells and CD8+ T cells recognize and eliminate cancer cells [308]. Nevertheless, certain tumor types have developed strategies to evade immune recognition and prevent immune cell infiltration through molecular and cellular mechanisms, such as pH changes and changes in the expression of surface molecules [309,310]. However, immune cells can also positively influence tumor progression and promote tumor cell growth [311]. For example, neutrophils can promote tumor angiogenesis by secreting vascular endothelial growth factor [308]. Such immunosuppressive cells also include tumor-associated macrophages (TAMs) [252]. In recent years, much attention has been focused on TAMs as they are correlated with poor prognosis and reduced survival [308]. How cellular changes in the tumor microenvironment impacts TAMs and how this modulates TAM function is not clear yet [312]. Since several oncogenes are G4-rich and cancer cells have altered G4 levels, G4 stabilization by G4 ligands is discussed as a target in cancer therapy and tested in a clinical trial [174,176,182,194]. Thus, I aimed to understand if and how G4 formation, in particular G4 stabilization by G4 ligands, impacts macrophage function during infection.

My PhD thesis provides a system-wide analysis of the consequences of G4 stabilization in mouse macrophages. Interestingly, G4s were detected in macrophages and were sensitive to ligand treatment (Figure 7). G4 stabilization altered the cytokine expression and secretion (Figure 9 - Figure 11), while it had no effect on the phagocytic behavior (Figure 8). The reduced cytokine expression could be explained by changes in the NF-κB

transcription factor signaling pathway (Figure 12 and Figure 14). Finally, G4 formation altered the chromatin landscape by keeping the chromatin less accessible at the loci that were highly accessible in LPS treatment alone (Figure 13 - Figure 16). In the following chapters, the newly obtained data will be discussed in topic-focused chapters, culminating in the presentation of the resulting model illustrating the new role of G4 formation in mouse macrophages (Figure 17).

4.1 G4 stabilization has no impact on phagocytosis and mitochondrial fitness

The data presented showed that G4 formation has no effect on the phagocytic behavior and mitochondrial fitness of macrophages (Figure 8). The key function of macrophages is phagocytosis [78], and thus it was the first process to be analyzed for the effect of G4 formation. G4 formation did not interfere with this central process, as the rate of phagocytosis did not change between the treatments (Figure 8). It has been shown that exogenous G4s in human neutrophils increase the phagocytosis in the presence of *Salmonella* [313]. It is possible that treatment with the exogenous G4s in the human neutrophils was recognized by cGAS/STING and this activation of the immune system resulted in increased phagocytosis rates. However, activation of the immune system was not tested by the authors [313]. This study used exogenous G4s and therefore the results are not comparable to my study where endogenous G4s were stabilized by PDS ligand treatment. Thus, my data show for the first time that endogenous G4 stabilization does not alter the phagocytic rate in mouse macrophages (Figure 8).

Since the effect of G4 stabilization on macrophage-derived mitochondria has not been tested, it was crucial to investigate whether ligand treatment by PDS induces mitochondrial metabolic changes that would affect subsequent studies. It has been shown that cellular stress and inflammation, such as pathogen infection, leads to the release of mitochondrial DNA as DAMP, changes in membrane potential, and the production of reactive oxygen species [314]. Mitochondrial metabolism, in turn, regulates macrophage activation, differentiation, and survival [314]. G4 formation did not affect the mitochondrial activity of macrophages (Supplementary figure 2). ROS production, as well as mitochondrial size and membrane potential were not affected by G4 ligand treatment

(Supplementary figure 2). Thus, it could be excluded that the effects observed in the later experiments were driven by a mitochondrial stress response.

4.2 PDS stabilizes G4s in mouse macrophages

Macrophages are important phagocytes of the innate immune system [78]. I was able to show by immunofluorescence and flow cytometry data (BG-flow [259]) that G4s form in mouse iBMDMs and can be stabilized by PDS treatment (Figure 7). Similar to macrophages, G4s in most other cells were stabilized by PDS in a time- and concentration-dependent manner [158,315,316]. In contrast to other cancer cells such as U2OS cells, macrophages are less sensitive to G4 stabilization as higher concentrations of PDS can be used (Supplementary figure 2) [158]. Previously, it has been shown that prolonged exposure to PDS (24-72 hours) leads to DNA damage and cell cycle arrest [186]. In contrast, the use of subtoxic doses of 25 µM PDS for four hours in my study did not lead to double strand breaks, as indicated by lack of γH2AX bands (Figure 7) and no change in cell viability (Supplementary figure 2). Furthermore, it has been shown that PDS induces a type I interferon response in human cancer cells after 24 hours incubation at 10 µM due to increased genome instability and accumulation of DNA in the cytosol [255]. The PDS treatment caused micronuclei formation, cGAS/STING and NF-κB activation [255]. It could be that genome instability and DNA double-strand break events caused a broad immune response via cGAS/STING recognition or that the prolonged timing of PDS treatment timing caused a stress response leading to the type I interferon response. However, since they used cancer cells with prolonged PDS treatment time resulting in DNA damage, the results are not comparable to my study.

In the PDS and LPS cotreatment, the G4 level is at the same level as in the untreated sample (Figure 7). Previously, a non-canonical signaling pathway was described in which caspase-11 leads to a drop of intracellular potassium levels during LPS stimulation [317]. Ionic fluxes such as potassium efflux are required for NLRP3 inflammasome activation [62]. Consequently, it could be that the potassium efflux has a negative effect on G4 levels, as potassium is required as a cation for G4 stabilization [140]. This could explain why the G4 level is not increased in the PDS and LPS co-treatment compared to untreated. Consistent with this, in the time course experiment, when PDS was added before LPS, G4 levels

were increased again (Figure 7). Probably, the G4s levels were already stabilized before the addition of LPS and the potassium efflux could not change the G4 level anymore. Conversely, when LPS was added before PDS, G4 levels were similar to untreated levels (Figure 7). Putatively, LPS treatment led to potassium efflux and G4s cannot be effectively stabilized afterwards due to the lack in potassium.

Alternatively, LPS is known to be involved in chromatin remodeling and chromatin structure is linked to gene expression [189,297–300]. Thus, LPS-induced chromatin remodeling could block the G4 formation, since G4s can only fold in open, accessible chromatin regions [196]. The chromatin landscape is discussed in detail in Chapter 4.4. How and which G4s regulate the cellular response in macrophages is essential to know in a genome-wide assay to understand the exact role of G4s. The CUT&Tag assay revealed that 479 peaks were detected in the LPS treated samples compared to the untreated samples (Chapter 3.5). Although untreated and LPS treated samples have a similar total G4 level (Figure 7), this result proves that different G4s are folded. This supports the role of G4s as functional elements in transcription as described in the literature [196,216].

According to the CUT&Tag data, a distinct set of kinases were detected in the peaks of LPS treated samples (Table 2 and Supplementary figure 3), suggesting that G4s are involved in kinase expression. Among the G4-containing kinases in the LPS treated samples was Hck (Supplementary figure 3). This kinase has been shown to play a role in the LPS/TLR4-induced TNF and IL-6 expression independent of NF-κB [318]. How G4 stabilization affects the Hck expression, remains elusive. It could be speculated that LPS and PDS treatment leads to the formation of different G4s within Hck, that have different effects on the Hck expression. G4s have already been discussed as a target to modulate kinase transcription as an anticancer therapy [217]. A prominent example is the KIT proto-oncogene, which encodes a tyrosine protein kinase involved in cell proliferation [319] and whose constitutive activation plays a role in gastrointestinal stromal tumors [320]. G4 stabilization in the human KIT promoter has been shown to downregulate the mRNA and protein levels in human cell lines [321].

The CUT&Tag assay did not show different peaks between PDS and untreated, indicating a technical problem with the PDS treated sample. PDS may weaken the binding site for BG4 in pulldown assays, since PDS and BG4 compete for the same binding site at the G-tetrad (Supplementary figure 7), whereas BG4 can still bind in immunofluorescence with less stringent washes. Optimization by less stringent washes did not solve the problem in CUT&Tag. Nowadays, the method has been modified and called Chem-map [322]. This method uses precomplexed biotinylated ligands with the antibiotin antibody that will bind to the target chromatin and a second antibody that tethers the Tn5 transposase to the ligand binding sites [322]. Alternatively, biotinylated ligands can also be used to detect G4s, such as biotinylated PDS, which has been used to pull down telomeric G4s from human cells [323]. The biotinylated, triazole-assembled template assembled synthetic G-quartet (BioCyTASQ) was shown to isolate DNA and RNA G4s from solution by affinity purification [324], bypassing the problematic PDS blocking for the BG4 binding site. This ligand research is a very promising approach for future genome-wide detection of the G4 landscape. The implementation of this assay will be a key experiment in the near future to address how LPS and PDS affect the G4 landscape genome-wide and to unravel how G4s as a functional element contribute to and shape macrophage function. In conclusion, G4s form in macrophages and are sensitive to ligand treatment. G4 stabilization and LPS co-treatment resulted in an altered G4 landscape compared to LPS treatment alone or untreated. The G4 landscape needs to be further investigated by further experiments to address which G4s contribute to macrophage function.

4.3 G4 stabilization reduces the immune response to bacteria involving modulation of the NF-κB pathway

The data presented here demonstrate for the first time that G4 formation affects the immune response to bacterial infection through decreased expression of maturation marker (Figure 8), decreased cytokine expression (Figure9 and Figure 10) and secretion (Figure 11), and modulation of the NF-κB pathway (Figure 12). The only previously known link of maturation markers and G4s is that spleen cells incubated with the G4-forming telomeric repeat sequence $(TTAGGG)_4$ had decreased CD40 levels after 24 hours [325]. Probably these cytoplasmic G4s trigger a cGAS/STING activation like toxic PDS concentrations (see Chapter 4.2 [255]). In my study endogenous G4s caused a decrease in

maturation marker expression (Figure 8) and thus a different mechanism of G4s plays a role. Probably PDS stabilizes G4s at promoters important for the maturation markers or alters the accessibility of the promoters via chromatin remodeling (see also Chapter 4.4). As the maturation marker expression is one required signal for T cell activation and clonal expansion [89], it is likely that T cells are no longer activated by macrophages when co-treated with PDS and LPS. In order to prove that the macrophages no longer activate T cells due to decreased CD40 and CD80 production after G4 stabilization, a T cell activation assay could be performed as described in the literature [22].

Exposure to LPS caused strong expression changes (Figure 9) as it was already shown by others, e.g. 1525 genes were upregulated and 1113 genes were downregulated in macrophages, and similar GO annotations were found, such as innate immune response, TNF and NF-κB signaling [326], and thus is comparable to my 3´ RNA-Seq data. PDS expression caused 653 differentially expressed genes in rat cells [327], although this number is much higher compared to my 3´RNA-Seq (Figure 9), it is difficult to compare these values as different cells and concentrations were used. The strongest effect caused by the double treatment is described for the first time in my study (Figure 9) and suggests that G4 stabilization in combination with LPS stimulation not only modifies the expression of some genes such as c-Myc [179,328], but on a global scale. While others have shown that 24 hours after LPS treatment led to cytokine secretion [329], I demonstrated that four hours is sufficient to induce a cytokine secretion response (Figure 11), except for IL-1 beta, which requires at least eight hours (Figure 10). All cytokines tested were down-regulated and their secretion levels decreased after PDS treatment (Figure 10 and Figure 11). The majority (nine out of eleven) tested cytokines in the secretion assays have in common that they are regulated by the transcription factor NF-κB, as reviewed [330]. Accordingly, NF-κB motifs are enriched only within the LPS peaks in the ATAC-Seq data (Figure 14). Transcription factor occupancy prediction revealed that breast cancer cells with altered G4 levels were enriched for NF-κB pathway factors compared to untreated cells [331]. Most likely these conflicting findings are due to the fact that different breast cancer cells have specific transcriptional programs [332] and I used a macrophage model simulating a bacterial infection with LPS. In general, however, it demonstrates the ability of G4s to modulate transcription factor occupancy and thus alter gene expression, confirming previous

data [196,333]. The NF-κB p65 subunit was shown to be phosphorylated at serine 536 in response to IL-1 beta [334]. After G4 stabilization, reduced NF-κB phosphorylation level (Figure 12) was observed, correlating with reduced IL-1 beta expression and secretion (Figure 10). This led to less nuclear translocation and in turn impaired NF-κB-dependent transcriptional activity was measured using a NF-κB reporter cell line (Figure 12). Although NF-κB is not the only transcription factor modulated by the double treatment, it is a key player in orchestrating the immune response and could explain many of the observed effects.

There are several possibilities why NF-κB activity and motif enrichment are altered after G4 stabilization. It may be that NF-κB cannot bind the promoter region of its target genes when a G4 is present. It is also possible that NF-κB can bind G4s in the absence of a G4 ligand and the binding site on the G4 is blocked in the presence of PDS. Alternatively, it could be speculated that the chromatin at the NF-κB binding sites is inaccessible and inhibits its binding. The influence of LPS and PDS on the chromatin landscape is discussed in Chapter 4.4. To elaborate on this, specific NF-κB binding was assessed using ChIP Seq. However, NF-κB ChIP Seq showed no enrichment of NF-κB occupancy in LPS treated samples and a low overall pulldown efficiency (data not shown). First, NF-κB has multiple subunits, which may decrease pulldown efficiency since only the p65 subunit was used for the pulldown. Second, other ChIP protocols have used TNF priming in order to increase the presence of NF-κB and thus the pulldown efficiency [335]. The NF-κB consensus motif is 5´-GGGRNYYYCC-3´ (R= purine, N= any nucleotide, Y= pyrimidine) [107], so it may be interesting to test whether certain promoter sequences can fold into G4s and how NF-κB binding is affected by these secondary structures. An *in vitro* approach could test whether purified NF-κB protein can bind G4 oligonucleotides and thus would clarify which model of NF-κB binding is correct. In conclusion, G4 stabilization affects the immune response by decreasing the maturation marker expression, cytokine expression and secretion. These effects can be explained by changes in the NF-κB activity, but how NF-κB binding is affected by G4 stabilization in detail remained elusive.

4.4 G4 formation alters the chromatin landscape

The role of G4s as epigenetic modulators has recently emerged, and G4s have been found to directly interact with chromatin remodeling factors such as SWI/SNF (SWItch/Sucrose Non-Fermentable) [336]. Therefore, ATAC-Seq was performed to rule out whether and how G4 stabilization affects the chromatin landscape in macrophages. Indeed, G4s had an impact on the chromatin accessibility and the transcription factor motif occupancy (Figure 13-Figure 16). ATAC-Seq showed similar abundances of open chromatin regions in untreated and LPS treated samples that were enriched at transcription start sites (Figure 13). Thus, the open chromatin regions correlated with the highly transcribed regions in LPS treatment (Supplementary figure 4).

It has been shown that LPS activates the p38 MAPK pathway leading to phosphorylation of histone 3 at serine 10 (H3S10) and phosphorylation/ acetylation of histone 3 at serine 19 or lysine 14 (H3S10/K14) [299]. These modifications were essential for the recruitment of the transcription factor NF-κB to specific genes such as IL-12 [299]. Thus, it is postulated that some NF-κB dependent genes require phosphorylation and phosphoacetylation to make the promoters accessible for binding and to allow transcription to start [300]. Thus, LPS modulates the chromatin to express host defense related genes and makes NF-κB target promoters accessible. PDS and PDS plus LPS treatment resulted in less open chromatin regions compared to untreated and LPS (Figure 13). The chromatin at the transcription start sites was less accessible compared to untreated and LPS (Figure 13). Why the PDS chromatin regions did not correlate with the gene expression (data not shown) remains unclear. Further investigation of how G4s modify chromatin is needed to address this issue. G4s have been discussed to influence epigenetic control in cells and contribute to disease progression, such as in cancerous tissues, and G4s have also been suggested to play a role in interactions within DNA methyltransferase proteins, key enzymes in epigenetic modulation [216,336–338]. Interaction of the DNA methyltransferase 1 (DNTM1) with G4s decreased the enzyme function, resulting in a lack of methylation and putative changes in gene expression [339–341]. How G4s interact with methyltransferases, contribute to epigenetic modulation and lead to gene expression changes in detail requires further investigation.

The correlation of the ATAC-Seq peaks to G4 motifs revealed that G4 motif presence altered the chromatin landscape (Figure 15-Figure 16). The G4 motif containing peaks were broader (Figure 15), and in line it has been reported that G4s can only fold in open chromatin regions [342], thus G4s might keep the chromatin accessible after their formation. G4 motif-containing peaks were also more accessible in the surrounding chromatin (up to 5 kb), even after PDS treatment, compared to non-G4 motif-containing peaks (Figure 16), suggesting that G4 formation affects the chromatin landscape not only close to its formation site, but also in a broad window of 5 kb. How G4s influence the surrounding chromatin landscape remains an open question, it is possible that G4s interact directly with chromatin remodelers to modulate surrounding chromatin [336].

G4 stabilization by PDS had an impact on G4 motif composition (Figure 15). G4s are dynamically regulated [193], and presumably PDS stabilized the G4s that were less stable, as indicated by the stabilization of G4 motifs with longer loop size (Figure 15). In contrast, G4 motifs with more Gs in the G-tetrad and shorter loop length were detected in LPS treated samples compared to PDS (Figure 15), which are known to increase the stability [140]. The differences in the G4 topology also suggest that different G4s are folded between the treatments, which may have different cellular functions in macrophages. The G4 motif-containing peaks in the LPS treated samples were broader (Figure 16), suggesting that G4s may function as transcription factor binding hubs, as previously reported for human chromatin [196]. The peak regions that were highly accessible in LPS treatment were not accessible after co-treatment with PDS and LPS (Figure 16). This may explain the changes in gene expression observed in the 3´ RNA-Seq. The less accessible chromatin regions in PDS and LPS co-treatment compared to LPS could be located in regions important for orchestrating the immune response to bacteria, and inaccessibility could inhibit the binding of transcription factors such as NF-κB. In conclusion, G4 formation by PDS modulates the chromatin to a less accessible state at the loci that were accessible during LPS treatment. How G4 formation affects chromatin, for example by interacting with chromatin remodelers, remains to be elucidated.

4.5 G4s a possible target in sepsis

When humans are exposed to LPS due to a bacterial infection, it can cause sepsis, an endotoxic shock that is a significant cause of mortality in the intensive care unit [343,344]. Injection of the human telomeric sequence $(TTAGGG)_4$ downregulated the expression of proinflammatory cytokines by inhibiting the phosphorylation of the transcription factors signal transducer and activator of transcription 1 (STAT1) and STAT4 and protected mice from sepsis [345]. Consistent with this, STAT3, which is also a member of the Stat family, was enriched in LPS compared to LPS plus PDS in my ATAC-Seq analysis (10 times fold enrichment; data not shown).

Based on this I propose that STAT3 alterations upon G4 stabilization contribute to the downregulation of proinflammatory cytokines in mouse macrophages as well. G4 aptamers affecting the STAT3 signaling pathway were shown to have antiproliferative effects in human prostate and breast cancer cell lines [346]. STAT3 is a transcription factor involved in the expression of oncogenes in breast cancer [347] and thus STAT3 is a promising target in cancer therapy. The immunosuppressive activity of the telomeric $(TTAGGG)_n$ multimers correlated with their ability to form into G4s [325]. These studies strongly support my experiments to use G4s as a drug target to downregulate the LPS-mediated immune response and to apply this knowledge in a medical context.

In a medical context, these findings are relevant to patients suffering from an uncontrolled cytokine storm. An auto-amplifying cytokine production, known as a cytokine storm, is one of the main problems in sepsis patients [348]. Sepsis is the systemic inflammatory response to an infection, and the resulting organ failure can be life-threatening [349]. Systemic inflammatory response syndrome can also occur after surgery and has been reported as a complication after cardiovascular surgery [350].

G4 levels could be used as a biomarker before surgery, as low G4 levels may indicate an increased likelihood of a systemic inflammatory response syndrome. These patients could be treated with the telomeric $(TTAGGG)_n$ sequence before cardiovascular surgery, which inhibits phosphorylation of the STAT transcription factor family and thus presumably downregulates cytokine expression. Similarly, my study shows that G4 ligands may also

be appropriate for these patients as well. G4 stabilization putatively inhibits the binding of NF-κB to its target sequence and downregulates the expression and secretion of several cytokines. The G4 ligands already tested in clinical trials, such as CX-5461 [182], could be used for initial testing.

4.6 A model how G4s modulate the immune response to bacteria

The data presented here in combination with the current state of the research are summarized in a final putative model (Figure 17). Through a signaling cascade, LPS leads to the phosphorylation and translocation of NF-κB dimers such as p65 and p50, which bind to κB sites and activate the expression of their targets (Figure 17). The chromatin is open and accessible at the regions that are highly expressed after LPS stimulation. In turn, cytokines are expressed, and a second stimulus can lead to the inflammasome activation, resulting in the cleavage and secretion of cytokines such as IL-1 beta (Figure 17). In contrast, stabilization of G4s affects the chromatin landscape and leads to an altered less accessible chromatin at loci that are accessible after LPS stimulation. Putatively G4 formation and stabilization blocks the binding of NF-κB (Figure 17). As a result, cytokine levels are decreased. Lower levels of IL-1 beta secretion may lead to less phosphorylation of p65, thereby interrupting the positive feedback loop.

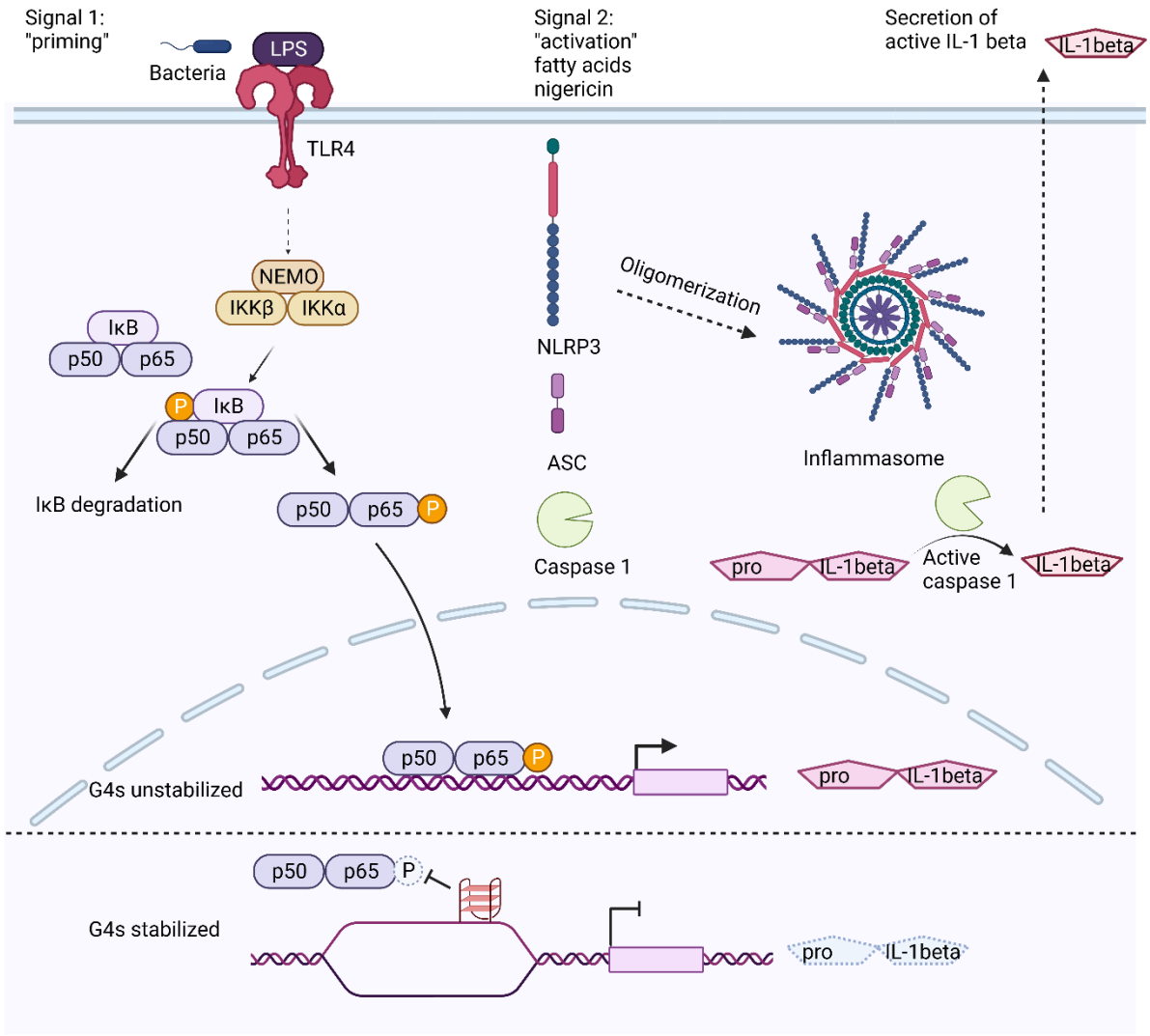

Figure 17: Putative model: G4 stabilization changes the immune response to bacterial infection.
In the upper panel of the figure the NF-κB-mediated immune response is shown with unstabilized G4 levels. G4 stabilization by PDS (lower panel) causes decreased NF-κB activity (phosphorylation of p65 and binding) because the positive feedback loop of NF-κB might be disrupted. This leads to low expression levels of cytokines like IL-1 beta that is turn also less cleaved and secreted. Low levels of secreted IL-1 beta are putatively not sufficient to regulate positively the NF-κB feedback loop. Figure created with Biorender.com.

4.7 Concluding remarks

My thesis provides a system-wide view of the role of G4s in mouse macrophages during infection by bacteria. G4 stabilization with the G4 ligand PDS results in a marked down-regulation of immune response-related gene expression and cytokine secretion after LPS stimulation. This phenotype is associated with reduced NF-κB activity. In addition, G4 stabilization alters the chromatin landscape and may thus block putative transcription start sites important for the LPS- mediated immune response and finally leading to a new model of how G4 formation alters the immune response after bacterial infection involving the NF-κB transcription factor pathway. Thus, G4s become an interesting drug target for sepsis treatment.

However, G4 stabilization by ligands such as PDS could affect all G4s currently forming in the cell, not just those relevant to inhibit cytokine expression (434,272 G4s in humans and 797,789 G4s in mice). Nevertheless, as ligand research and development continues, it may be possible in the future to target specific G4s, e.g. in the promoters of cytokines that are targeted by NF-κB.

In conclusion, the experiments in this thesis provide a new tool to down-regulate the immune response to bacteria via G4 stabilization involving modulation of the NF-κB transcription factor pathway. This not only sheds light on different functions/ roles of G4s, but highlights that G4s are an important therapeutic target and can be of great interest for treatment of sepsis patients.

5 Abstract

G-quadruplexes (G4s) are stable secondary structures that form in guanine-rich regions of DNA and RNA. Guanines bind via Hoogsteen hydrogen bonding and form G tetrads that stack upon each other and become stabilized by a cation in the center. Nowadays it is proven that G4s form *in vivo* and influence a variety of biological processes, including transcription, translation, replication, and telomere maintenance. More than 700,000 sites in the human and mouse genomes have the potential to form a G4. Since G4s are enriched in oncogenic promoters, they are targeted in cancer therapy. The contribution of tumor-associated macrophages (TAMs) in the tumor environment has been controversially discussed. Therefore, linking cancer and inflammation and analyzing the role of G4s in macrophages is an emerging research question.

The here presented doctoral thesis provides a detailed analysis of the role of G4s in mouse macrophages during bacterial infection mimicked by lipopolysaccharide (LPS). It was shown that G4s form in macrophages and can be stabilized by the G4-specific ligand pyridostatin (PDS). While the key macrophages function of phagocytosis was unaffected by G4 stabilization, G4 formation was shown to reduce the immune response-related cytokine expression and secretion. These transcriptome-wide changes affecting the immune response to bacteria are modulated by changes in the activity of the transcription factor NF-κB, a master regulator in orchestrating host defense. ATAC-Seq to map the chromatin landscape revealed that G4 stabilization modulates the accessibility of transcription start sites which could explain the transcriptomic changes.

The data presented here provide the basis for a novel role of G4s in the immune response to bacteria in macrophages. These findings open the possibility to discuss G4s as a drug target to control the immune response, for example during an endotoxic shock (sepsis) induced by exposure to LPS.

6 Supplement

IL-1 beta promoter:

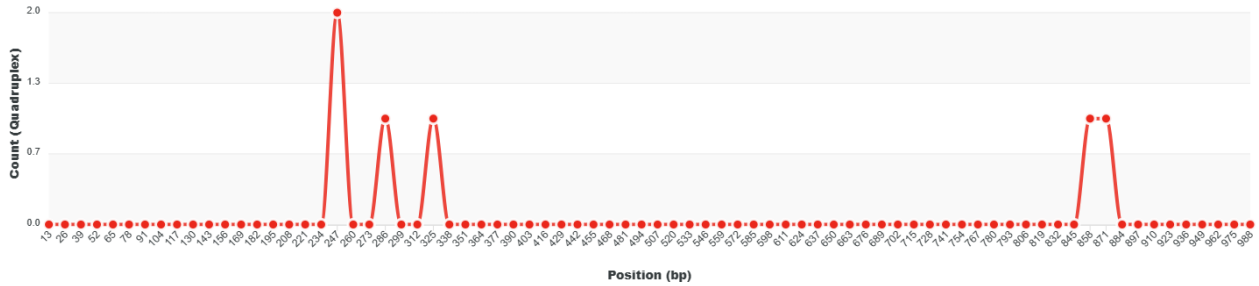

TNF alpha promoter:

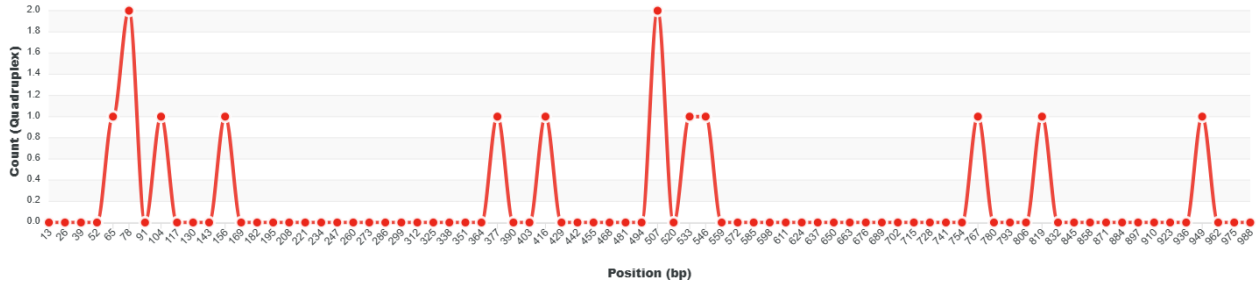

Supplementary figure 1: G4 prediction for IL-1 beta and TNF alpha promoters. G4 Hunter is a software for G4 prediction [351]. The principle of the algorithm is that every position in the sequence is given a score from -4 to 4. A score of 0 reflects A or T, whereas 1-4 represents the presence of 1-4 Gs and Cs are scored like Gs but with a negative score. The G4 hunter scores show how likely it is that a G4 could fold and the negative score how likely a G4 is on the complementary strand. The promoter sequence (1000 bp upstream) were analyzed for IL-1 beta (top) and TNF alpha (bottom). Both sequences have a G4 Hunter score of 2.

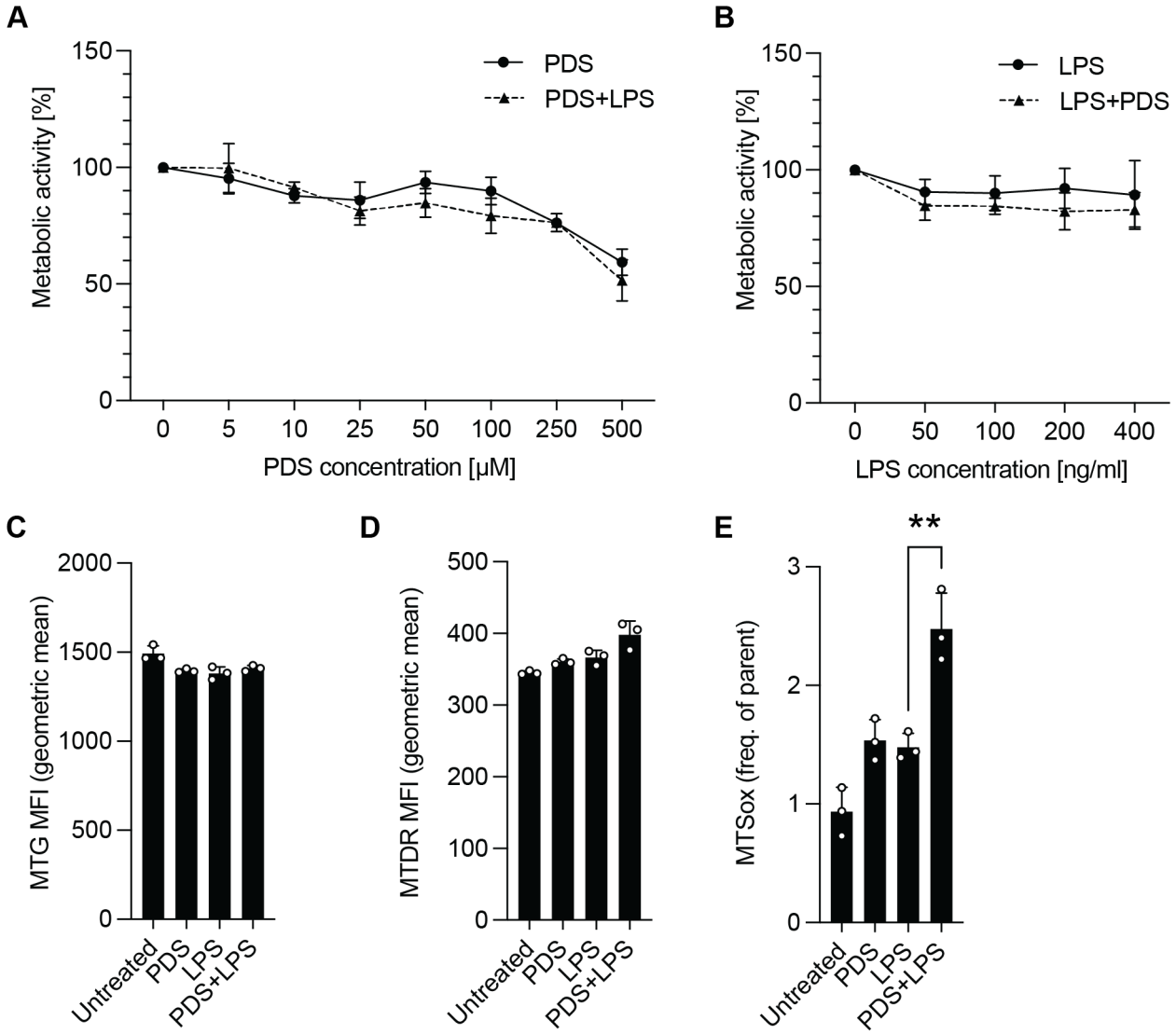

Supplementary figure 2: Metabolic and mitochondrial fitness of iBMDMs after treatment.

A-B) Alamarblue assay was used to calculate the metabolic activity of cells treated with indicated PDS and/or LPS concentrations for four hours (in this study 25 µM PDS and 200 ng/ml LPS were used, unless stated differently). C-D) iBMDMs were treated with PDS/ LPS and FACS analysis was used. MTG= MitoTracker® Green/ mitochondrial size; MTDR= MitoTracker® Deep Red/ mitochondrial membrane potential; MTSox= MitoTracker®=MitoSOX/ mitochondrial superoxide; MFI= mean fluorescence intensity; Three biological replicates are shown, p-value≤0.05=*; p-value≤0.01=** (unpaired t-test); scatter plot mean with SD.

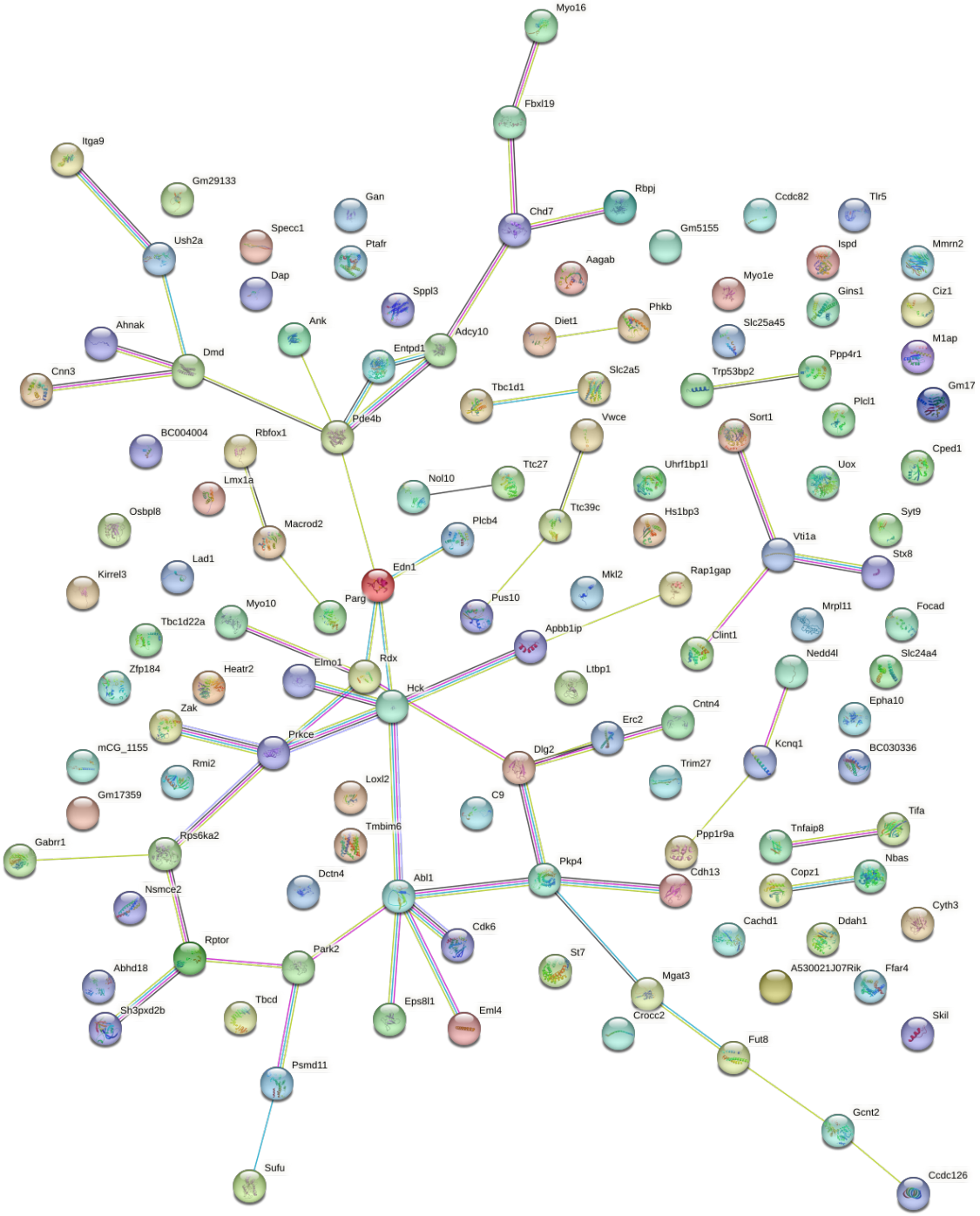

Supplementary figure 3: Protein interaction network for LPS treated samples (BG4 CUT&Tag).
The 479 peaks called with MACS2 in the LPS treatment in CUT&Tag were assigned to 146 gene coding proteins. The analysis displays the protein interaction network, physical and functional interactions were considered (created with STRING).

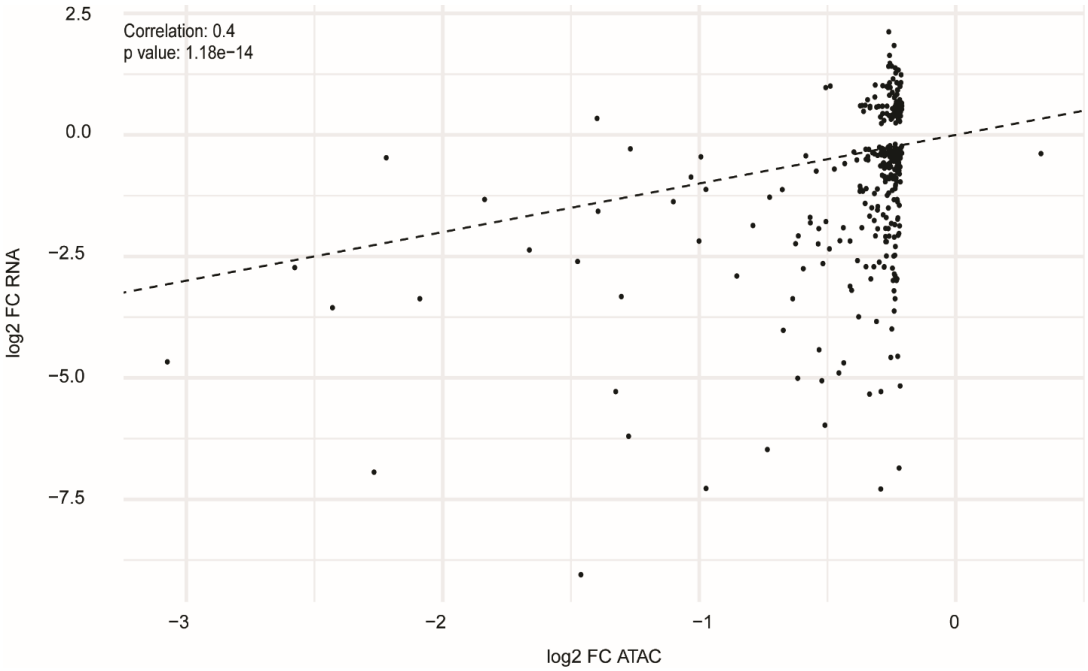

Supplementary figure 4: ATAC-Seq and 3´RNA-Seq correlation for LPS treated samples.
log2 fold changes (FC) correlate between ATAC-Seq and 3´RNA-Seq for the LPS treated sample. The correlation of the linear regression is 0.4 and is significantly ($p<0.005$). All three biological replicates of the 3´RNA-Seq and ATAC-Seq were considered. In cooperation with Jasper Spitzer (Schmidt laboratory).

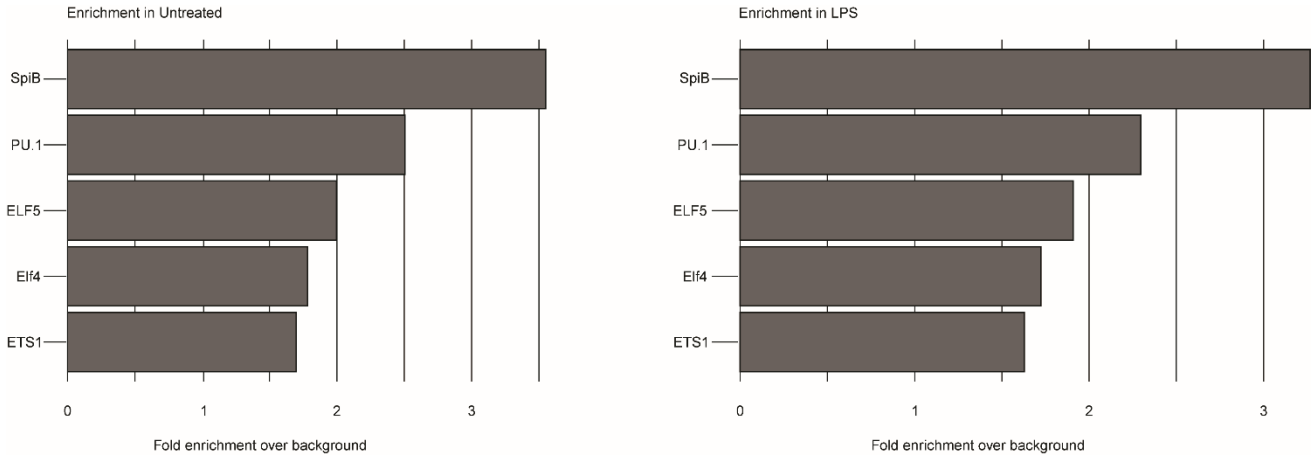

Supplementary figure 5: ATAC-Seq peak motif enrichment for untreated and LPS treated samples.
The motif enrichment for the ATAC-Seq peaks for untreated and LPS treated samples. Spi-B transcription factor (SpiB); Transcription factor PU.1 (PU.1); E74 Like ETS Transcription Factor 5 (ELF5); E74 Like ETS Transcription Factor 4 (Elf4); Protein C-ets-1 (ETS1). All three biological replicates of the ATAC-Seq were considered. In cooperation with Jasper Spitzer (Schmidt laboratory).

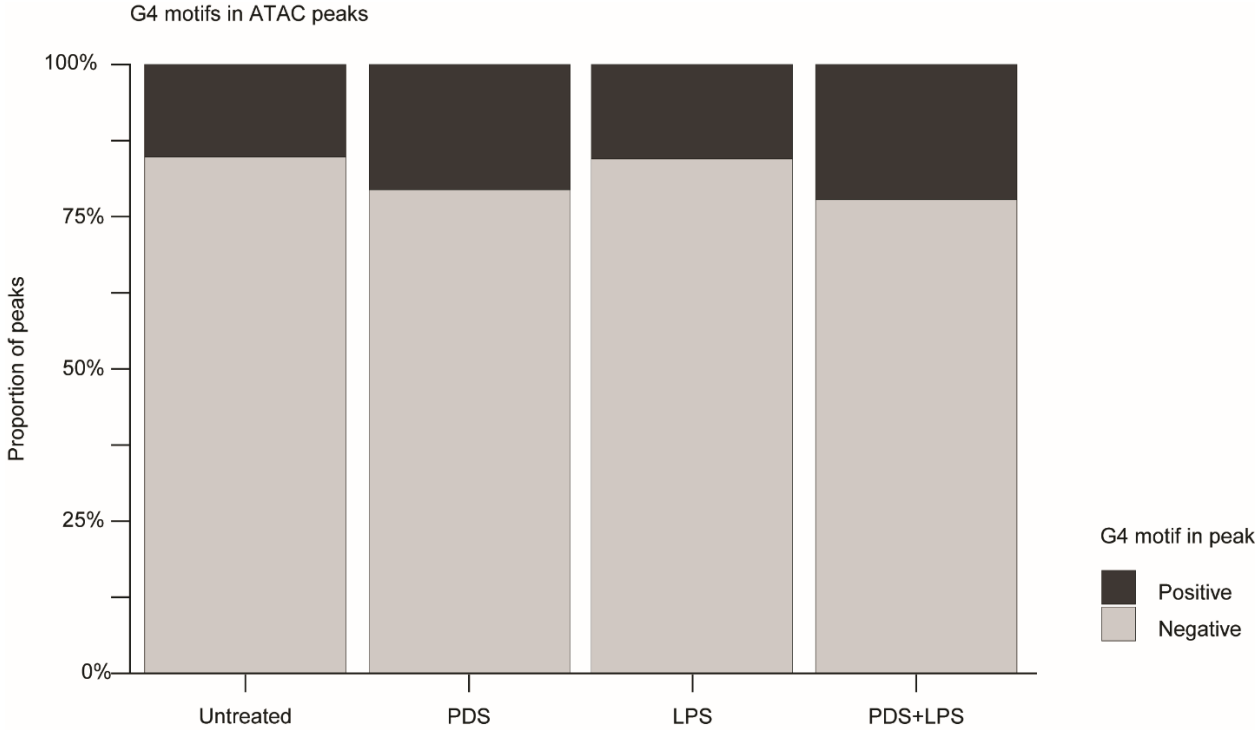

Supplementary figure 6: Correlation of G4 motifs to ATAC-Seq peaks.
The ATAC-Seq peaks were analyzed based on their proportions of G4 motifs or no G4 motif. All three biological replicates of the ATAC-Seq were considered. In cooperation with Jasper Spitzer (Schmidt laboratory).

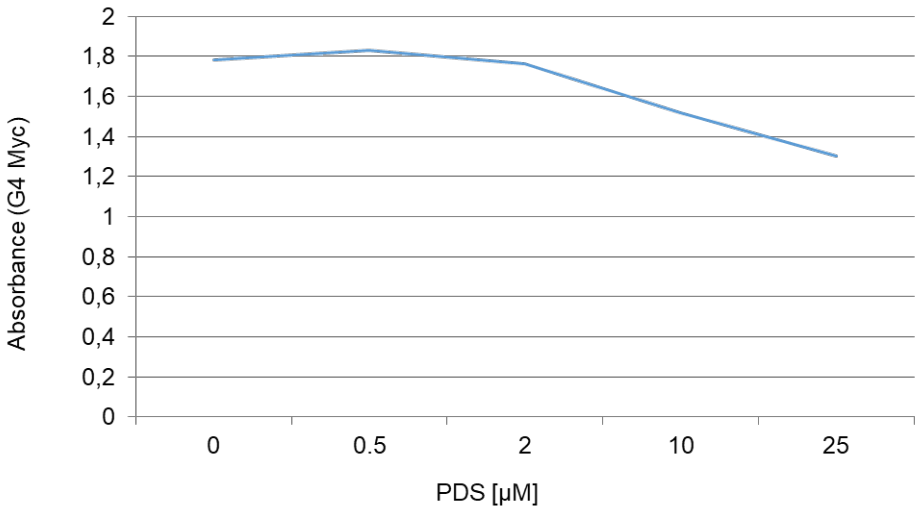

Supplementary figure 7: BG4 EILSA with increasing PDS concentrations.
The x-axis displays the PDS concentrations in µM and the y-axis shows the absorbance of the G4. With increasing PDS concentrations the absorbance decreases. The experiment was performed in cooperation with Theresa Zacheja.

7 List of figures

8 List of tables

9 Tables

The following tables are in addition to the Chapter 2 Material and Methods.

Table 3: Chemicals

Chemicals	Identifier	Supplier
Benzonase	E1014-25KU	Sigma-Aldrich
BSA	A6588.0050	AppliChem
Cobalt resin	89964	Thermo Fisher Scientific
Dynabeads Protein G	10003D	Thermo Fisher Scientific
Fluoroshield with DAPI	F6057-20ML	Sigma-Aldrich
Formaldehyde	4235.1	Roth
Glycine	3790.4	Roth
H_2O_2, 30 % (w/w)	H1009-5ML	Sigma-Aldrich
LPS	L7770-1MG	Sigma-Aldrich
Methanol	1060091011	Merck
Milk powder	T145.2	Roth
Nigericin	tlrl-nig-5	Invivogen
PDS	S7444-25MG	Selleckchem
Protease inhibitor	5056489001	Roche
Proteinase K	RP107B-5	7BioScience
Proteinmarker prestained	1123YL500	BioLabs

Table 4: Antibodies

Antibody	Dilution	Identifier	Supplier
Anti-FLAG	1:800	2368S	Cell Signaling
Anti-Rabbit Alexa Fluor	1:1000	A11008	Thermo Fisher Scientific
BG4	2 µg		self-purified
CD11b FITC	1:400	553310	Pharmingen
CD40 PE	1:200	12-0401-83	eBioScience
CD80-AF647	1:200	104718	eBioScience
Donkey anti-mouse 800 CW	1:10,000	926-32212	LI-COR
Donkey anti-rabbit 800 CW	1:10,000	926-32213	LI-COR
F4/80-BV421	1:400	123132	Biolegend
Fcblock	1:100	14-0161-86	Invitrogen
GAPDH	1:1000	sc69778	Sanra Cruz
Histone H3	1:1000	Ab1791	Abcam
L/D Near-IR	1:800	L34976A	Invitrogen
MitoSox-PE	1:4000	M36008	Invitrogen
MTDR-APC	1:4000	M22426	Invitrogen
MTG-FITC	1:4000	M7514	Invitrogen
p65	1:300	sc8008	Sanra Cruz
Phospho p65	1:1000	9936	Cell Signaling
Phospho-Histone H2A.X	1:1000	9718	Cell Signaling

Table 5: Primer

Name	Sequence (5´-3´)
GAPDH mouse fw	ACCACAGTCCATGCCATCAC
GAPDH mouse rv	TCCACCACCCTGTTGCTGTA
IL1-beta mouse fw	GCAACTGTTCCTGAACTCAACT
IL1-beta mouse rv	ATCTTTTGGGGTCCGTCAACT

Table 6: Buffers and solutions

Buffer	Composition
Antibody binding buffer (CUT&Tag)	wash buffer with 1% BSA, 2 mM EDTA, 0.05% digitonin
ATAC lysis buffer	10 mM Tris-Cl pH 7.4, 10 mM NaCl, 3 mM MgCl2, 0.1% (v/v) NP-40
Blocking buffer (BG4 IF)	2% milk (in PBS)
Blocking buffer (ChIP)	25 mM HEPES pH 7.5, 10.5 mM NaCl, 110 mM KCl, 1 mM MgCl2, 1% (w/v) BSA
Coomassie staining solution	0.25% Coomassie Brilliant Blue G-250, 50% EtOH, 10% acetic acid
DIG-Wash-BSA (CUT&Tag)	20 mM HEPES ph 7.5, 300 mM NaCl, 0.5 mM spermidine, 1% BSA, 0.01% digitonin
Elution (BG4)	PBS pH=8, 250 mM imidazole
FACS	1x PBS, 0.5 % FCS, 0.2 % sodium azide
Fix solution (BG4 IF)	methanol and acetic acid (3:1)
Intracellular cell salt	25 mM HEPES, 110 mM KCl, 10.5 mM NaCl, 1 mM MgCl2
NP40 lysis	50 mM HEPES pH 7.5, 150 mM KCl, 2 mM Na EDTA, 0.5% (v/v) NP-40 substitute, 1 mM NaF, freshly added before use: 0.5 mM DTT, 0.2 mM PMSF, 1 mM LP, 1 mM AP, 0.1 mM AEBSF
PBS	137 mM NaCl, 2.7 mM KCl, 8 mM Na2HPO4, 2 mM KH2PO4
Permeabilization solution (BG4 IF)	0.1% triton (in PBS)
Pre-fix solution (BG4 IF)	50% DMEM, 50% fix solution
SDS loading dye (6x)	300 mM Tris-HCl pH 6.8, 120 mM DTT, 9% (w/v) SDS, 48% (v/v) glycerol, 0.1% (v/v) Bromphenol blue
SDS running buffer (10x)	0.25 M Tris base, 1.92 M glycine, 1% (w/v) SDS
Separating gel buffer (4x)	1.5 M Tris-HCl pH 8.8, 0.4% (w/v) SDS
SOC	2% (w/v) tryptone, 10 mM NaCl, 0.5% (w/v) yeast extract, 10 mM MgSO4, 10 mM MgCl2, 2.5 mM KCl, 2% (w/v) glucose
Stacking gel buffer (4x)	0.5 M Tris-HCl pH 6.8, 0.4% (w/v) SDS
Tagmentation buffer (CUT&Tag)	DIG-Wash-BSA with 10 mM MgCl2

TBS-T	10 mM Tris-HCl pH 7.5, 150 mM NaCl, 0.05% (v/v) Tween20
TE buffer (ChIP)	10 mM Tris pH 8, 0.1 mM EDTA, 1% (w/v) SDS
TES (BG4)	50 mM Tris pH 8, 20% sucrose, 1 mM EDTA pH 8
Wash buffer (BG4)	PBS pH 8, 100 mM NaCl, 10 mM imidazole
Wash buffer (CUT&Tag)	20 mM HEPES pH 7.5, 150 mM NaCl, 0.5 mM spermidine
Washing buffer (BG4 IF)	0.1% Tween (in PBS)
Washing buffer (ChIP)	100 mM KCl, 0.1% (v/v) Tween 20, 10 mM Tris-HCl pH 7.4
Western blotting buffer	50 mM Tris base, 50 mM glycine, 20% (v/v) methanol

Table 7: Commercial systems

Kit/ System	Identifier	Supplier
AlamarBlue Cell Viability Assay Reagent	GENO786-921	VWR
IQ SYBR Green	170-8885	BioRad
QuantiTect Reverse Transcription Kit	205313	Qiagen
MinElute cleanup kit	28206	Qiagen
PROCARTAPLEX 9 PLEX	D4445144	Thermo Fisher Scientific
TRIzol	15596018	Thermo Fisher Scientific
Chromatrap hypotonic and lysis buffer	100008	Biozol
Quanti Blue solution	rep-qbs3	Invivogen
HTRF IL-1 beta	62MIL1BPEG	Cisbio

Table 8: Cell culture growth media and supplements

Solution	Identifier	Supplier
DMEM, high glucose	41965039	Thermo Fisher Scientific
DPBS, no calcium, no magnesium	14190094	Thermo Fisher Scientific
Fetal Bovine Serum (FBS)	10500064	Thermo Fisher Scientific
Penicillin-Streptomycin (10,000 U/ml) (PenStrep)	15140122	Thermo Fisher Scientific
Trypsin-EDTA (0.25%), phenol red	25200056	Thermo Fisher Scientific
Normocin	ant-nr-1	Invivogen
Zeocin	ant-zn-05	Invivogen

Table 9: Bacterial growth media and plates

Medium	Composition
2x TY medium	16 g/L tryptone, 10 g/L yeast extract, 5 g/L NaCl
LB agar	0.5% yeast extract, 1% tryptone, 0.5% NaCl, 2% agar
LB liquid	0.5% yeast extract, 1% tryptone, 0.5% NaCl
BHI plates	200 g calf brain infusion, 200 g beef heart infusion, 10 g proteose peptone, 5 g NaCl, 2.5 g Na2HPO4, 2 g dextrose, 15 g/L agar

Table 10: Antibiotics

Antibiotic	Identifier	Supplier
Ampicillin	K029.5	Carl Roth GmbH
Kanamycin	T832.3	Carl Roth GmbH

Table 11: Bacterial strains

Strain	Genotype	Supplier
DH5α	F- ϕ80lacZΔM15 Δ(lacZYA- argF)U169 deoR recA1 endA1 hsdR17(rk- , mk+) phoA supE44 thi-1 gyrA96 relA1 λ	Thermo Fisher Scientific
BL21	F– ompT hsdSB (rB–, mB–) gal dcm (DE3)	Thermo Fisher Scientific

Table 12: Eukaryotic cell lines

Cell line	Description	Supplier
iBMDMs (immortalized bone-marrow-derived macrophages)	[256]	Abdullah Lab
RAW-Blue NF-kB SEAP reporter	raw-sp	Invivogen

10 References

1. Feng, J. X. & Riddle, N. C. Epigenetics and genome stability. *Mamm Genome* **31**, 181–195 (2020).
2. Nicholson, L. B. The immune system. *Essays Biochem* **60**, (2016).
3. Parkin, J. & Cohen, B. An overview of the immune system. *Lancet* **357**, 1777–1789 (2001).
4. Drew, G. C., Stevens, E. J. & King, K. C. Microbial evolution and transitions along the parasite–mutualist continuum. *Nature Reviews Microbiology 2021 19:10* **19**, 623–638 (2021).
5. Thursby, E. & Juge, N. Introduction to the human gut microbiota. *Biochemical Journal* vol. 474 Preprint at https://doi.org/10.1042/BCJ20160510 (2017).
6. Boada-Romero, E., Martinez, J., Heckmann, B. L. & Green, D. R. The clearance of dead cells by efferocytosis. *Nature Reviews Molecular Cell Biology* vol. 21 Preprint at https://doi.org/10.1038/s41580-020-0232-1 (2020).
7. Vivier, E. & Malissen, B. Innate and adaptive immunity: specificities and signaling hierarchies revisited. *Nature Immunology 2005 6:1* **6**, 17–21 (2004).
8. Jastania, R., Geddie, W. R., Chapman, W. & Boerner, S. Secretion of lysosomal hydrolases by stimulated and nonstimulated macrophages. *J Exp Med* **148**, 435–428 (1978).
9. Tomar, N. & De, R. K. A brief outline of the immune system. *Methods in Molecular Biology* **1184**, (2014).
10. Finlay, B. B. & McFadden, G. Anti-immunology: Evasion of the host immune system by bacterial and viral pathogens. *Cell* vol. 124 Preprint at https://doi.org/10.1016/j.cell.2006.01.034 (2006).
11. Fällman, M., Persson, C. & Wolf-Watz, H. Yersinia proteins that target host cell signaling pathways. *Journal of Clinical Investigation* vol. 99 Preprint at https://doi.org/10.1172/JCI119270 (1997).
12. The History of Plague – Part 1. The Three Great Pandemics - JMVH. https://jmvh.org/article/the-history-of-plague-part-1-the-three-great-pandemics/.
13. Lewis, K. The Science of Antibiotic Discovery. *Cell* vol. 181 Preprint at https://doi.org/10.1016/j.cell.2020.02.056 (2020).

14. Hutchings, M., Truman, A. & Wilkinson, B. Antibiotics: past, present and future. *Current Opinion in Microbiology* vol. 51 Preprint at https://doi.org/10.1016/j.mib.2019.10.008 (2019).
15. The innate and adaptive immune systems. Institute for Quality and Efficiency in Health Care (2020). https://www.ncbi.nlm.nih.gov/books/NBK279396/
16. Gadjeva, M. The complement system. Overview. *Methods Mol Biol* **1100**, 1–9 (2014).
17. Li, D. & Wu, M. Pattern recognition receptors in health and diseases. *Signal Transduction and Targeted Therapy* vol. 6 Preprint at https://doi.org/10.1038/s41392-021-00687-0 (2021).
18. Takeda, K. & Akira, S. Toll-like receptors. *Curr Protoc Immunol* **109**, 14.12.1-14.12.10 (2015).
19. Nikolakopoulou, C., Willment, J. A. & Brown, G. D. C-Type Lectin Receptors in Antifungal Immunity. *Adv Exp Med Biol* **1204**, 1–30 (2020).
20. Rehwinkel, J. & Gack, M. U. RIG-I-like receptors: their regulation and roles in RNA sensing. *Nat Rev Immunol* **20**, 537–551 (2020).
21. Marshall, J. S., Warrington, R., Watson, W. & Kim, H. L. An introduction to immunology and immunopathology. *Allergy, Asthma and Clinical Immunology* vol. 14 Preprint at https://doi.org/10.1186/s13223-018-0278-1 (2018).
22. Underhill, D. M., Bassetti, M., Rudensky, A. & Aderem, A. Dynamic Interactions of Macrophages with T Cells during Antigen Presentation. *J Exp Med* **190**, 1909 (1999).
23. Geissmann, F. *et al.* Development of monocytes, macrophages, and dendritic cells. *Science* vol. 327 Preprint at https://doi.org/10.1126/science.1178331 (2010).
24. Cabeza-Cabrerizo, M., Cardoso, A., Minutti, C. M., Pereira Da Costa, M. & Reis E Sousa, C. Dendritic Cells Revisited. *Annual Review of Immunology* vol. 39 Preprint at https://doi.org/10.1146/annurev-immunol-061020-053707 (2021).
25. Lacy, P. Mechanisms of Degranulation in Neutrophils. *Allergy, Asthma & Clinical Immunology* **2**, (2006).
26. Vivier, E., Tomasello, E., Baratin, M., Walzer, T. & Ugolini, S. Functions of natural killer cells. *Nature Immunology* vol. 9 Preprint at https://doi.org/10.1038/ni1582 (2008).

27. Min, B., Brown, M. A. & Legros, G. Understanding the roles of basophils: Breaking dawn. *Immunology* vol. 135 Preprint at https://doi.org/10.1111/j.1365-2567.2011.03530.x (2012).
28. Shah, H., Eisenbarth, S., Tormey, C. A. & Siddon, A. J. Behind the scenes with basophils: an emerging therapeutic target. *Immunotherapy Advances* vol. 1 Preprint at https://doi.org/10.1093/immadv/ltab008 (2021).
29. Ackerman, S. J. *et al.* Ex Vivo Models for the Study of Eosinophils. *Eosinophils in Health and Disease* 39–71 (2013) doi:10.1016/B978-0-12-394385-9.00004-3.
30. Wen, T. & Rothenberg, M. E. The Regulatory Function of Eosinophils. *Microbiol Spectr* **4**, (2016).
31. Lichterman, J. N. & Reddy, S. M. Mast cells: A new frontier for cancer immunotherapy. *Cells* **10**, (2021).
32. Dunkelberger, J. R. & Song, W. C. Complement and its role in innate and adaptive immune responses. *Cell Research 2010 20:1* **20**, 34–50 (2009).
33. Sarma, J. V. & Ward, P. A. The complement system. *Cell Tissue Res* **343**, 227 (2011).
34. Natoli, G. & Ostuni, R. Adaptation and memory in immune responses. *Nature Immunology 2019 20:7* **20**, 783–792 (2019).
35. Kumar, B. V., Connors, T. J. & Farber, D. L. Human T Cell Development, Localization, and Function throughout Life. *Immunity* vol. 48 Preprint at https://doi.org/10.1016/j.immuni.2018.01.007 (2018).
36. Seder, R. A. & Ahmed, R. Similarities and differences in CD4+ and CD8+ effector and memory T cell generation. *Nature Immunology* vol. 4 Preprint at https://doi.org/10.1038/ni969 (2003).
37. Luckheeram, R. V., Zhou, R., Verma, A. D. & Xia, B. $CD4^+$T cells: differentiation and functions. *Clin Dev Immunol* **2012**, (2012).
38. Raskov, H., Orhan, A., Christensen, J. P. & Gögenur, I. Cytotoxic CD8+ T cells in cancer and cancer immunotherapy. *British Journal of Cancer* vol. 124 Preprint at https://doi.org/10.1038/s41416-020-01048-4 (2021).
39. Neefjes, J., Jongsma, M. L. M., Paul, P. & Bakke, O. Towards a systems understanding of MHC class i and MHC class II antigen presentation. *Nature Reviews Immunology* vol. 11 Preprint at https://doi.org/10.1038/nri3084 (2011).

40. Eibel, H., Kraus, H., Sic, H., Kienzler, A.-K. & Rizzi, M. B cell Biology: An Overview. *Curr Allergy Asthma Rep* **14**, (2014).
41. Lu, L. L., Suscovich, T. J., Fortune, S. M. & Alter, G. Beyond binding: Antibody effector functions in infectious diseases. *Nature Reviews Immunology* vol. 18 Preprint at https://doi.org/10.1038/nri.2017.106 (2018).
42. Gaudino, S. J. & Kumar, P. Cross-talk between antigen presenting cells and T cells impacts intestinal homeostasis, bacterial infections, and tumorigenesis. *Frontiers in Immunology* vol. 10 Preprint at https://doi.org/10.3389/fimmu.2019.00360 (2019).
43. Cancro, M. P. & Tomayko, M. M. Memory B cells and plasma cells: The differentiative continuum of humoral immunity. *Immunological Reviews* vol. 303 Preprint at https://doi.org/10.1111/imr.13016 (2021).
44. Palm, A. K. E. & Henry, C. Remembrance of Things Past: Long-Term B Cell Memory After Infection and Vaccination. *Frontiers in immunology* vol. 10 Preprint at https://doi.org/10.3389/fimmu.2019.01787 (2019).
45. Dranoff, G. Cytokines in cancer pathogenesis and cancer therapy. *Nature Reviews Cancer 2004 4:1* **4**, 11–22 (2004).
46. Comparing the Innate and Adaptive Immune Systems | Seattle, WA Patch. https://patch.com/washington/seattle/comparing-innate-adaptive-immune-systems.
47. Kogut, M. H., Lee, A. & Santin, E. Microbiome and pathogen interaction with the immune system. *Poult Sci* **99**, (2020).
48. Sameer, A. S. & Nissar, S. Toll-Like Receptors (TLRs): Structure, Functions, Signaling, and Role of Their Polymorphisms in Colorectal Cancer Susceptibility. *BioMed Research International* vol. 2021 Preprint at https://doi.org/10.1155/2021/1157023 (2021).
49. Beutler, B. Innate immunity: An overview. *Mol Immunol* **40**, (2004).
50. Brubaker, S. W., Bonham, K. S., Zanoni, I. & Kagan, J. C. Innate immune pattern recognition: a cell biological perspective. *Annu Rev Immunol* **33**, 257–290 (2015).
51. Ciesielska, A., Matyjek, M. & Kwiatkowska, K. TLR4 and CD14 trafficking and its influence on LPS-induced pro-inflammatory signaling. *Cell Mol Life Sci* **78**, 1233–1261 (2021).
52. Vaure, C. & Liu, Y. A comparative review of toll-like receptor 4 expression and functionality in different animal species. *Front Immunol* **5**, (2014).

53. Yang, H. *et al.* MD-2 is required for disulfide HMGB1-dependent TLR4 signaling. *J Exp Med* **212**, 5–14 (2015).
54. Jiang, D. *et al.* Regulation of lung injury and repair by Toll-like receptors and hyaluronan. *Nat Med* **11**, 1173–1179 (2005).
55. Ryu, J. K. *et al.* Reconstruction of LPS Transfer Cascade Reveals Structural Determinants within LBP, CD14, and TLR4-MD2 for Efficient LPS Recognition and Transfer. *Immunity* **46**, (2017).
56. Lizundia, R., Sauter, K. S., Taylor, G. & Werling, D. Host species-specific usage of the TLR4-LPS receptor complex. *Innate Immun* **14**, 223–231 (2008).
57. Suttles, J. & Stout, R. D. Macrophage CD40 signaling: a pivotal regulator of disease protection and pathogenesis. *Semin Immunol* **21**, 257–264 (2009).
58. Bullock, T. N. J. CD40 stimulation as a molecular adjuvant for cancer vaccines and other immunotherapies. *Cellular & Molecular Immunology 2021 19:1* **19**, 14–22 (2021).
59. Lu, Y. C., Yeh, W. C. & Ohashi, P. S. LPS/TLR4 signal transduction pathway. *Cytokine* **42**, 145–151 (2008).
60. Mazgaeen, L. & Gurung, P. Recent advances in lipopolysaccharide recognition systems. *International Journal of Molecular Sciences* vol. 21 Preprint at https://doi.org/10.3390/ijms21020379 (2020).
61. Ting, J. P. Y. *et al.* The NLR gene family: An official nomenclature. *Immunity* **28**, (2008).
62. Swanson, K. V., Deng, M. & Ting, J. P. Y. The NLRP3 inflammasome: molecular activation and regulation to therapeutics. *Nature Reviews Immunology* vol. 19 Preprint at https://doi.org/10.1038/s41577-019-0165-0 (2019).
63. Kelley, N., Jeltema, D., Duan, Y. & He, Y. The NLRP3 inflammasome: An overview of mechanisms of activation and regulation. *International Journal of Molecular Sciences* vol. 20 Preprint at https://doi.org/10.3390/ijms20133328 (2019).
64. Mariathasan, S. *et al.* Cryopyrin activates the inflammasome in response to toxins and ATP. *Nature* **440**, 228–232 (2006).
65. Surprenant, A., Rassendren, F., Kawashima, E., North, R. A. & Buell, G. The Cytolytic P2Z Receptor for Extracellular ATP Identified as a P2X Receptor (P2X7). *Science (1979)* (1996) doi:10.1126/SCIENCE.272.5262.735.

66. Walev, I., Reske, K., Palmer, M., Valeva, A. & Bhakdi, S. Potassium-inhibited processing of IL-1 beta in human monocytes. *EMBO J* **14**, 1607–1614 (1995).
67. Perregaux, D. & Gabel, C. A. Interleukin-1β maturation and release in response to ATP and nigericin. Evidence that potassium depletion mediated by these agents is a necessary and common feature of their activity. *Journal of Biological Chemistry* **269**, (1994).
68. Shostak, K. & Chariot, A. NF-κB, stem cells and breast cancer: The links get stronger. *Breast Cancer Research* **13**, 1–7 (2011).
69. O'Brien, W. T. *et al.* The NLRP3 inflammasome in traumatic brain injury: potential as a biomarker and therapeutic target. *Journal of Neuroinflammation 2020 17:1* **17**, 1–12 (2020).
70. Peng, C., Ouyang, Y., Lu, N. & Li, N. The NF-κB Signaling Pathway, the Microbiota, and Gastrointestinal Tumorigenesis: Recent Advances. *Front Immunol* **11**, 1387 (2020).
71. Blevins, H. M., Xu, Y., Biby, S. & Zhang, S. The NLRP3 Inflammasome Pathway: A Review of Mechanisms and Inhibitors for the Treatment of Inflammatory Diseases. *Front Aging Neurosci* **14**, (2022).
72. Metchnikoff, E. The Comparative Pathology of Inflammation. *Nature 1894 50:1287* **50**, 194–195 (1894).
73. Pittet, M. J., Nahrendorf, M. & Swirski, F. K. The journey from stem cell to macrophage. *Ann N Y Acad Sci* **1319**, 1–18 (2014).
74. Epelman, S., Lavine, K. J. & Randolph, G. J. Origin and Functions of Tissue Macrophages. *Immunity* vol. 41 Preprint at https://doi.org/10.1016/j.immuni.2014.06.013 (2014).
75. Moore, M. A. S. & Metcalf, D. Ontogeny of the Haemopoietic System: Yolk Sac Origin of In Vivo and In Vitro Colony Forming Cells in the Developing Mouse Embryo*. *Br J Haematol* **18**, 279–296 (1970).
76. Mass, E., Nimmerjahn, F., Kierdorf, K. & Schlitzer, A. Tissue-specific macrophages: how they develop and choreograph tissue biology. *Nature Reviews Immunology 2023* 1–17 (2023) doi:10.1038/s41577-023-00848-y.

77. Hoeksema, M. A. & Glass, C. K. Nature and nurture of tissue-specific macrophage phenotypes. *Atherosclerosis* vol. 281 Preprint at https://doi.org/10.1016/j.atherosclerosis.2018.10.005 (2019).
78. Lendeckel, U., Venz, S. & Wolke, C. Macrophages: shapes and functions. *ChemTexts* **8**, 1–12 (2022).
79. Yunna, C., Mengru, H., Lei, W. & Weidong, C. Macrophage M1/M2 polarization. *European Journal of Pharmacology* vol. 877 Preprint at https://doi.org/10.1016/j.ejphar.2020.173090 (2020).
80. Liu, J., Geng, X., Hou, J. & Wu, G. New insights into M1/M2 macrophages: key modulators in cancer progression. *Cancer Cell International* vol. 21 Preprint at https://doi.org/10.1186/s12935-021-02089-2 (2021).
81. Chávez-Galán, L., Olleros, M. L., Vesin, D. & Garcia, I. Much more than M1 and M2 macrophages, there are also CD169+ and TCR+ macrophages. *Frontiers in Immunology* vol. 6 Preprint at https://doi.org/10.3389/fimmu.2015.00263 (2015).
82. El-Zayat, S. R., Sibaii, H. & Mannaa, F. A. Toll-like receptors activation, signaling, and targeting: an overview. *Bulletin of the National Research Centre 2019 43:1* **43**, 1–12 (2019).
83. Mosser, D. M., Hamidzadeh, K. & Goncalves, R. Macrophages and the maintenance of homeostasis. *Cellular & Molecular Immunology 2020 18:3* **18**, 579–587 (2020).
84. Brown, G. C. & Neher, J. J. Microglial phagocytosis of live neurons. *Nat Rev Neurosci* **15**, 209–216 (2014).
85. Grigoryeva, L. S. & Cianciotto, N. P. Human macrophages utilize a wide range of pathogen recognition receptors to recognize Legionella pneumophila, including Toll-Like Receptor 4 engaging Legionella lipopolysaccharide and the Toll-like Receptor 3 nucleic-acid sensor. *PLoS Pathog* **17**, e1009781 (2021).
86. Law, S. K. A. C3 receptors on macrophages. *J Cell Sci* (1988) doi:10.1242/jcs.1988.supplement_9.4.
87. Ward, D. M., Leslie, J. D. & Kaplan, J. Homotypic lysosome fusion in macrophages: analysis using an in vitro assay. *J Cell Biol* **139**, 665–673 (1997).
88. Watts, C. Capture and processing of exogenous antigens for presentation on MHC molecules. *Annu. Rev. Immunol* **15**, 821–50 (1997).

89. Guerriero, J. L. Macrophages: Their Untold Story in T Cell Activation and Function. *Int Rev Cell Mol Biol* **342**, 73–93 (2019).
90. Craig, M. & Slauch, J. M. Phagocytic superoxide specifically damages an extracytoplasmic target to inhibit or kill Salmonella. *PLoS One* **4**, (2009).
91. Zigmond, E. *et al.* Infiltrating monocyte-derived macrophages and resident kupffer cells display different ontogeny and functions in acute liver injury. *J Immunol* **193**, 344–353 (2014).
92. Duque, G. A. & Descoteaux, A. Macrophage cytokines: Involvement in immunity and infectious diseases. *Frontiers in Immunology* vol. 5 Preprint at https://doi.org/10.3389/fimmu.2014.00491 (2014).
93. McWhorter, F. Y., Wang, T., Nguyen, P., Chung, T. & Liu, W. F. Modulation of macrophage phenotype by cell shape. *Proc Natl Acad Sci U S A* **110**, 17253–17258 (2013).
94. Royall, J. A. *et al. Tumor necrosis factor and interleukin ICU increase vascular endothelial permeability*. (1989).
95. Chan, S. H. *et al. Induction of Interferon y Production by Natural Killer Cell Stimulatory Factor: Characterization of the Responder Cells and Synergy with Other Inducers*. http://rupress.org/jem/article-pdf/173/4/869/1101450/869.pdf (1991).
96. Bressler, P. *et al.* Mutational analysis of the p50 subunit of NF-kappa B and inhibition of NF-kappa B activity by trans-dominant p50 mutants. *J Virol* **67**, 288 (1993).
97. Steward, R. Dorsal, an Embryonic Polarity Gene in Drosophila, Is Homologous to the Vertebrate Proto-Oncogene, c-rel. *Science (1979)* **238**, 692–694 (1987).
98. Wilhelmsen, K. C., Eggleton, K. & Temin, H. M. Nucleic acid sequences of the oncogene v-rel in reticuloendotheliosis virus strain T and its cellular homolog, the proto-oncogene c-rel. *J Virol* **52**, 172–182 (1984).
99. Brownell,', E., O'brien, S. J., Nash, W. G. & Rice', N. Genetic characterization of human c-rel sequences. *Mol Cell Biol* **5**, 2826 (1985).
100. Gilmore, T. D. Introduction to NF-κB: Players, pathways, perspectives. *Oncogene* vol. 25 Preprint at https://doi.org/10.1038/sj.onc.1209954 (2006).
101. Müller, C. W., Van Duyne, F. A., Sodeoka, M., Verdine, G. L. & Harrison, S. C. Structure of the nf-κb p50 homodimer bound to dna. *Nature* **373**, (1995).

102. Biancalana, M., Natan, E., Lenardo, M. J. & Fersht, A. R. NF-κB Rel subunit exchange on a physiological timescale. *Protein Science* **30**, (2021).
103. Hayden, M. S. & Ghosh, S. Shared Principles in NF-κB Signaling. *Cell* vol. 132 Preprint at https://doi.org/10.1016/j.cell.2008.01.020 (2008).
104. Ballard, D. W. *et al.* The we/ Oncogene Encodes a KB Enhancer Binding Protein That Inhibits NFKB Function. *Cell* **63**, 603–614 (1990).
105. Liu, T., Zhang, L., Joo, D. & Sun, S. C. NF-κB signaling in inflammation. *Signal Transduction and Targeted Therapy* vol. 2 Preprint at https://doi.org/10.1038/sigtrans.2017.23 (2017).
106. Hoffmann, A., Levchenko, A., Scott, M. L. & Baltimore, D. The IkappaB-NF-kappaB signaling module: temporal control and selective gene activation. *Science* **298**, 1241–1245 (2002).
107. Chen, F. E., Huang, D. Bin, Chen, Y. Q. & Ghosh, G. Crystal structure of p50/p65 heterodimer of transcription factor NF-κB bound to DNA. *Nature 1998 391:6665* **391**, 410–413 (1998).
108. Perkins, N. D. Post-translational modifications regulating the activity and function of the nuclear factor kappa B pathway. *Oncogene* **25**, 6717–6730 (2006).
109. Buss, H. *et al.* Constitutive and interleukin-1-inducible phosphorylation of p65 NF-{kappa}B at serine 536 is mediated by multiple protein kinases including I{kappa}B kinase (IKK)-{alpha}, IKK{beta}, IKK{epsilon}, TRAF family member-associated (TANK)-binding kinase 1 (TBK1), and an unknown kinase and couples p65 to TATA-binding protein-associated factor II31-mediated interleukin-8 transcription. *J Biol Chem* **279**, 55633–55643 (2004).
110. Pahl, H. L. Activators and target genes of Rel/NF-κB transcription factors. *Oncogene* **18**, 6853–6866 (1999).
111. Holdsworth, S. R. & Can, P. Y. Cytokines: Names and numbers you should care about. *Clinical Journal of the American Society of Nephrology* vol. 10 Preprint at https://doi.org/10.2215/CJN.07590714 (2015).
112. Biron, C. A. Role of early cytokines, including alpha and beta interferons (IFN-alpha/beta), in innate and adaptive immune responses to viral infections. *Semin Immunol* **10**, 383–390 (1998).

113. Karin, N. & Razon, H. Chemokines beyond chemo-attraction: CXCL10 and its significant role in cancer and autoimmunity. *Cytokine* **109**, 24–28 (2018).
114. Couper, K. N., Blount, D. G. & Riley, E. M. IL-10: the master regulator of immunity to infection. *J Immunol* **180**, 5771–5777 (2008).
115. Dinarello, C. A. Biologic Basis for Interleukin-1 in Disease. *Blood* **87**, 2095–2147 (1996).
116. Eder, C. Mechanisms of interleukin-1beta release. *Immunobiology* **214**, 543–553 (2009).
117. Lopez-Castejon, G. & Brough, D. Understanding the mechanism of IL-1β secretion. *Cytokine and Growth Factor Reviews* vol. 22 Preprint at https://doi.org/10.1016/j.cytogfr.2011.10.001 (2011).
118. Sims, J. E. & Smith, D. E. The IL-1 family: regulators of immunity. *Nature Reviews Immunology 2010 10:2* **10**, 89–102 (2010).
119. Horai, R. *et al.* Production of Mice Deficient in Genes for Interleukin (IL)-1α, IL-1β, IL-1α/β, and IL-1 Receptor Antagonist Shows that IL-1β Is Crucial in Turpentine-induced Fever Development and Glucocorticoid Secretion. *J Exp Med* **187**, 1463 (1998).
120. Borden, E. C. Interferons α and β in cancer: therapeutic opportunities from new insights. *Nature Reviews Drug Discovery* vol. 18 Preprint at https://doi.org/10.1038/s41573-018-0011-2 (2019).
121. Markowitz, C. E. Interferon-beta: Mechanism of action and dosing issues. *Neurology* **68**, (2007).
122. Kumaran Satyanarayanan, S. *et al.* IFN-β is a macrophage-derived effector cytokine facilitating the resolution of bacterial inflammation. *Nat Commun* **10**, (2019).
123. Uciechowski, P. & Dempke, W. C. M. Interleukin-6: A Masterplayer in the Cytokine Network. *Oncology* **98**, 131–137 (2020).
124. Hirano, T. *et al.* Purification to homogeneity and characterization of human B-cell differentiation factor (BCDF or BSFp-2). *Proc Natl Acad Sci U S A* **82**, 5490–5494 (1985).
125. Idriss, H. T. & Naismith, J. H. TNF and the TNF Receptor Superfamily: Structure-Function Relationship(s). *Microsc. Res. Tech* **50**, 184–195 (2000).

126. Jang, D. I. *et al.* The Role of Tumor Necrosis Factor Alpha (TNF-α) in Autoimmune Disease and Current TNF-α Inhibitors in Therapeutics. *International Journal of Molecular Sciences 2021, Vol. 22, Page 2719* **22**, 2719 (2021).
127. Kaplanski, G. Interleukin-18: Biological properties and role in disease pathogenesis. *Immunological Reviews* vol. 281 Preprint at https://doi.org/10.1111/imr.12616 (2018).
128. Van Den Borne, P., Quax, P. H. A., Hoefer, I. E. & Pasterkamp, G. The multifaceted functions of CXCL10 in cardiovascular disease. *Biomed Res Int* **2014**, (2014).
129. Luster, A. D., Unkeless, J. C. & Ravetch, J. V. Gamma-interferon transcriptionally regulates an early-response gene containing homology to platelet proteins. *Nature* **315**, 672–676 (1985).
130. Liu, M. *et al.* CXCL10/IP-10 in infectious diseases pathogenesis and potential therapeutic implications. *Cytokine Growth Factor Rev* **22**, 121–130 (2011).
131. Sui, Y. *et al.* Neuronal apoptosis is mediated by CXCL10 overexpression in simian human immunodeficiency virus encephalitis. *Am J Pathol* **164**, 1557–1566 (2004).
132. Ullrich, K. *et al.* Immunology of IL-12: An update on functional activities and implications for disease. *EXCLI J* **19**, (2020).
133. Bochman, M. L., Paeschke, K. & Zakian, V. A. DNA secondary structures: stability and function of G-quadruplex structures. *Nature Reviews Genetics 2012 13:11* **13**, 770–780 (2012).
134. Shen, Q. & Lin, C. RNA returns to the fold. *Nature Chemistry 2020 12:3* **12**, 221–222 (2020).
135. Bang, I. Untersuchungen über die Guanylsäure. *Biochemie* 293–231 (1910) doi:10.1515/BCHM2.1901.32.3-4.201.
136. Gellert, M., Lipsett, M. N. & Davies, D. R. Helix formation by guanylic acid. *Proc Natl Acad Sci U S A* **48**, 2013–2018 (1962).
137. Huppert, J. L. & Balasubramanian, S. Prevalence of quadruplexes in the human genome. *Nucleic Acids Res* **33**, 2908–2916 (2005).
138. Varshney, D., Spiegel, J., Zyner, K., Tannahill, D. & Balasubramanian, S. The regulation and functions of DNA and RNA G-quadruplexes. *Nature Reviews Molecular Cell Biology 2020 21:8* **21**, 459–474 (2020).

139. Bolduc, F., Garant, J. M., Allard, F. & Perreault, J. P. Irregular G-quadruplexes Found in the Untranslated Regions of Human mRNAs Influence Translation. *J Biol Chem* **291**, 21751 (2016).
140. Jana, J., Mohr, S., Vianney, Y. M. & Weisz, K. Structural motifs and intramolecular interactions in non-canonical G-quadruplexes. *RSC Chemical Biology* vol. 2 Preprint at https://doi.org/10.1039/d0cb00211a (2021).
141. Schultze, P., Macaya, R. F. & Feigon, J. Three-dimensional solution structure of the thrombin-binding DNA aptamer d(GGTTGGTGTGGTTGG). *J Mol Biol* **235**, 1532–1547 (1994).
142. Macaya, R. F., Schultze, P., Smith, F. W., Roe, J. A. & Feigon, J. Thrombin-binding DNA aptamer forms a unimolecular quadruplex structure in solution. *Proc Natl Acad Sci U S A* **90**, 3745–3749 (1993).
143. Liu, W. *et al.* Kinetics and mechanism of G-quadruplex formation and conformational switch in a G-quadruplex of PS2.M induced by Pb2+. *Nucleic Acids Res* **40**, (2012).
144. Hardin, C. C., Watson, T., Corregan, M. & Bailey, C. Cation-dependent transition between the quadruplex and Watson-Crick hairpin forms of d(CGCG3GCG). *Biochemistry* **31**, 833–841 (1992).
145. Guédin, A., Gros, J., Alberti, P. & Mergny, J. L. How long is too long? Effects of loop size on G-quadruplex stability. *Nucleic Acids Res* **38**, 7858–7868 (2010).
146. Ma, Y., Iida, K. & Nagasawa, K. Topologies of G-quadruplex: Biological functions and regulation by ligands. *Biochem Biophys Res Commun* **531**, 3–17 (2020).
147. Fogolari, F. *et al.* Molecular models for intrastrand DNA G-quadruplexes. *BMC Struct Biol* **9**, (2009).
148. Dvorkin, S. A., Karsisiotis, A. I. & da Silva, M. W. Encoding canonical DNA quadruplex structure. *Sci Adv* **4**, (2018).
149. Capra, J. A., Paeschke, K., Singh, M. & Zakian, V. A. G-quadruplex DNA sequences are evolutionarily conserved and associated with distinct genomic features in Saccharomyces cerevisiae. *PLoS Comput Biol* **6**, 9 (2010).
150. Wu, F. *et al.* Genome-wide analysis of DNA G-quadruplex motifs across 37 species provides insights into G4 evolution. *Communications Biology 2021 4:1* **4**, 1–11 (2021).

151. Mishra, S. K. *et al.* Characterization of highly conserved G-quadruplex motifs as potential drug targets in Streptococcus pneumoniae. *Sci Rep* **9**, (2019).
152. Rhodes, D. & Lipps, H. J. Survey and summary G-quadruplexes and their regulatory roles in biology. *Nucleic Acids Research* vol. 43 Preprint at https://doi.org/10.1093/nar/gkv862 (2015).
153. Maizels, N. & Gray, L. T. The G4 Genome. *PLoS Genet* **9**, (2013).
154. Georgakopoulos-Soares, I. *et al.* Alternative splicing modulation by G-quadruplexes. *Nat Commun* **13**, (2022).
155. Marsico, G. *et al.* Whole genome experimental maps of DNA G-quadruplexes in multiple species. *Nucleic Acids Res* **47**, (2019).
156. Chambers, V. S. *et al.* High-throughput sequencing of DNA G-quadruplex structures in the human genome. *Nat Biotechnol* **33**, 877–881 (2015).
157. Simon, P., Schult, P. & Paeschke, K. Binding and Modulation of G-quadruplex DNA and RNA Structures by Proteins. in *Handbook of Chemical Biology of Nucleic Acids* (2023). doi:10.1007/978-981-16-1313-5_102-1.
158. Biffi, G., Tannahill, D., Mccafferty, J. & Balasubramanian, S. Quantitative Visualization of DNA G-quadruplex Structures in Human Cells Europe PMC Funders Group. *Nat Chem* **5**, 182–186 (2013).
159. Zyner, K. G. *et al.* G-quadruplex DNA structures in human stem cells and differentiation. *Nature Communications 2022 13:1* **13**, 1–17 (2022).
160. Meier-Stephenson, V. G4-quadruplex-binding proteins: review and insights into selectivity. *Biophys Rev* **14**, 635 (2022).
161. Bian, W. X. *et al.* Binding of cellular nucleolin with the viral core RNA G-quadruplex structure suppresses HCV replication. *Nucleic Acids Res* **47**, 56–68 (2019).
162. Cogoi, S., Shchekotikhin, A. E. & Xodo, L. E. HRAS is silenced by two neighboring G-quadruplexes and activated by MAZ, a zinc-finger transcription factor with DNA unfolding property. *Nucleic Acids Res* **42**, 8379–8388 (2014).
163. Sato, K., Martin-Pintado, N., Post, H., Altelaar, M. & Knipscheer, P. Multistep mechanism of G-quadruplex resolution during DNA replication. *Sci Adv* **7**, (2021).
164. Johnson, J. E., Cao, K., Ryvkin, P., Wang, L. S. & Johnson, F. B. Altered gene expression in the Werner and Bloom syndromes is associated with sequences having G-quadruplex forming potential. *Nucleic Acids Res* **38**, 1114–1122 (2010).

165. Brosh, R. M. & Bohr, V. A. Human premature aging, DNA repair and RecQ helicases. *Nucleic Acids Research* vol. 35 Preprint at https://doi.org/10.1093/nar/gkm1008 (2007).
166. Wu, Y. & Brosh, R. M. G-quadruplex nucleic acids and human disease. *FEBS Journal* vol. 277 Preprint at https://doi.org/10.1111/j.1742-4658.2010.07760.x (2010).
167. Tsuge, K. & Shimamoto, A. Research on Werner Syndrome: Trends from Past to Present and Future Prospects. *Genes* vol. 13 Preprint at https://doi.org/10.3390/genes13101802 (2022).
168. Huber, M. D., Duquette, M. L., Shiels, J. C. & Maizels, N. A Conserved G4 DNA Binding Domain in RecQ Family Helicases. *J Mol Biol* **358**, (2006).
169. Sun, H., Karow, J. K., Hickson, I. D. & Maizels, N. The Bloom's syndrome helicase unwinds G4 DNA. *Journal of Biological Chemistry* **273**, (1998).
170. Maizels, N. G4-associated human diseases. *EMBO Rep* **16**, 910–922 (2015).
171. Santos, T., Salgado, G. F., Cabrita, E. J. & Cruz, C. G-Quadruplexes and Their Ligands: Biophysical Methods to Unravel G-Quadruplex/Ligand Interactions. *Pharmaceuticals 2021, Vol. 14, Page 769* **14**, 769 (2021).
172. Li, Q. *et al.* G4LDB: a database for discovering and studying G-quadruplex ligands. *Nucleic Acids Res* **41**, (2013).
173. Sayers, E. W. *et al.* Database resources of the national center for biotechnology information. *Nucleic Acids Res* **50**, D20–D26 (2022).
174. Cogoi, S. & Xodo, L. E. G-quadruplex formation within the promoter of the KRAS proto-oncogene and its effect on transcription. *Nucleic Acids Res* **34**, (2006).
175. Cogoi, S., Paramasivam, M., Spolaore, B. & Xodo, L. E. Structural polymorphism within a regulatory element of the human KRAS promoter: Formation of G4-DNA recognized by nuclear proteins. *Nucleic Acids Res* **36**, (2008).
176. Awadasseid, A., Ma, X., Wu, Y. & Zhang, W. G-quadruplex stabilization via small-molecules as a potential anti-cancer strategy. *Biomedicine and Pharmacotherapy* vol. 139 Preprint at https://doi.org/10.1016/j.biopha.2021.111550 (2021).
177. Zhu, G., Pei, L., Xia, H., Tang, Q. & Bi, F. Role of oncogenic KRAS in the prognosis, diagnosis and treatment of colorectal cancer. *Molecular Cancer 2021 20:1* **20**, 1–17 (2021).

178. Hurley, L. H., Von Hoff, D. D., Siddiqui-Jain, A. & Yang, D. Drug targeting of the c-MYC promoter to repress gene expression via a G-quadruplex silencer element. *Semin Oncol* **33**, 498–512 (2006).
179. Siddiqui-Jain, A., Grand, C. L., Bearss, D. J. & Hurley, L. H. Direct evidence for a G-quadruplex in a promoter region and its targeting with a small molecule to repress c-MYC transcription. *Proc Natl Acad Sci U S A* **99**, 11593–11598 (2002).
180. Ou, T. M. *et al.* Stabilization of G-quadruplex DNA and down-regulation of oncogene c-myc by quindoline derivatives. *J Med Chem* **50**, (2007).
181. Yang, D. & Hurley, L. Structure of the biologically relevant G-quadruplex in the c-MYC promoter. *Nucleosides Nucleotides Nucleic Acids* **25**, 951–968 (2006).
182. Xu, H. *et al.* CX-5461 is a DNA G-quadruplex stabilizer with selective lethality in BRCA1/2 deficient tumours. *Nat Commun* **8**, (2017).
183. Liu, L. Y., Ma, T. Z., Zeng, Y. L., Liu, W. & Mao, Z. W. Structural Basis of Pyridostatin and Its Derivatives Specifically Binding to G-Quadruplexes. *J Am Chem Soc* **144**, (2022).
184. Rodriguez, R. *et al.* A novel small molecule that alters shelterin integrity and triggers a DNA-damage response at telomeres. *J Am Chem Soc* **130**, 15758–15759 (2008).
185. Koirala, D. *et al.* A single-molecule platform for investigation of interactions between G-quadruplexes and small-molecule ligands. *Nature Chemistry 2011 3:10* **3**, 782–787 (2011).
186. Rodriguez, R. *et al.* Small molecule-induced DNA damage identifies alternative DNA structures in human genes. *Nat Chem Biol* **8**, 301 (2012).
187. del Villar-Guerra, R., Trent, J. O. & Chaires, J. B. G-Quadruplex Secondary Structure Obtained from Circular Dichroism Spectroscopy. *Angewandte Chemie - International Edition* **57**, (2018).
188. Puig Lombardi, E. & Londoño-Vallejo, A. A guide to computational methods for G-quadruplex prediction. *Nucleic Acids Research* vol. 48 Preprint at https://doi.org/10.1093/nar/gkz1097 (2020).
189. Hänsel-Hertsch, R., Spiegel, J., Marsico, G., Tannahill, D. & Balasubramanian, S. Genome-wide mapping of endogenous G-quadruplex DNA structures by chromatin immunoprecipitation and high-throughput sequencing. *Nature Protocols 2018 13:3* **13**, 551–564 (2018).

190. Lipps, H. J. & Rhodes, D. G-quadruplex structures: in vivo evidence and function. *Trends Cell Biol* **19**, 414–422 (2009).
191. Paeschke, K. *et al.* Pif1 family helicases suppress genome instability at G-quadruplex motifs. *Nature* **497**, (2013).
192. Schaffitzel, C. *et al.* In vitro generated antibodies specific for telomeric guanine-quadruplex DNA react with Stylonychia lemnae macronuclei. *Proc Natl Acad Sci U S A* **98**, (2001).
193. Di Antonio, M. *et al.* Single-molecule visualization of DNA G-quadruplex formation in live cells. *Nat Chem* **12**, (2020).
194. Hänsel-Hertsch, R. *et al.* Landscape of G-quadruplex DNA structural regions in breast cancer. *Nat Genet* **52**, 878–883 (2020).
195. Caterino, M. & Paeschke, K. Action and function of helicases on RNA G-quadruplexes. *Methods* **204**, (2022).
196. Spiegel, J. *et al.* G-quadruplexes are transcription factor binding hubs in human chromatin. *Genome Biol* **22**, (2021).
197. Tan, J. & Lan, L. The DNA secondary structures at telomeres and genome instability. *Cell and Bioscience* vol. 10 Preprint at https://doi.org/10.1186/s13578-020-00409-z (2020).
198. Todd, A. K., Johnston, M. & Neidle, S. Highly prevalent putative quadruplex sequence motifs in human DNA. *Nucleic Acids Res* **33**, 2901–2907 (2005).
199. Smith, J. S. *et al.* Rudimentary G-quadruplex-based telomere capping in Saccharomyces cerevisiae. *Nat Struct Mol Biol* **18**, (2011).
200. Vallur, A. C. & Maizels, N. Activities of human exonuclease 1 that promote cleavage of transcribed immunoglobulin switch regions. *Proc Natl Acad Sci U S A* **105**, 16508–16512 (2008).
201. Zahler, A. M., Williamson, J. R., Cech, T. R. & Prescott, D. M. Inhibition of telomerase by G-quartet DNA structures. *Nature* **350**, 718–720 (1991).
202. Paeschke, K. *et al.* Telomerase recruitment by the telomere end binding protein-β facilitates G-quadruplex DNA unfolding in ciliates. *Nat Struct Mol Biol* **15**, (2008).
203. Bryan, T. M. G-Quadruplexes at Telomeres: Friend or Foe? *Molecules* **25**, (2020).

204. Besnard, E. *et al.* Unraveling cell type-specific and reprogrammable human replication origin signatures associated with G-quadruplex consensus motifs. *Nat Struct Mol Biol* **19**, (2012).
205. Cayrou, C. *et al.* Genome-scale analysis of metazoan replication origins reveals their organization in specific but flexible sites defined by conserved features. *Genome Res* **21**, (2011).
206. Cayrou, C., Grégoire, D., Coulombe, P., Danis, E. & Méchali, M. Genome-scale identification of active DNA replication origins. *Methods* **57**, (2012).
207. Valton, A. L. & Prioleau, M. N. G-Quadruplexes in DNA Replication: A Problem or a Necessity? *Trends in Genetics* vol. 32 Preprint at https://doi.org/10.1016/j.tig.2016.09.004 (2016).
208. Kruisselbrink, E. *et al.* Mutagenic Capacity of Endogenous G4 DNA Underlies Genome Instability in FANCJ-Defective C. elegans. *Current Biology* **18**, (2008).
209. London, T. B. C. *et al.* FANCJ is a structure-specific DNA helicase associated with the maintenance of genomic G/C tracts. *Journal of Biological Chemistry* **283**, (2008).
210. Safa, L. *et al.* 5′ to 3′ Unfolding Directionality of DNA Secondary Structures by Replication Protein A: G-QUADRUPLEXES AND DUPLEXES*. *J Biol Chem* **291**, 21246 (2016).
211. Lerner, L. K. & Sale, J. E. Replication of G quadruplex DNA. *Genes* vol. 10 Preprint at https://doi.org/10.3390/genes10020095 (2019).
212. Eddy, J. & Maizels, N. Gene function correlates with potential for G4 DNA formation in the human genome. *Nucleic Acids Res* **34**, (2006).
213. Huppert, J. L. & Balasubramanian, S. G-quadruplexes in promoters throughout the human genome. *Nucleic Acids Res* **35**, (2007).
214. Lam, E. Y. N., Beraldi, D., Tannahill, D. & Balasubramanian, S. G-quadruplex structures are stable and detectable in human genomic DNA. *Nat Commun* **4**, (2013).
215. Zhang, C., Liu, H. H., Zheng, K. W., Hao, Y. H. & Tan, Z. DNA G-quadruplex formation in response to remote downstream transcription activity: long-range sensing and signal transducing in DNA double helix. *Nucleic Acids Res* **41**, 7144–7152 (2013).

216. Robinson, J., Raguseo, F., Nuccio, S. P., Liano, D. & Di Antonio, M. DNA G-quadruplex structures: more than simple roadblocks to transcription? *Nucleic Acids Res* **49**, 8419–8431 (2021).
217. Balasubramanian, S., Hurley, L. H. & Neidle, S. Targeting G-quadruplexes in gene promoters: A novel anticancer strategy? *Nat Rev Drug Discov* **10**, (2011).
218. Hänsel-Hertsch, R. *et al.* G-quadruplex structures mark human regulatory chromatin. *Nat Genet* **48**, (2016).
219. Lago, S. *et al.* Promoter G-quadruplexes and transcription factors cooperate to shape the cell type-specific transcriptome. *Nat Commun* **12**, (2021).
220. Fleming, A. M. & Burrows, C. J. Interplay of Guanine Oxidation and G-Quadruplex Folding in Gene Promoters. *Journal of the American Chemical Society* vol. 142 Preprint at https://doi.org/10.1021/jacs.9b11050 (2020).
221. Wang, K. B. *et al.* Oxidative Damage Induces a Vacancy G-Quadruplex That Binds Guanine Metabolites: Solution Structure of a cGMP Fill-in Vacancy G-Quadruplex in the Oxidized BLM Gene Promoter. *J Am Chem Soc* **144**, (2022).
222. Ribeyre, C. *et al.* The yeast Pif1 helicase prevents genomic instability caused by G-quadruplex-forming CEB1 sequences in vivo. *PLoS Genet* **5**, (2009).
223. Paeschke, K., Capra, J. A. & Zakian, V. A. DNA Replication through G-Quadruplex Motifs Is Promoted by the Saccharomyces cerevisiae Pif1 DNA Helicase. *Cell* **145**, (2011).
224. Cheung, I., Schertzer, M., Rose, A. & Lansdorp, P. M. Disruption of dog-1 in Caenorhabditis elegans triggers deletions upstream of guanine-rich DNA. *Nat Genet* **31**, (2002).
225. Kumar, C., Batra, S., Griffith, J. D. & Remus, D. The interplay of rna:Dna hybrid structure and g-quadruplexes determines the outcome of r-loop-replisome collisions. *Elife* **10**, (2021).
226. Lee, W. T. C. *et al.* Single-molecule imaging reveals replication fork coupled formation of G-quadruplex structures hinders local replication stress signaling. *Nat Commun* **12**, (2021).
227. Sauer, M. & Paeschke, K. G-quadruplex unwinding helicases and their function in vivo. *Biochemical Society Transactions* vol. 45 Preprint at https://doi.org/10.1042/BST20170097 (2017).

228. Linke, R., Limmer, M., Juranek, S. A., Heine, A. & Paeschke, K. The relevance of g-quadruplexes for dna repair. *International Journal of Molecular Sciences* vol. 22 Preprint at https://doi.org/10.3390/ijms222212599 (2021).
229. Yang, Z., Takai, K. K., Lovejoy, C. A. & de Lange, T. Break-induced replication promotes fragile telomere formation. *Genes Dev* **34**, (2020).
230. Vannier, J. B. *et al.* RTEL1 is a replisome-associated helicase that promotes telomere and genome-wide replication. *Science* **342**, 239–242 (2013).
231. Gauthier, L. R. *et al.* Rad51 and DNA-PKcs are involved in the generation of specific telomere aberrations induced by the quadruplex ligand 360A that impair mitotic cell progression and lead to cell death. *Cellular and Molecular Life Sciences* **69**, (2012).
232. Sfeir, A. *et al.* Mammalian Telomeres Resemble Fragile Sites and Require TRF1 for Efficient Replication. *Cell* **138**, (2009).
233. Zacheja, T. *et al.* Mgs1 protein supports genome stability via recognition of G-quadruplex DNA structures. *FASEB Journal* **34**, (2020).
234. Lopes, J. *et al.* G-quadruplex-induced instability during leading-strand replication. *EMBO Journal* **30**, (2011).
235. Masuda-Sasa, T., Polaczek, P., Peng, X. P., Chen, L. & Campbell, J. L. Processing of G4 DNA by Dna2 helicase/nuclease and replication protein A (RPA) provides insights into the mechanism of Dna2/RPA substrate recognition. *J Biol Chem* **283**, 24359–24373 (2008).
236. Ghosal, G. & Muniyappa, K. Saccharomyces cerevisiae Mre11 is a high-affinity G4 DNA-binding protein and a G-rich DNA-specific endonuclease: Implications for replication of telomeric DNA. *Nucleic Acids Res* **33**, (2005).
237. Salas, T. R. *et al.* Human replication protein A unfolds telomeric G-quadruplexes. *Nucleic Acids Res* **34**, (2006).
238. Zhang, X., Spiegel, J., Martínez Cuesta, S., Adhikari, S. & Balasubramanian, S. Chemical profiling of DNA G-quadruplex-interacting proteins in live cells. *Nat Chem* **13**, (2021).
239. Kosiol, N., Juranek, S., Brossart, P., Heine, A. & Paeschke, K. G-quadruplexes: a promising target for cancer therapy. *Molecular Cancer* vol. 20 Preprint at https://doi.org/10.1186/s12943-021-01328-4 (2021).

240. Moye, A. L. *et al.* Telomeric G-quadruplexes are a substrate and site of localization for human telomerase. *Nat Commun* **6**, (2015).
241. Kim, N. W. *et al.* Specific association of human telomerase activity with immortal cells and cancer. *Science (1979)* **266**, (1994).
242. Beauvarlet, J. *et al.* Modulation of the ATM/autophagy pathway by a G-quadruplex ligand tips the balance between senescence and apoptosis in cancer cells. *Nucleic Acids Res* **47**, (2019).
243. Zimmer, J. *et al.* Targeting BRCA1 and BRCA2 Deficiencies with G-Quadruplex-Interacting Compounds. *Mol Cell* **61**, (2016).
244. Ohnmacht, S. A. *et al.* A G-quadruplex-binding compound showing anti-tumour activity in an in vivo model for pancreatic cancer. *Sci Rep* **5**, 11385–11385 (2015).
245. Hanahan, D. Hallmarks of Cancer: New Dimensions. *Cancer Discovery* vol. 12 Preprint at https://doi.org/10.1158/2159-8290.CD-21-1059 (2022).
246. Hiam-Galvez, K. J., Allen, B. M. & Spitzer, M. H. Systemic immunity in cancer. *Nature Reviews Cancer* vol. 21 Preprint at https://doi.org/10.1038/s41568-021-00347-z (2021).
247. Itakura, E. *et al.* IL-10 expression by primary tumor cells correlates with melanoma progression from radial to vertical growth phase and development of metastatic competence. *Modern Pathology 2011 24:6* **24**, 801–809 (2011).
248. Coussens, L. M. Neutralizing tumor-promoting chronic inflammation: A magic bullet? (Science (286)). *Science* vol. 340 Preprint at https://doi.org/10.1126/science.339.6127.1522-c (2013).
249. Zhang, H. *et al.* Poor Clinical Outcomes and Immunoevasive Contexture in Intratumoral IL-10-Producing Macrophages Enriched Gastric Cancer Patients. *Ann Surg* **275**, (2022).
250. Turovskaya, O., Kim, G., Cheroutre, H., Kronenberg, M. & Madan, R. Interleukin 10 acts on regulatory t cells to maintain expression of the transcription factor foxp3 and suppressive function in mice with colitis. *Nat Immunol* **10**, (2009).
251. DeNardo, D. G. *et al.* CD4+ T Cells Regulate Pulmonary Metastasis of Mammary Carcinomas by Enhancing Protumor Properties of Macrophages. *Cancer Cell* **16**, (2009).

252. Gabrilovich, D. I., Ostrand-Rosenberg, S. & Bronte, V. Coordinated regulation of myeloid cells by tumours. *Nature Reviews Immunology* vol. 12 Preprint at https://doi.org/10.1038/nri3175 (2012).
253. Kuang, D. M. *et al.* Activated monocytes in peritumoral stroma of hepatocellular carcinoma foster immune privilege and disease progression through PD-L1. *Journal of Experimental Medicine* **206**, (2009).
254. Steidl, C. *et al.* Tumor-associated macrophages and survival in classic Hodgkin's lymphoma. *N Engl J Med* **362**, 875–885 (2010).
255. Miglietta, G., Russo, M., Duardo, R. C. & Capranico, G. G-quadruplex binders as cytostatic modulators of innate immune genes in cancer cells. *Nucleic Acids Res* **49**, (2021).
256. Abdullah, Z. *et al.* RIG-I detects infection with live Listeria by sensing secreted bacterial nucleic acids. *EMBO J* **31**, 4153–4164 (2012).
257. Schindelin, J. *et al.* Fiji: an open-source platform for biological-image analysis. *Nat Methods* **9**, 676–682 (2012).
258. Dobin, A. *et al.* STAR: ultrafast universal RNA-seq aligner. *Bioinformatics* **29**, 15–21 (2013).
259. De Magis, A., Kastl, M., Brossart, P., Heine, A. & Paeschke, K. BG-flow, a new flow cytometry tool for G-quadruplex quantification in fixed cells. *BMC Biol* **19**, (2021).
260. Lyu, J., Shao, R., Kwong Yung, P. Y. & Elsässer, S. J. Genome-wide mapping of G-quadruplex structures with CUT&Tag. *Nucleic Acids Res* **50**, E13 (2022).
261. Langmead, B. & Salzberg, S. L. Fast gapped-read alignment with Bowtie 2. *Nature Methods 2012 9:4* **9**, 357–359 (2012).
262. Martin, M. Cutadapt removes adapter sequences from high-throughput sequencing reads. *EMBnet J* **17**, 10–12 (2011).
263. Danecek, P. *et al.* Twelve years of SAMtools and BCFtools. *Gigascience* **10**, (2021).
264. Zhang, Y. *et al.* Model-based analysis of ChIP-Seq (MACS). *Genome Biol* **9**, 1–9 (2008).
265. Li, Q., Brown, J. B., Huang, H. & Bickel, P. J. Measuring reproducibility of high-throughput experiments. *https://doi.org/10.1214/11-AOAS466* **5**, 1752–1779 (2011).

266. Heinz, S. *et al.* Simple combinations of lineage-determining transcription factors prime cis-regulatory elements required for macrophage and B cell identities. *Mol Cell* **38**, 576–589 (2010).
267. Ross-Innes, C. S. *et al.* Differential oestrogen receptor binding is associated with clinical outcome in breast cancer. *Nature 2011 481:7381* **481**, 389–393 (2012).
268. Pagés, H., Aboyoun, P., Gentleman, R. & DebRoy, S. Biostrings: Efficient manipulation of biological strings. *R package version 2.58.0.* Preprint at (2020).
269. Ramírez, F. *et al.* deepTools2: a next generation web server for deep-sequencing data analysis. *Nucleic Acids Res* **44**, W160–W165 (2016).
270. R Core Team. R: A Language and Environment for Statistical Computing. *R Foundation for Statistical Computing* Preprint at (2021).
271. Wickham, H. *et al.* Welcome to the Tidyverse. *J Open Source Softw* **4**, 1686 (2019).
272. Siddiqui-Jain, A., Grand, C. L., Bearss, D. J. & Hurley, L. H. *Direct evidence for a G-quadruplex in a promoter region and its targeting with a small molecule to repress c-MYC transcription*. www.pnas.org (2002).
273. Simonsson, T. & Henriksson, M. C-myc suppression in Burkitt's lymphoma cells. *Biochem Biophys Res Commun* **290**, (2002).
274. Phan, A. T., Kuryavyi, V., Gaw, H. Y. & Patel, D. J. Small-molecule interaction with a five-guanine-tract g-quadruplex structure from the human myc promoter. *Nat Chem Biol* **1**, 167–173 (2005).
275. Prorok, P. *et al.* Involvement of G-quadruplex regions in mammalian replication origin activity. *Nat Commun* **10**, (2019).
276. Zamarron, B. F. & Chen, W. Dual roles of immune cells and their factors in cancer development and progression. *Int J Biol Sci* **7**, (2011).
277. Davis, B. K. Derivation of macrophages from mouse bone marrow. in *Methods in Molecular Biology* vol. 1960 (2019).
278. Forman, H. J. & Torres, M. Reactive oxygen species and cell signaling: Respiratory burst in macrophage signaling. in *American Journal of Respiratory and Critical Care Medicine* vol. 166 (2002).
279. Chandak, P. G. *et al.* Efficient phagocytosis requires triacylglycerol hydrolysis by adipose triglyceride lipase. *J Biol Chem* **285**, 20192–20201 (2010).

280. Wu, T. T., Chen, T. L. & Chen, R. M. Lipopolysaccharide triggers macrophage activation of inflammatory cytokine expression, chemotaxis, phagocytosis, and oxidative ability via a toll-like receptor 4-dependent pathway: Validated by RNA interference. *Toxicol Lett* **191**, (2009).
281. Uribe-Querol, E. & Rosales, C. Phagocytosis: Our Current Understanding of a Universal Biological Process. *Frontiers in Immunology* vol. 11 Preprint at https://doi.org/10.3389/fimmu.2020.01066 (2020).
282. Sanders, P. G. T., Cotterell, J., Sharpe, J. & Isalan, M. Transfecting RNA quadruplexes results in few transcriptome perturbations. *RNA Biol* **10**, 205 (2013).
283. Chui, R. & Dorovini-Zis, K. Regulation of CCL2 and CCL3 expression in human brain endothelial cells by cytokines and lipopolysaccharide. *J Neuroinflammation* **7**, (2010).
284. Fukumoto, S. *et al.* Suppression of IP-10/CXCL10 gene expression in LPS- and/or IFN-γ-stimulated macrophages by parasite-secreted products. *Cell Immunol* **276**, 101–109 (2012).
285. Hobbs, S., Reynoso, M., Geddis, A. V., Mitrophanov, A. Y. & Matheny, R. W. LPS-stimulated NF-κB p65 dynamic response marks the initiation of TNF expression and transition to IL-10 expression in RAW 264.7 macrophages. *Physiol Rep* **6**, (2018).
286. Rossol, M. *et al.* LPS-induced cytokine production in human monocytes and macrophages. *Critical Reviews in Immunology* vol. 31 Preprint at https://doi.org/10.1615/critrevimmunol.v31.i5.20 (2011).
287. Murray, R. Z. & Stow, J. L. Cytokine secretion in macrophages: SNAREs, Rabs, and membrane trafficking. *Frontiers in Immunology* vol. 5 Preprint at https://doi.org/10.3389/fimmu.2014.00538 (2014).
288. Hiscott, J. *et al.* Characterization of a functional NF-kappa B site in the human interleukin 1 beta promoter: evidence for a positive autoregulatory loop. *Mol Cell Biol* **13**, 6231–6240 (1993).
289. Hiscott, J. *et al.* Induction of human interferon gene expression is associated with a nuclear factor that interacts with the NF-kappa B site of the human immunodeficiency virus enhancer. *J Virol* **63**, (1989).
290. Libermann, T. A. & Baltimore, D. Activation of interleukin-6 gene expression through the NF-kappa B transcription factor. *Mol Cell Biol* **10**, (1990).

291. Cao, S., Zhang, X., Edwards, J. P. & Mosser, D. M. NF-κB1 (p50) homodimers differentially regulate pro- and anti-inflammatory cytokines in macrophages. *Journal of Biological Chemistry* **281**, (2006).
292. Collart, M. A., Baeuerle, P. & Vassalli, P. Regulation of tumor necrosis factor alpha transcription in macrophages: involvement of four kappa B-like motifs and of constitutive and inducible forms of NF-kappa B. *Mol Cell Biol* **10**, (1990).
293. Yeruva, S., Ramadori, G. & Raddatz, D. NF-κB-dependent synergistic regulation of CXCL10 gene expression by IL-1β and IFN-γ in human intestinal epithelial cell lines. *Int J Colorectal Dis* **23**, (2008).
294. Murphy, T. L., Cleveland, M. G., Kulesza, P., Magram, J. & Murphy, K. M. Regulation of interleukin 12 p40 expression through an NF-kappa B half-site. *Mol Cell Biol* **15**, (1995).
295. Moreno, R., Sobotzik, J. M., Schultz, C. & Schmitz, M. L. Specification of the NF-κB transcriptional response by p65 phosphorylation and TNF-induced nuclear translocation of IKKε. *Nucleic Acids Res* **38**, (2010).
296. Szklarczyk, D. *et al.* The STRING database in 2023: protein–protein association networks and functional enrichment analyses for any sequenced genome of interest. *Nucleic Acids Res* **51**, (2023).
297. Weinmann, A. S., Plevy, S. E. & Smale, S. T. Rapid and selective remodeling of a positioned nucleosome during the induction of IL-12 p40 transcription. *Immunity* **11**, (1999).
298. Weinmann, A. S. *et al.* Nucleosome remodeling at the IL-12 p40 promoter is a TLR-dependent, Rel-independent event. *Nat Immunol* **2**, (2001).
299. Saccani, S., Pantano, S. & Natoli, G. p38-dependent marking of inflammatory genes for increased NF-κB recruitment. *Nat Immunol* **3**, (2002).
300. Hamon, M. A. & Cossart, P. Histone Modifications and Chromatin Remodeling during Bacterial Infections. *Cell Host and Microbe* vol. 4 Preprint at https://doi.org/10.1016/j.chom.2008.07.009 (2008).
301. Vaillant, A. A. J. & Qurie, A. Immunodeficiency. *StatPearls* (2022).
302. Yu, H. H., Yang, Y. H. & Chiang, B. L. Chronic Granulomatous Disease: a Comprehensive Review. *Clin Rev Allergy Immunol* **61**, 101–113 (2021).

303. Yusuf, K., Sampath, V. & Umar, S. Bacterial Infections and Cancer: Exploring This Association And Its Implications for Cancer Patients. *International Journal of Molecular Sciences* vol. 24 Preprint at https://doi.org/10.3390/ijms24043110 (2023).
304. Rolston, K. V. I. Infections in Cancer Patients with Solid Tumors: A Review. *Infectious Diseases and Therapy* vol. 6 Preprint at https://doi.org/10.1007/s40121-017-0146-1 (2017).
305. Bhat, S., Muthunatarajan, S., Mulki, S. S., Archana Bhat, K. & Kotian, K. H. Bacterial Infection among Cancer Patients: Analysis of Isolates and Antibiotic Sensitivity Pattern. *Int J Microbiol* **2021**, (2021).
306. Challagundla, N., Saha, B. & Agrawal-Rajput, R. Insights into inflammasome regulation: cellular, molecular, and pathogenic control of inflammasome activation. *Immunologic Research 2022 70:5* **70**, 578–606 (2022).
307. Ozturk, M. M. & Wu, W. Microglia: The protectors of the brain. (2022).
308. Gonzalez, H., Hagerling, C. & Werb, Z. Roles of the immune system in cancer: From tumor initiation to metastatic progression. *Genes and Development* vol. 32 Preprint at https://doi.org/10.1101/GAD.314617.118 (2018).
309. Whiteside, T. L. Immune suppression in cancer: Effects on immune cells, mechanisms and future therapeutic intervention. *Semin Cancer Biol* **16**, 3–15 (2006).
310. Hao, G., Xu, Z. P. & Li, L. Manipulating extracellular tumour pH: an effective target for cancer therapy. *RSC Adv* **8**, 22182–22192 (2018).
311. Dougan, M. & Dranoff, G. The immune response to tumors. *Curr Protoc Immunol* **Chapter 20**, (2009).
312. Pan, Y., Yu, Y., Wang, X. & Zhang, T. Tumor-Associated Macrophages in Tumor Immunity. *Front Immunol* **11**, 583084 (2020).
313. Viryasova, G. M. *et al.* G-quadruplex-forming oligodeoxyribonucleotides activate leukotriene synthesis in human neutrophils. *J Biomol Struct Dyn* **37**, 3649–3659 (2019).
314. Wang, Y., Li, N., Zhang, X. & Horng, T. Mitochondrial metabolism regulates macrophage biology. *Journal of Biological Chemistry* vol. 297 Preprint at https://doi.org/10.1016/j.jbc.2021.100904 (2021).

315. Zou, M. *et al.* G-quadruplex binder pyridostatin as an effective multi-target ZIKV inhibitor. *Int J Biol Macromol* **190**, 178–188 (2021).
316. Tseng, T. Y., Chu, I. Te, Lin, S. J., Li, J. & Chang, T. C. Binding of small molecules to G-quadruplex DNA in cells revealed by fluorescence lifetime imaging microscopy of o-BMVC foci. *Molecules* **24**, (2019).
317. Rühl, S. & Broz, P. Caspase-11 activates a canonical NLRP3 inflammasome by promoting K(+) efflux. *Eur J Immunol* **45**, 2927–2936 (2015).
318. Smolinska, M. J., Page, T. H., Urbaniak, A. M., Mutch, B. E. & Horwood, N. J. Hck tyrosine kinase regulates TLR4-induced TNF and IL-6 production via AP-1. *J Immunol* **187**, 6043–6051 (2011).
319. Yarden, Y. *et al.* Human proto-oncogene c-kit: a new cell surface receptor tyrosine kinase for an unidentified ligand. *EMBO J* **6**, (1987).
320. Sakurai, S., Fukasawa, T., Chong, J. M., Tanaka, A. & Fukayama, M. C-kit gene abnormalities in gastrointestinal stromal tumors (tumors of interstitial cells of cajal). *Japanese Journal of Cancer Research* **90**, (1999).
321. Zorzan, E. *et al.* Screening of candidate G-quadruplex ligands for the human c-KIT promotorial region and their effects in multiple in-vitro models. *Oncotarget* **7**, (2016).
322. Yu, Z. *et al.* Chem-map profiles drug binding to chromatin in cells. *Nature Biotechnology 2023* 1–7 (2023) doi:10.1038/s41587-022-01636-0.
323. Müller, S., Kumari, S., Rodriguez, R. & Balasubramanian, S. Small-molecule-mediated G-quadruplex isolation from human cells. *Nat Chem* **2**, 1095–1098 (2010).
324. Rota Sperti, F. *et al.* Click-Chemistry-Based Biomimetic Ligands Efficiently Capture G-Quadruplexes in Vitro and Help Localize Them at DNA Damage Sites in Human Cells. *JACS Au* **2**, (2022).
325. Gursel, I. *et al.* Repetitive Elements in Mammalian Telomeres Suppress Bacterial DNA-Induced Immune Activation. *The Journal of Immunology* **171**, (2003).
326. Alasoo, K. *et al.* Transcriptional profiling of macrophages derived from monocytes and iPS cells identifies a conserved response to LPS and novel alternative transcription. *Sci Rep* **5**, (2015).
327. Wang, X. *et al.* Genomic G-quadruplex folding triggers a cytokine-mediated inflammatory feedback loop to aggravate inflammatory diseases. *iScience* **25**, (2022).

328. Simonsson, T., Pecinka, P. & Kubista, M. DNA tetraplex formation in the control region of c-myc. *Nucleic Acids Res* **26**, (1998).
329. Monguió-Tortajada, M., Franquesa, M., Sarrias, M. R. & Borràs, F. E. Low doses of LPS exacerbate the inflammatory response and trigger death on TLR3-primed human monocytes article. *Cell Death Dis* **9**, (2018).
330. Oeckinghaus, A. & Ghosh, S. The NF-κB Family of Transcription Factors and Its Regulation. *Cold Spring Harb Perspect Biol* (2009).
331. Hunold, P. *et al.* G-quadruplex DNA structures mediate non-autonomous instruction of breast tumour microenvironments. *bioRxiv* 2023.01.16.524243 (2023) doi:10.1101/2023.01.16.524243.
332. Hu, W. *et al.* Systematic characterization of cancer transcriptome at transcript resolution. *Nature Communications 2022 13:1* **13**, 1–16 (2022).
333. Eddy, J. & Maizels, N. Conserved elements with potential to form polymorphic G-quadruplex structures in the first intron of human genes. *Nucleic Acids Res* **36**, 1321–1333 (2008).
334. Wang, B. *et al.* Role of Novel Serine 316 Phosphorylation of the p65 Subunit of NF-κB in Differential Gene Regulation. *J Biol Chem* **290**, 20336–20347 (2015).
335. Ngo, K. A. *et al.* Dissecting the Regulatory Strategies of NF-κB RelA Target Genes in the Inflammatory Response Reveals Differential Transactivation Logics. *Cell Rep* **30**, (2020).
336. Varizhuk, A., Isaakova, E. & Pozmogova, G. DNA G-Quadruplexes (G4s) Modulate Epigenetic (Re)Programming and Chromatin Remodeling: Transient Genomic G4s Assist in the Establishment and Maintenance of Epigenetic Marks, While Persistent G4s May Erase Epigenetic Marks. *Bioessays* **41**, (2019).
337. Rauchhaus, J., Robinson, J., Monti, L. & Di Antonio, M. G-quadruplexes Mark Sites of Methylation Instability Associated with Ageing and Cancer. *Genes (Basel)* **13**, (2022).
338. Mukherjee, A. K., Sharma, S. & Chowdhury, S. Non-duplex G-Quadruplex Structures Emerge as Mediators of Epigenetic Modifications. *Trends Genet* **35**, 129–144 (2019).
339. Halder, R. *et al.* Guanine quadruplex DNA structure restricts methylation of CpG dinucleotides genome-wide. *Mol Biosyst* **6**, 2439–2447 (2010).

340. Cree, S. L. *et al.* DNA G-quadruplexes show strong interaction with DNA methyltransferases in vitro. *FEBS Lett* **590**, 2870–2883 (2016).
341. Bell, C. G. *et al.* DNA methylation aging clocks: challenges and recommendations. *Genome Biol* **20**, (2019).
342. Esnault, C. *et al.* G4access identifies G-quadruplexes and their associations with open chromatin and imprinting control regions. *Nat Genet* **55**, 1359–1369 (2023).
343. Riedemann, N. C., Guo, R.-F. & Ward, P. A. The enigma of sepsis. *J Clin Invest* **112**, 460–467 (2003).
344. Alexander, C. & Rietschel, E. T. Bacterial lipopolysaccharides and innate immunity. *Journal of Endotoxin Research* vol. 7 Preprint at https://doi.org/10.1179/096805101101532675 (2001).
345. Shirota, H., Gursel, I., Gursel, M. & Klinman, D. M. Suppressive Oligodeoxynucleotides Protect Mice from Lethal Endotoxic Shock. *The Journal of Immunology* **174**, (2005).
346. Esposito, V. *et al.* Structural and Biological Features of G-Quadruplex Aptamers as Promising Inhibitors of the STAT3 Signaling Pathway. *International Journal of Molecular Sciences 2023, Vol. 24, Page 9524* **24**, 9524 (2023).
347. Ma, J. H., Qin, L. & Li, X. Role of STAT3 signaling pathway in breast cancer. *Cell Communication and Signaling* vol. 18 Preprint at https://doi.org/10.1186/s12964-020-0527-z (2020).
348. Chousterman, B. G., Swirski, F. K. & Weber, G. F. Cytokine storm and sepsis disease pathogenesis. *Seminars in Immunopathology* vol. 39 Preprint at https://doi.org/10.1007/s00281-017-0639-8 (2017).
349. Levy, M. M. *et al.* 2001 SCCM/ESICM/ACCP/ATS/SIS International Sepsis Definitions Conference. in *Critical Care Medicine* vol. 31 (2003).
350. Gorla, R., Erbel, R., Eagle, K. A. & Bossone, E. Systemic inflammatory response syndromes in the era of interventional cardiology. *Vascular Pharmacology* vol. 107 Preprint at https://doi.org/10.1016/j.vph.2018.04.003 (2018).
351. Bedrat, A., Lacroix, L. & Mergny, J. L. Re-evaluation of G-quadruplex propensity with G4Hunter. *Nucleic Acids Res* **44**, 1746–1759 (2016).

11 Acknowledgments

I would like to take this opportunity to say thank you to all the people who have encouraged, motivated and supported me along the way. I am very grateful to have had the opportunity to experience the PhD journey or the rather roller coaster ride sometimes.

First of all, I would like to thank Katrin for giving me the opportunity to work freely in her admirable group and for her open door policy.

I would like to thank the whole group for the great time I had when working with all of you. Thanks for the scientific discussions and of course the fun we had during the coffee breaks. Thanks to my teacher of sarcasm Eike, the guardian of wisdom Markus, the king of word jokes Phillip jr, the sunshine and cheerful Saul, the Italian temper Alessio and the swordsman Phillip sen.
I would like to thank the best technicians a lab can have: Theresa and Lea! Thank you Stefan for your lectures in the kitchen about science and thank you for your help and advice.
I cannot imagine my PhD time without having coffee with Mona and Michi, the “Triple M”. Thanks to Zeinab for her patience and for teaching me so much about immunology and for letting me work in her lab, and thanks to Kostas and Jenni for their technical support.
Thanks to Jasper and Susanne for their bioinformatical support and ideas and the fruitful discussions!

Thank you for always being there for me, Daniel! Not only have you been my favorite colleague, but you have become an even closer friend. Thank you for the time we spent bouldering together and thanks for your honesty.

Having friends who share the same passion and are always ready for a joke is precious! Thanks to “Akademisch Blau”!
Thanks to all the members of Hochschulsport Rowing, a bunch of great people. The time I spent with you on the Rhine and hearing the “click” of our skulls calmed me down and always made me forget the rest of the world.
Thanks for always listening to me and traveling around the world with me, Sara!

Thank you, Alex, for your love and patience. Thanks for making me laugh when I want to cry.

Finally, I would like to thank my family for always supporting me. Especially thanks to my “Oldies”, Mama and Claus, for your love and for believing in me no matter what I do and for letting me know that I can always come home and get homemade “Hühnerfrikassee”.